UNIVERSITY OF CAMBRIDGE

HIF2α regulates ccRCC tumorigenesis through activation of cell cycle regulators

Erika Vojtasova

Clare Hall

This dissertation is submitted for the degree of Doctor of Philosophy

February 2019

Preface

This dissertation is the result of my own work and includes nothing which is the outcome of work done in collaboration except as declared and specified in the text. I hereby declare some of the works done in this dissertation were in collaboration with Sakari Vanharanta, Paulo Rodrigues, Saiful Effendi Bin Syafruddin, Saroor Patel, Luca Pellegrinet, Dora Bihary and Shamith Samarajiwa.

It is not substantially the same as any that I have submitted, or, is being concurrently submitted for a degree or diploma or other qualification at the University of Cambridge or any other University or similar institution except as declared in the Preface and specified in the text. I further state that no substantial part of my dissertation has already been submitted, or, is being concurrently submitted for any such degree, diploma or other qualification at the University of Cambridge or any other university or similar institution except as declared in the Preface and specified in the text.

It does not exceed the prescribed word limit for the relevant Degree Committee.

Acknowledgements

I would like to express my sincere gratitude to my supervisor Sakari, who gave me the opportunity to work on this PhD project. He was a great mentor and was always available to discuss any questions or concerns I had. He also helped me with the analysis of the raw data from all the RNA-seq and ChIP-seq experiments.

The postdocs in the lab were of great help throughout my PhD. Saroor and I started at the same time and she became my day to day mentor. I thank her for teaching me all the useful cloning techniques, TC techniques and for having countless conversations about my project.

I was never bored sitting next to Paulo. Thank you, Paulo, for your patience and always answering my questions. Paulo was also very kind and performed the RNA-seq and ChIP-seq experiments showed in this thesis.

I am very thankful to all the other members of the lab- Naz, Fendi, Ludo, Emma, Anabel and Jianfeng for their help and support throughout my PhD. Thank you for all the dinner parties and Friday breakfasts! A special thanks to Fendi, who was also performing the RNA-seq experiments.

I would like to thank Shamith and Dora from the computational group for their help with the RNA-seq data analysis.

I am very thankful to Alyson, with whom I spent many fun Thursdays in the animal facility. Thank you for teaching me how to handle animals and overcome my fear.

Thanks to Luca from Evan's lab, for helping me with the IHC protocols.

Last, but not least, I want to thank to my parents and my sister Dominika who was a reliable source of support and encouragement.

Abstract

Clear cell renal cell carcinoma (ccRCC) is the most frequent type of kidney cancer, with 50% 5-year survival. Genetically, ccRCCs are characterised by inactivation of VHL which is lost in 90% of cases. Inactivating mutations of VHL lead to stabilisation of HIF2α which in turn drives the expression of multiple target genes involved in ccRCC initiation. However, it is unclear whether HIF2α activation is necessary for tumour maintenance. This is of particular interest because current ccRCC therapies are not sufficient and a significant fraction of patients develop resistance. The need for new therapeutic strategies led to development of inhibitors of HIF2α which showed great efficacy *in vitro*, however, patient clinical studies showed high variability in outcome. This further highlights the importance of understanding the role of HIF2α and its downstream regulated pathways in ccRCC.

In order to study the role of HIF2α in ccRCC maintenance, a tetracycline-controlled HIF2α system was developed and introduced into HIF2α depleted cell lines. Tumour growth upon HIF2α reintroduction confirmed the importance of HIF2α for tumour initiation *in vivo*. Subsequent loss of HIF2α led to significant tumour regression and no relapse was observed for 6 weeks.

Using the genetic model described above, the molecular mechanisms underlying HIF2α-mediated tumour maintenance were studied. RNA-seq analysis comparing HIF2α activated versus HIF2α inactivated tumours revealed significant downregulation of genes involved in cell cycle progression such as *MYC, CCND1* and *TGFa*. Furthermore, enhancer profiling performed through H3K27ac ChIP-seq demonstrated the activation of enhancer elements in the close vicinity of these genes. Moreover, HIF2α ChIP-seq showed that it bound the same

enhancers suggesting that HIF2α interaction with these elements contributes to the activation of cell cycle progression genes.

Understanding the mechanisms behind HIF2α-regulated pathways will contribute to understand the variability in patient outcome and may offer new therapeutic targets to improve patient survival in ccRCC.

Table of Contents

List of abbreviations

ADD2	Adducin 2
AR	Androgen Receptor
ARNT	Aryl Hydrocarbon Receptor Nuclear Translocator
BAP1	*BRCA1* Associated Protein-1
bHLH	basic Helix-Loop-Helix
Cas9	CRISPR Associated Protein 9
CCND1	Cyclin D1
ccRCC	clear cell Renal Cell Carcinoma
CDK	Cyclin Dependent Kinase
ChIP	Chromatin Immuno-Precipitation
CRISPR	Clustered Regularly Interspaced Short Palindromic Repeats
CRISPRi	CRISPR interference
Cas3	Caspase 3
CTAD	C- terminal Transcriptional Activation Domain
CTLA-4	Cytotoxic T-Lymphocyte Associated Antigen 4
CXCR4	C-X-C chemokine Receptor type 4
dCas9	Dead Cas9
DDR	DNA-Damage Response
DMSO	Dimethyl Sulfoxide
DOX	Doxycycline
EV	Empty Vector
EGFR	Epithelial Growth Factor Receptor
FACS	Fluorescence-Activated Cell Sorting
FBS	Fetal Bovine Serum
FIH	Factor-Inhibiting HIF
FIMO	Find Individual Motif Occurrences
GOI	Gene of Interest
GSEA	Gene Set Enrichment Analysis
GWAS	Genome-Wide Association Studies
HIF	Hypoxia Induced Factor
HR	Homologous Recombination
HRE	Hypoxia Responsive Elements
HLRCC	Hereditary Leiomyomatosis and Renal Cell Cancer
IHC	Immunohistochemistry
IL-2	Interleukin-2
INFα	Interferon alpha
IPA	Ingenuity Pathway Analysis
IRES	Internal Ribosome Entry Site
KD	Knock Down

KO	Knock Out
LTBP1	Latent-Transforming growth factor Beta-binding Protein 1
mTOR	Mammalian Target of Rapamycin
NK	Natural Killer
NOA	Non-Oncogene Addiction
NOD	Non-obese diabetic
NTAD	N- terminal Transcriptional Activation Domain
OA	Oncogene Addiction
PAM	Protospacer-Associated Motif
PAS	Per-ARNT-Sim
PBRM1	Polybromo 1
PDGF-β	Platelet-Derived Growth Factor beta
PD-L1	Programmed Death Ligand 1
PDX	Patient-Derived Xenografts
PGK	Phosphoglycerate Kinase
PHD	Prolyl Hydroxylase Domain
PuroR	Puromycin Resistance
RCC	Renal Cell Carcinoma
ROS	Reactive Oxygen Species
RT	Room Temperature
rTetR	reverse Tetracycline repressor
SCR	Scramble
SEM	Standard Error of the Mean
SETD2	SET Domain containing 2
SDHB	Succinate Dehydrogenase Complex Subunit B
SNP	Single Nucleotide Polymorphism
TAM	Tumour-Associated Macrophages
TCGA	The Cancer Genome Atlas
TET	Tetracycline
TetR	Tetracycline Repressor
TGF-α	Transforming Growth Factor alpha
TME	Tumour Microenvironment
TRACERx	Tracking Cancer Evolution
TRE	Tetracycline Responsive Element
VEGF	Vascular Endothelial Growth Factor
VHL	von Hippel- Lindau
WT	Wild type

List of Figures

List of Tables

Chapter 1. Introduction

1.1 Kidney: Anatomy and Function

The urinary system is comprised of kidneys, ureter, bladder, prostate (in man) and urethra (**Figure 1.1**). Kidneys are bean-like organs located in the back of peritoneal cavity. The kidney is the main osmoregulatory organ in the body: it filters the blood and regulates acid-base balance, electrolyte concentration and extracellular fluid volume [1].

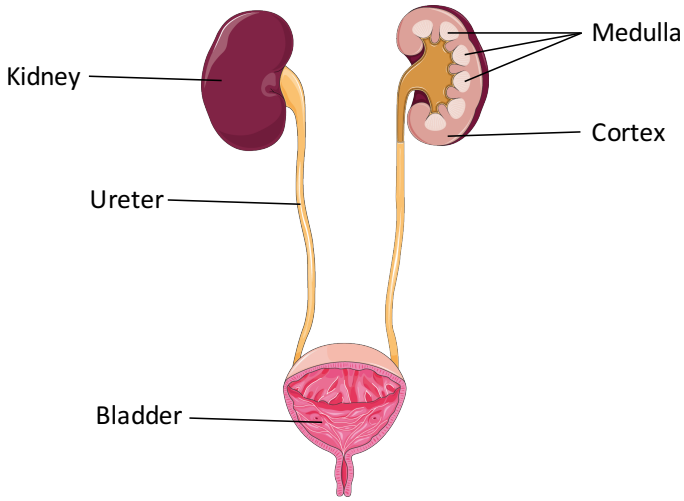

Figure 1.1 Anatomy of the urinary system. Illustration was adapted from freely distributed clipart obtained from https://smart.servier.com.

The kidney is divided into two major structures: outer renal cortex and inner renal medulla (**Figure 1.2**). The medulla consists of several renal pyramids and the renal cortex consists of nephrons. The nephron is the main structural and functional unit of the kidney. Each kidney is made up of several million nephrons which actively filter the blood and form urine. Each nephron consists of three parts: the renal corpuscle (located in the renal cortex), the renal tubule and the associated capillary network. Blood is filtered in the renal corpuscle, where cells and large proteins are retained, and small molecules are passed from the glomerulus into the Bowman's capsule. Reabsorption of water and nutrients takes place in the renal

tubules. Filtered waste is then secreted and emptied into the collecting duct, passed into the bladder via ureter and excreted via urethra[1].

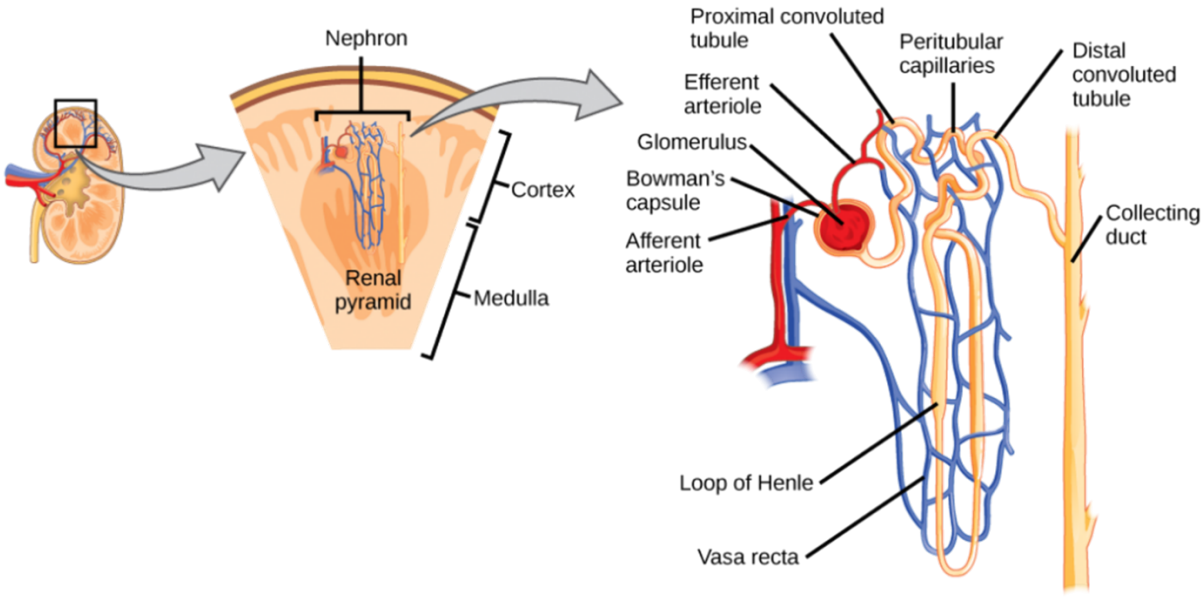

Figure 1.2 Microscopic anatomy of the kidney. Source: https://opentextbc.ca/biology/chapter/22-2-the-kidneys-and-osmoregulatory-organs/

Apart from its excretive and osmoregulatory functions, the kidney also functions as a hormone secreting organ. It regulates secretion of erythropoietin which is essential for red blood cell formation, renin which helps in regulation of blood pressure and 1, 25-dihydroxycholecalciferol which is an active form of vitamin D3 found in the kidney[1,2].

1.2 Overview of kidney cancers

Renal Cell Carcinoma (RCC) accounts for 3% of all adult cancers, being the ninth most common cancer in men and the fourteenth most common in women worldwide[3]. The incidence of this cancer strongly correlates with age, more than third of diagnosed patients in the UK between 2013-2015 were over 75 years old[4]. Risk of developing RCC has been linked to obesity, hypertension and cigarette smoking[4–7]. In the UK, 25% of RCCs were associated to excess weight and 13% to obesity[4]: a BMI increase of 5kg/m^2 has been associated with RCC prevalence[6].

Both familial and sporadic cases of RCCs occur. Sporadic RCCs are the most common ones and only 2-4% of cases are associated with hereditary syndromes[3]. There are four major histologic subgroups of RCC: clear cell (75%), papillary (15%), chromophobe (5%), and collecting duct (2%)[8] (**Figure 1.3**). In addition, other rare types of RCC exist. There are several hereditary syndromes associated with these subtypes such as: von Hippel- Lindau (VHL) syndrome associated with clear cell RCC, hereditary papillary renal carcinoma is linked to *c-Met* mutations and familial renal oncocytoma and chromophobe RCC are associated with Birt-Hogg-Dube syndrome which is caused by mutations in the folliculin tumour suppressor gene; hereditary leiomyomatosis and renal cell cancer (HLRCC) which is observed in patients with fumarate hydratase mutations and tend to result in papillary RCC; succinate dehydrogenase complex subunit B (SDHB)-associated hereditary paraganglioma/phaeochromocytoma linked to mutations in SDHB gene and resulting in variety of renal tumours[9,10].

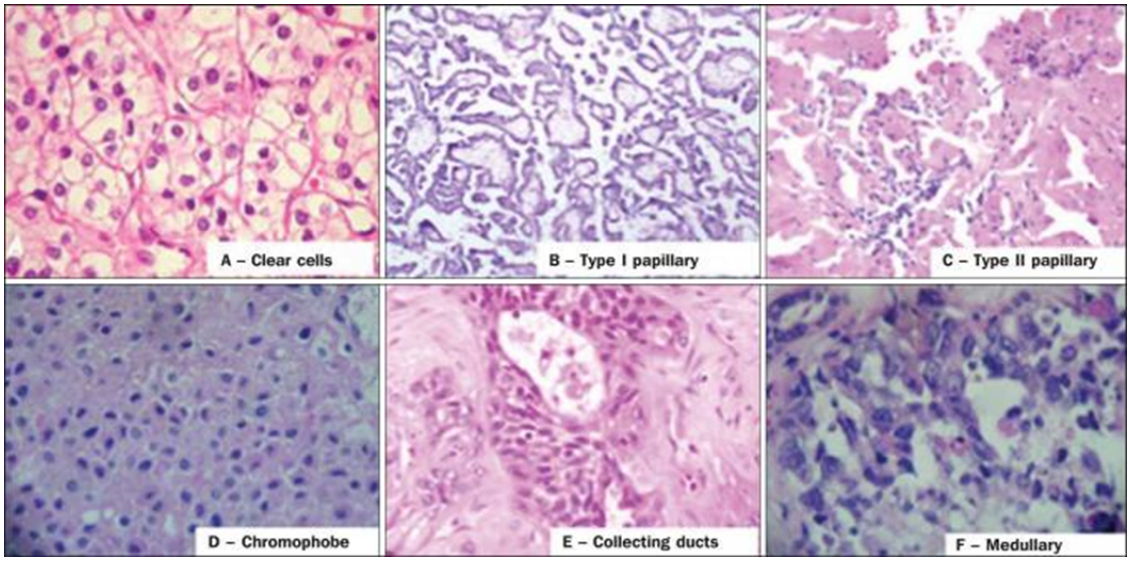

Figure 1.3 Histology of the most common RCC subtypes. Source: Muglia VF, Prando A. Renal cell carcinoma: histological classification and correlation with imaging findings. Radiol Bras. 2015

1.3 Clear cell renal cell carcinoma

Overview

Clear cell RCC (ccRCC) is the most frequent subtype of renal cancer, accounting for 75% of all adult RCC cases[8]. Macroscopically, ccRCC tumours are characterised by a yellow surface caused by the high lipid content within the cells. On the cellular level, ccRCC is composed of cells with clear or eosinophilic cytoplasm[3] (**Figure 1.3A**). In most cases (>90%) ccRCC arises as a result of *VHL* inactivation[11]. *VHL* is a tumour suppressor gene located on the short arm of chromosome 3 (3p25-26). VHL syndrome is an autosomal dominant disease, where patients inherit one non-functional allele of *VHL* gene and the second functional allele becomes inactivated or lost in affected organs, hence ccRCC in these patients tends to be early onset and multifocal. The majority of non-familial ccRCC cases (90%) have one *VHL* allele inactivated

through a deletion, leading to loss of heterozygosity, and the other allele becomes inactivated via gene mutation (>50% of cases) or by gene silencing (5-10% of cases)[12].

Molecular characterisation

ccRCC are highly heterogeneous at the genetic and/or epigenetic level[13,14]. Whole exome sequencing of 417 tumours revealed that 19 genes are significantly mutated [15]. Genes such as *VHL*, polybromo 1 (*PBRM1*) a component of chromatin remodelling complex SWI/SNF, histone methyltransferase SET domain containing 2 (*SETD2*) and the nuclear deubiquitinase *BRCA1* associated protein-1 (*BAP1*) are the most commonly mutated genes in ccRCC. Other genes such as chromatin-modifying enzymes lysine (K)- specific demethylase 6A (*UTX*), lysine (K)-specific demethylase 5C (*JARID1C*), phosphatase and tensin homologue (*PTEN),* mammalian target of rapamycin (*mTOR)* and *p53* have been also observed to be frequently mutated in ccRCC[15]. Interestingly, *PBRM1, SETD2* and *BAP1* genes are all located on the chromosome 3 short arm in the vicinity of the *VHL* locus.

Current understanding of ccRCC tumorigenesis highlights *VHL* inactivation as the initial step, followed by mutations in one or more of the above-mentioned genes. For instance, recent studies in mice models, have shown that that only combined inactivation of *VHL* and *BAP1*, as opposed to single KO of each of these genes*,* resulted in tumour development[16]. Moreover, a recent project (Tracking Renal Cancer Evolution – TRACERx) was undertaken with the objective of defining the drivers and intertumoral heterogeneity in ccRCC and the relationship between the heterogeneity and disease stage, clinical outcome and treatment response. This study analysed 1206 regions from primary tumours of 101 ccRCC patients and detected 751 somatic copy number alterations[17]. Up to 30 driver events per tumour were found. The

analysis of event co-occurrences at the clonal level showed an enrichment for mutual exclusivity in *BAP1* and *BPRM1, BAP1* and *SET2*. However, these events were found to co-occur at separate tumour subclones at the patient level. A subset of cases that harboured two or more additional clonal drivers apart from *VHL* were observed*. BPRM1* was found to be one of the early events in ccRCC, being present in 74% of cases. In another study performed by the same group, 575 primary and 335 metastatic biopsies across 100 patients with metastatic ccRCC were analyzed[18]. Metastatic sites tended to be more homogenous, with less somatic driver alterations compared to their matched primary tumours. Only 5.4% of driver events were found to be *de novo* in metastasis, suggesting that most of the driver diversity are present at the primary tumour site. 9p loss (the Cyclin-dependant kinase inhibitor *CDKN2A* gene is located on 9p21[19]) was found to be a potent driver of metastasis and ccRCC mortality risk. 14q loss (the *HIF1α* gene is located on 14q23.2[20]) was also found to be significant, in fact 71% of the metastatic cases had lost both, 9p and 14q, compared to 35% in cases where metastasis had not occurred. Whole genome analysis from 95 biopsies across 33 ccRCC patients showed that early ccRCC development follows strongly preferred trajectories where loss of 3p is often the initial driver [21]. However, this study suggests a latency of many decades between 3p loss and the onset of cancer.

1.4 VHL-HIF pathway in ccRCC

The VHL protein has many functions, such as regulation of extracellular fibronectin matrix assembly[22], interaction with alpha-chains of collagen IV[23] and control of ciliogenesis by interacting with microtubules[24]. However, the most studied function of pVHL is serving as a

recognition subunit of the E3 ubiquitin ligase complex capable of targeting proteins for proteosomal degradation. The pVHL E3 ubiquitin ligase complex targets protein kinase C[25], Rbp1 (a subunit of RNA polymerase 2)[26] but the best described interaction of pVHL to date is regulation of hypoxia induced factor (HIF) activity[27] (**Figure 1.4**). HIF is a heterodimer consisting of two basic helix-loop-helix Per-ARNT-Sim (PAS) domains (bHLH PAS) named HIF1α/HIF2α and HIF1β (also referred to as Aryl Hydrocarbon Receptor Nuclear Translocator or ARNT). Both HIFα subunits contain two transcriptional activation domains- N-terminal transcriptional activation domains (NTAD) and C- terminal transcriptional activation domains (CTAD) (**Figure 1.5**). Under normoxic conditions, HIFα becomes hydroxylated at two highly conserved proline residues within the oxygen-dependent degradation domain by prolyl hydroxylases (PHD). The β domain of pVHL recognises the PHD hydroxylated HIFα at one or both proline residues, binds to it along with elongin-C, elongin-B, cullin-2 and ring-box 1 to form an E3 ubiquitin ligase which targets HIFα for ubiquitination and degradation[28]. In addition, CTAD can be hydroxylated on its asparagine residue by Factor-inhibiting HIF (FIH), impairing CTAD activity[29]. In hypoxia, PHDs are inactive; FIH remains active in intermediate levels of hypoxia[30]. In hypoxic conditions, unhydroxylated proline residues of HIFα cannot be recognized by pVHL and therefore, HIFα accumulates in the cell. HIFα is then translocated to the nucleus, where it heterodimerises with HIFβ. HIFβ is constitutively expressed at the protein level and is not affected by oxygen levels. The HIF heterodimer complex binds to hypoxia responsive elements (HREs), recruits transcriptional coactivators (p300/CBP) and turns on the transcription of HIF regulated genes such as vascular endothelial growth factor (VEGF), platelet-derived growth-factor B chain (PDGF-β), transforming growth-factor-α (TGF-α) and others. HIF regulated genes are involved in processes such as angiogenesis, metabolism, cell cycle, apoptosis and metastasis and their dysregulation has been observed

in many cancers[31]. HIFα stabilisation and accumulation due to microenvironmental hypoxia within the tumour is observed in many cancers. Tumour hypoxia has been associated with increased metastasis, poor prognosis and resistance to radiation therapy[32]. In ccRCC, VHL mutations render it unable to target HIFα for degradation, leading to the stabilisation of the latter with subsequent upregulation of glycolysis and angiogenesis typically observed in tumours[32,33]. Moreover, the importance of HIF2α deregulation in hereditary and sporadic *VHL*-associated RCC was shown by Li and colleagues[34], demonstrating that the risk of developing ccRCC correlates with the degree of pVHL impairment to target HIFα for degradation and low and high risk of developing ccRCC can be predicted depending on the type of *VHL* mutations. Based on these observations HIFα has been identified as a putative therapeutic target for ccRCC.

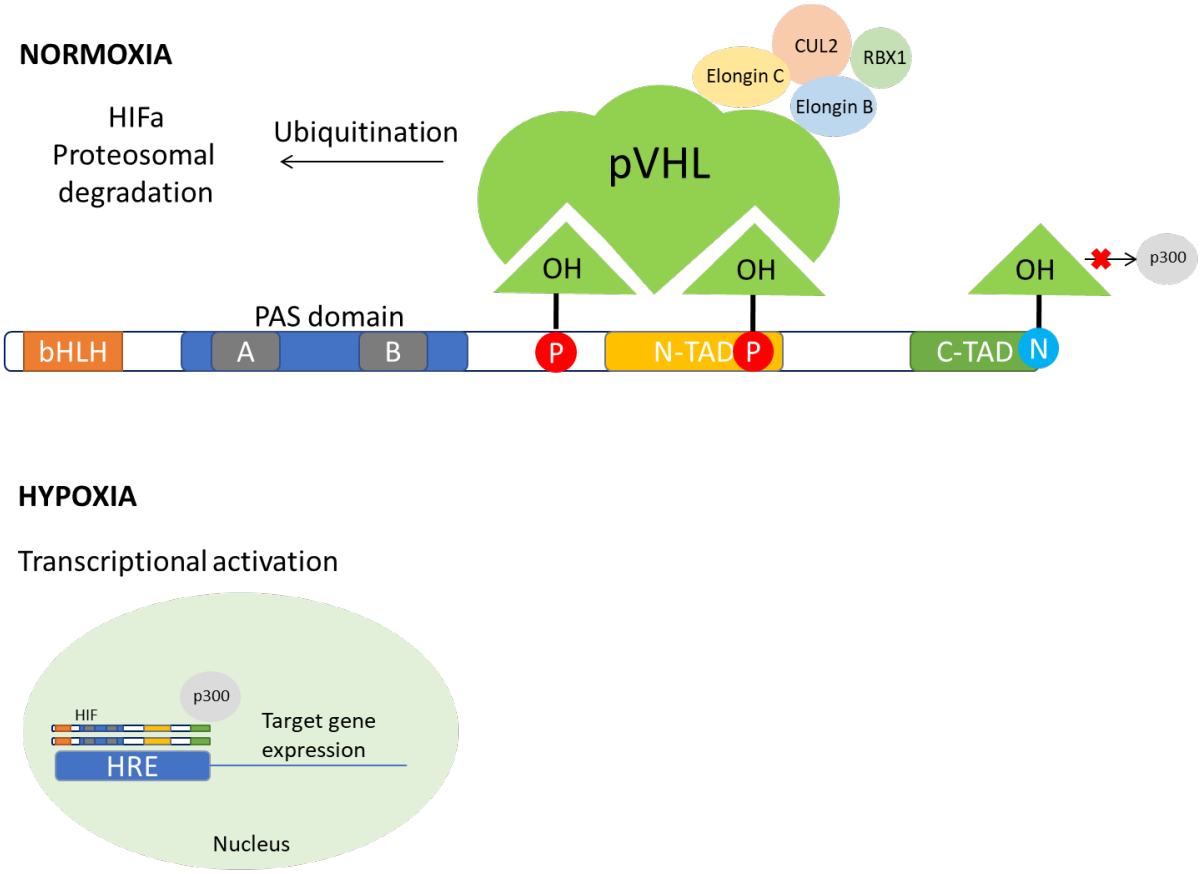

Figure 1.4 VHL-HIF pathway in normoxic and hypoxic conditions. In normoxia, HIFα is hydroxylated and targeted by VHL for proteosomal degradation. In hypoxia, HIFα is not recognised by VHL, it accumulates, translocates to nucleus and dimerizes with HIFβ, driving the expression of HIF downstream target genes. (adapted from Chen *et al.*, 2009 28)

1.5 HIFα isoforms

HIF1α was initially identified in studies involving oxygen-regulated expression of erythropoietin by Semenza and Wang[35]. Shortly after, HIF2α, sharing 48% sequence identity with HIF1α, was discovered[36,37]. Tian and colleagues[37] showed that both HIFα subunits heterodimerise with HIFβ and bind to the same DNA recognition sites. HIFβ subunit was shown to be an essential component of HIF1α/HIFβ heterodimer, especially important for recognition of HIF1α DNA-binding sites[38], however, Choi and colleagues[39] demonstrated that some HIF1α target genes (*SUI1-RS1, FKBP4* and *PSMA3*) are induced independently of HIFβ.

In regard to pVHL recognition of hydroxylated HIFα, both isoforms are hydroxylated by PHD, however, CTAD hydroxylation by FIH differentially affects HIFα isoforms and its downstream targets. HIF2α is relatively resistant to FIH hydroxylation compared to HIF1α[40]. A third isoform of HIFα, HIF3α, has not been extensively studied compared to the other HIFα subunits. It lacks a CTAD (**Figure 1.5**) and is not capable of efficient HRE induction. Nonetheless, HIF3α was still shown to regulate the expression of HIF target genes, indicating it may be more important than previously anticipated[41]. Even though both HIF1α and HIF2α have similar characteristics, Ema and colleagues[36] observed that their expression levels differ. HIF2α mRNA is abundantly expressed in the majority of organs such as lungs, heart and liver in normoxia, whereas HIF1α mRNA is ubiquitously expressed at a lower level. Not only do their expression levels differ, but also experiments have shown that HIF1α and HIF2α in VHL defective RCC cells have opposing effects on gene expression and tumorigenesis *in vitro.* For instance, HIF1α positively regulates BNip3 (a pro-apoptotic, anti-tumorigenic Bcl-2 family protein), while HIF2α promotes expression of pro-tumorigenic cyclin D (involved in G1 to S transition in cell cycle), TFG-α (potent renal cell mitogen) and VEGF (vascular endothelial growth factor promoting angiogenesis)[33]. Moreover, HIF1α has been shown to antagonise MYC and induce cell cycle arrest[42], whereas HIF2α promotes MYC transcriptional activity in hypoxia resulting in cell proliferation[43]. Therefore, in the case of RCC, HIF2α seems to be more tumorigenic than HIF1α. In fact, Shen and colleagues[44] demonstrated that wild type HIF1α supress tumour growth in ccRCC and acts as a tumour suppressor gene. Also, stabilisation of HIF1α alone is insufficient to promote tumorigenesis[45]. On the other hand, downregulation of HIF2α by shRNA dramatically impaired tumour growth *in vivo*, demonstrating that loss of HIF2α alone is sufficient to supress VHL-mediated tumorigenesis[46,47]. Additionally, experiments using VHL-reintroduced cell lines together with a HIF2α variant which lacks its pVHL binding site restored

the tumour-forming ability of these cells. These experiments demonstrated that stabilisation of HIF2α is sufficient for tumorigenesis[48]. The importance of HIF2α for tumorigenesis was further supported by observation that some VHL deficient patient cell lines express both isoforms of HIFα but others, such as 786-O and KTCL140 only express HIF2α and importantly, there are no known ccRCC cell lines that only expresses HIF1α[27]. It was also observed that early kidney lesions of VHL patients showed higher expression of HIF1α whereas advanced lesions tend to express HIF2α at higher level[33]. Moreover, genome-wide association studies (GWAS) of RCC found two variants in a locus mapping to *EPAS1* gene (*HIF2α*) on 2p21 to be associated with susceptibility to RCC[49]. Nonetheless, the expression of both HIFα seem to be essential for early stage of tumour development based of the observation that deletion of either *HIF1α* or *HIF2α* abrogated the formation of renal cysts and tumours in *VHL/Trp53* mutant mice[50].

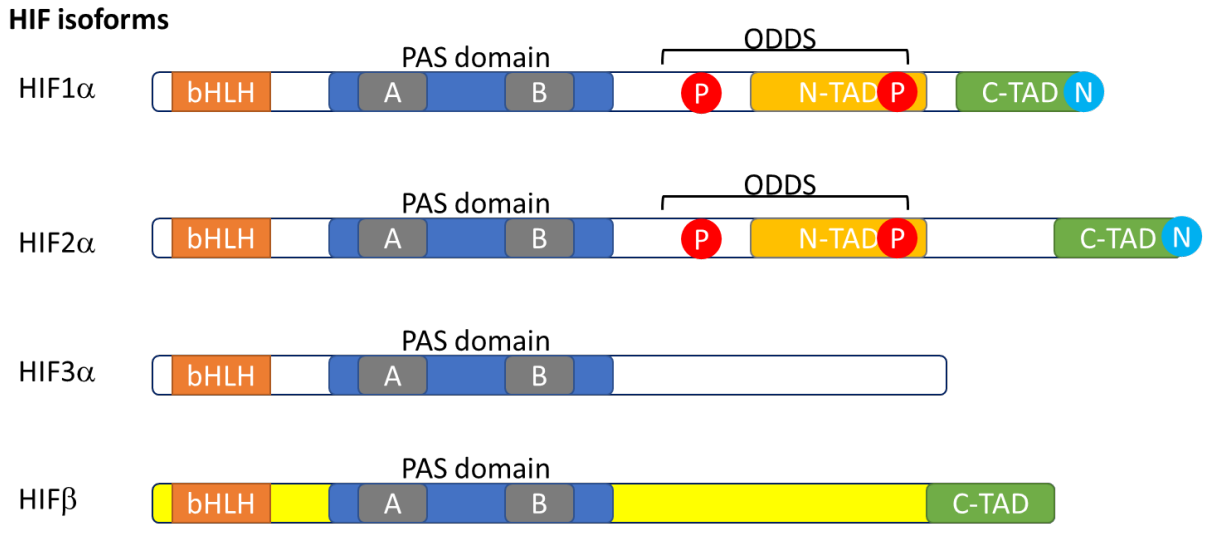

Figure 1.5 Structure of HIF isoforms. All HIF proteins share a domain involved in DNA-binding - basic Helix-Loop-Helix domain (bHLH) and in protein to protein interaction and dimerization- Per-Arnt-Sim domain (PAS). The C-terminal domain (C-TAD) and N-terminal domain (N-TAD) are involved in transcriptional activation. ODDS are oxygen dependent degradation domains. (adapted from Chen *et al.*, 2009[51])

1.6 Current treatments

Renal cancer is often asymptomatic and usually diagnosed incidentally during imaging diagnostic tests for other clinical reasons. The first symptoms of renal cancer are often due to metastatic spread. Radical nephrectomy or nephron-sparing tumorectomy is the first line of treatment for early stage disease. Radical nephrectomy is the surgical removal of the whole kidney, including perirenal fat tissue, adrenal gland and regional lymph nodes[52]. Nephron-sparing tumorectomy, also known as partial nephrectomy removes only the primary tumour, while preserving the rest of the renal tissue. Nonetheless, disease relapse and spread to the secondary sites is common, as with most cancer types, inoperable and fatal in most cases[53]. One third of ccRCC patients have metastasis when diagnosed with 5-year survival rates of only less than 10%. Patients with advanced ccRCC are not responsive to conventional radio- and chemotherapies, accounting for their poor prognosis and high mortality[54].

Until 20 years ago, cytokine-based treatment was the only available therapy for metastatic ccRCC. Treatment with interferon alpha (INFα) and interleukin-2 (IL-2) had very adverse side effects and very poor patient survival rate[55,56]. Currently, there are several approved targeted treatments available for metastatic RCC.

Due to the highly vascular nature of this disease, several tyrosine kinase inhibitors targeting the VEGF signalling pathway were approved. These include sorafenib, sunitinib, pazopanib and axitinib[57–59]. First-line treatment options include orally administered multi-targeted receptor tyrosin kinase inhibitors (eg. VEGFR, PDGFR) such as sunitinib and pazopanib[60]. Sunitinib treatment demonstrated better response rates and longer progression-free survival compared to INFα treatment[58]. Pazopanib was also associated with improved tumour response and longer progression-free survival compared to placebo[61]. In addition to that, bevacizumab,

a monoclonal antibody against VEGFA has also been clinically approved as a first-line treatment for metastatic ccRCC[62]. Axitinib and sorafenib were tested as second-line treatments for metastatic RCC following failure of previous therapy with sunitinib, bevacizumab, temsirolimus, or cytokines. Axitinib, compared to sorafenib, was associated with better efficacy and longer progression-free survival[59].

mTOR inhibitors, such as everolimus and temsirolimus, have been approved as a single treatment for advanced ccRCC[63,64]. Temsirolimus is another first-line treatment in patients with poor-risk ccRCC. Metabolic toxic effects of mTOR inhibitors such as hyperglycemia, hypercholesterolemia and hyperlipidemia have been reported[60]. Everolimus is a second-line treatment mTOR inhibitor which demonstrated prolonged progression-free survival compared to placebo in patients that had progressed on therapy with sunitinib, sorafenib or both[63]. Resistance to both, VEGF-targeted and mTOR-targeted treatments has been observed in a significant number of patients[12]. To improve the patient's outcome, a combination of anti-angiogenic and mTOR inhibitors has been tested. Adverse side effect and no benefit was observed in some of these trials[65,66].However, a combination of everolimus and lenvantinib (a multi-target receptor tyrosine kinases inhibitor that include PDGFRA and PDGFRB[65]) treatment showed improved progression-free and overall survival of advanced ccRCC patents who have been previously treated with anti-VEGF inhibitors[67].

Recently, immune checkpoint inhibitors have been developed as a novel strategy to treat various solid tumours, including advanced ccRCC[68]. Antibody inhibitors targeting programmed death (PD-1) and programmed death ligand (PD-L1), nivolumab and atezolizumab, respectively, have been approved as second line treatment for patients who have received prior therapy with the VEGF-targeted agents and mTOR inhibitors. Nivolumab

treatment showed improved response and overall survival in patients who progressed on VEGF-targeted therapy compared to treatment with everolimus[69]. Other checkpoint inhibitors, including the cytotoxic T-lymphocyte associated antigen (CTLA-4) inhibitor ipilimumab in combination with several agents and programmed death ligand 1 (PD-L1) inhibitor atezolizumab, are currently at various stages of clinical trials for ccRCC treatment[70].

1.7 Targeting HIF2α

Inefficiency of the drugs mentioned above, and the persistence of poor patient prognosis have led to attempts to target HIF2α therapeutically. Targeting a transcription factor is usually very challenging due to difficulties of identifying suitable molecular targets, failure to achieve high specificity and avoiding off-target effects[71]. Recently, Scheuermann and colleagues[72] discovered that the PAS-B domain of HIF2α contains a large cavity that can be used as a small molecule binding target. They identified and characterised artificial ligands binding within this pocket resulting in HIF2α structural and functional changes, which prevent its heterodimerisation with HIFβ *in vitro*. Importantly, these small molecules are HIF2α specific and do not have any affinity for HIF1α and so present a potential HIF2α selective therapeutic treatment for RCC patients. More than 130 small molecule inhibitors have been discovered and two, namely PT2385 and PT2399 have been selected for further testing[73,74].

PT2385 is a HIF2α inhibitor which is completely engulfed in the HIF2α cavity, preventing its interaction with HIF1β. It strongly inhibited the expression of HIF2α regulated genes such as *VEGF, CCND1, CXCR4* and *GLUT1 in vitro* and in tumour xenografts. Importantly, HIF1α regulated genes were not affected. Compared to current established ccRCC treatments,

PT2385 showed better safety profile and faster tumour reduction in subcutaneous tumour models[75]. Phase I dose escalation trial of PT2385 in 49 patients with previously treated advanced ccRCC showed no dose-limiting toxicity and good safety, pharmacokinetic and pharmacodynamic profile. Observed patients response was variable: 2% complete response, 12% partial response and 52% stable disease[76].

The PT2399 antagonist is also under preclinical development. It successfully dissociated HIF heterodimers in human ccRCC cell lines and supressed tumorigenesis in 56% of such cell lines[77,78]. It showed greater activity than sunitinib, was active in sunitinib-progressing tumours, and was better tolerated. However, some VHL-mutant ccRCC became resistant to this treatment, even though HIF dissociation occurred. PT2399 sensitive tumours showed a distinguishing gene signature and generally higher levels of HIF2α. Prolonged treatment led to resistance due to mutation in HIF2α / HIF1β binding sites.

Furthermore, a novel, orally administered small molecule HIF2α inhibitor PT2977 was recently tested. PT2977 showed improved potency compared to PT2385[79]. Patients with advanced ccRCC who have been treated with at least one therapy were included in a Phase 1 dose-escalation trial. PT2977 was well tolerated and showed favourable safety profile. The study also showed variable patients' response- of five patients with ccRCC, one showed partial response and four stable disease with tumour reductions from 8-26%. PT2677 is currently under evaluation and expansion for Phase II trial.

1.8 Oncogene and non-oncogene addiction

The term "Oncogene Addiction" (OA) was first mentioned by Bernard Weinstein[80] to describe the dependency of some cancers on the activity of a single gene product for cancer cells'

survival. This theory was supported by studies of well-known oncogenes such as *MYC* in various cancers[81], where switching on the *MYC* oncogene led to tumour development and subsequent switching off the gene inhibited cancer cell division, leading to apoptosis. For example, Felsher and Bishop[82] used a tetracycline regulated transgenic mouse model to conditionally express *MYC* in hematopoietic cells. *MYC* transgene expression led to development of T cell lymphomas and acute myeloid leukemias and *MYC* inactivation resulted in tumour regression associated with rapid proliferative arrest, differentiation and apoptosis of tumour cells, and resumption of normal host hematopoiesis. Another study, that using tamoxifen controlled *Myc-ER* in pancreatic β cells, showed that *MYC* activation alone is sufficient to induce proliferation of pancreatic β cells, and its deactivation induces rapid regression associated with vascular degeneration and β cell apoptosis[83]. Such studies prove that targeting a single oncogene may be sufficient to reverse malignancy. Similar observations have been reported for other oncogenes such as *K-ras* in lung cancer, *Wnt-1* in breast cancer, *Bcr-Abl* in leukaemia[84]. Oncogene targeted therapies initially work well, however, resistance and tumour relapse are eventually observed in the clinic[85]. Common ways of observed resistance include alterations of the oncogene drug target (eg. with Imatinib, an inhibitor of the BCR-ABL pathway in chromic myeloid leukaemia, resistance arises by acquisition of second-site mutations in BCR-ABL itself[86]) or activating mutations in other component of the oncogenic pathway (eg. with Vemurafinib, an inhibitor of BRAF in melanoma, resistance is acquired by activating other components of MAPK pathway such as NRAS[87]).

Solimini and colleagues[88,89] described another, potentially larger group of drug targets that explores dependency of some cancers on normal cellular function of genes involved in oncogenic pathways, but genes themselves are not oncogenic. This phenomenon was termed

"non-oncogene addiction" (NOA). Targeting NOA is categorised as tumour intrinsic and extrinsic. Tumour intrinsic NOA is referring to targeting genes involved in supporting oncogenic state of the tumour cells in a cell autonomous manner. Examples of targeting an intrinsic NOA include inhibition of DNA damage response (DDR) (inhibition of DDR kinase Chk1 show selective toxicity towards tumour cells with defective p53 and RB pathways[90]), sensitizing to Reactive oxygen species (ROS) (agents stimulating ROS production can selectively induce apoptosis in cancer cells[91]) and modulation of immune response (prostaglandin PGE2 supresses activation of cytotoxic T cells, inhibition of PGE2 improves immune response to tumour cells in murine lung cancer models[92]). Tumour extrinsic NOA genes function in stromal and vascular cells supporting the tumour. Tumour supporting cells are genetically more stable than tumour cells and present a more favourable drug target as they are less likely to develop drug resistance, on the other hand tumours may evolve to be less dependent on those cells[89]. An example of extrinsic NOA is angiogenesis which supplies tumours with nutrients and oxygen. VEGF inhibitors mentioned above, or inhibitors of any protein required for angiogenesis, can be explored for NOA therapy. Mechanisms of resistance to angiogenic inhibitors include amplification of pro-angiogenic genes in the cancer cell genome, change of mode of vascularisation to ensure cancer cell nutrition or expression of alternative angiogenic proteins[93]. Some oncogenes and non-oncogenes may play an important role in tumour initiation, but may not be required for tumour maintenance, therefore more extensive studies of alternative pathways involved in tumorigenesis of specific cancers are necessary and this knowledge can be used to prevent resistance by targeting multiple gene products at the same time.

The role of the immune system in oncogene addiction

Oncogene activation can modulate the expression of some critical immune regulatory receptors, interfere with the normal immune cell development and modulate the expression of cytokines[94,95]. Thus, oncogene inactivation can restore these immune responses. Furthermore, oncogene inactivation depends on immune system to induce tumour regression in many cancers through different mechanisms[96]. For example, Rakhra and colleagues[97] showed that transgenic models of MYC or BCR-ABL tumorigenesis only undergo oncogene inactivation induced tumour regression when the hosts immune system is intact. The kinetics of regression, the extent of regression and the ability to maintain regression were affected by the immune compromised host. Only $CD4^+$, and not $CD8^+$ T cells seem to be necessary for sustained tumour regression. $CD4^+$ T cells can express a variety of cytokines, important for regulation of cellular senescence and angiogenesis[98–100]. Change in cytokines was observed following oncogene inactivation: anti-tumour cytokines are recruited and pro-tumour cytokines are supressed[97]. Another study showed the role of *MYC* in reprogramming of tumour stroma in *KRAS* driven lung cancer models with controllable *MYC* expression[101]. *MYC* deactivation led to changes in tumour stroma and tumour regression was dependent on natural killer (NK) cells. Other mouse models of oncogene-induced tumours showed tumour growth and regression is dependent on innate immune cells such as mast cells or macrophages[102,103]. These studies suggest the importance of innate and adaptive immune cells as well as other host cells for sustained tumour regression.

1.9 Conditional genetic systems in cancer biology

In the last 50 years, many advances have occurred in the development and usage of mouse models used, starting from transplantation-based mouse models (xenografts) to genetically engineered mouse models. Though they provided a lot of knowledge, they also have their limitations[104]. Xenografts are frequently used in cancer research to test for cancer related genes and for preclinical drug testing. Nevertheless, cancer cell lines contain multiple mutations from the start and develop more when cultured for long time. These models do not always represent the morphology and genetic heterogeneity of human cancers and therefore are often poor predictors of clinical response[104]. Genetically engineered mouse models contributed greatly to cancer biology by proving that an oncogene expression in normal cells could lead to tumour formation[105–107]. However, the transgenes are expressed in all cells at all times of a particular tissue, which fails to mimic a sporadic cancer development where a single cell accumulates mutations resulting in tumorigenesis. More sophisticated systems allowing for somatic inactivation of a tumour suppressor or activation of an oncogene in defined tissue at defined time are now available. The most commonly used technologies are Cre-LoxP system and tetracycline (Tet)-inducible systems. This is particularly useful especially when studying a gene that is toxic to the animal, and so the gene can be activated only when appropriate. These strategies have and will contribute to substantially improve the understanding of the function of individual genes in development and disease[104].

Cre-Lox system

The Cre-Lox recombination system was derived from bacteriophage P1. Cre recombinase cuts specifically a DNA sequence flanked by two *lox P* sites. *Lox P* are specific sequences of 34bp consisting of an 8bp core sequence, where recombination takes place, and two flanking 13bp inverted repeats. One of the first examples was the generation of colorectal cancer mouse model where the *Apc* gene was flanked by *loxP* recombination sites and Cre recombinase was delivered via adenovirus-mediated delivery[108]. Following the Cre activation, colorectal adenomas resembling adenomas in familial adenomatous polyposis coli patients, were formed. Temporal and spatial induction of a somatic mutation can also be achieved using Cre-ERT fusion protein, where Cre is fused to a mutated hormone binding domain of the oestrogen receptor (ERT). In this setting, Cre-ERT recombinase is active in presence of oestrogen analogue tamoxifen[109]. ERT have also been fused to known oncogenes, in order to study their role in tumour initiation and maintenance. For example, Pelengaris and colleagues[83] used a *MYC-ERT* transgene which showed that *MYC* activation led to tumorigenesis in model of pancreatic cancer, and *MYC* deactivation induced rapid tumour regression.

Tetracycline (TET)- inducible systems

TET-inducible systems are the most commonly used inducible systems allowing for spatiotemporal and reversible gene expression regulation. The TET OFF system was the first to be developed. It comprises of a tetracycline repressor (TetR) which in presence of tetracycline or its analogue doxycycline (DOX), precludes its binding to tetracycline regulating elements within the TET promoter, and hence prevent the expression of the target gene[110]. An adaptation of TetR to a reverse TetR (rTetR) resulted in the generation of the TET ON system allowing for gene expression activation by DOX[111]. This system was used to generate DOX-inducible cDNAs and shRNAs which allowed for controlled gene expression without modifying the genome. DOX-inducible gene expression systems have been successfully used to study oncogene addiction by either turning on the expression of the oncogenic transgene, or by turning it off to determine how the tumours respond to oncogene inactivation[112,113]. For instance, Dow and colleagues[114], have shown, that using DOX-inducible shRNA against *APC,* colorectal cancer cells can revert to functioning normal cells *in vivo*, even though *KRAS* and *p53* mutations are present. Recently, discovery of CRISPR-Cas9 genome editing technique allowed for development of DOX-inducible Cas9 systems: DOX regulated induction of Cas9 enabled widespread gene disruption and effectively created biallelic mutations [115].

1.10 Problem statement and project aims

Over the last two decades, there has been significant progress in understanding the ccRCC pathogenesis and molecular mechanisms involved in ccRCC. This knowledge has led to the development of therapeutics such as agents targeting angiogenesis and mTOR signalling pathways. However, these therapies are not always effective, and patients are often refractory to treatment. Several studies have shown the importance of HIF2α in ccRCC tumorigenesis, particularly in tumour initiation[47,48]. Recent development of HIF2α inhibitors has shown some efficacy in xenograft models, however, patients response was very variable[75–78]. The aim of this study is to identify the key targets through which HIF2α drives tumour growth and progression. Understanding the mechanisms behind HIF2α-regulated pathways will help to understand the variability in patient outcome and may offer new therapeutic targets or suggest a combination therapy to combat resistance and improve patient survival. In order to study the role of HIF2α, a HIF2α-controllable system is needed. Such a system to control the HIF2α expression has not been described. The following outlines the aims of this study:

Aim 1: To develop a genetic tool which will aid to understand the role of HIF2α in ccRCC maintenance

Objective 1. Establish a genetic model for controllable HIF2α expression in ccRCC

To develop a genetic model that allows for temporal control of HIF2α expression in VHL mutant ccRCC cell lines, I first generated HIF2α KO cell lines using CRISPR-Cas9 genome engineering. Then, I developed an exogenous HIF2α construct which can be controlled in a doxycycline (DOX) inducible manner.

Objective 2. Test the HIF2α inducible genetic model in vitro

I introduced the exogenous HIF2α DOX-inducible construct into the HIF2α KO clones and validated this genetic system *in vitro* in multiple ccRCC HIF2α KO clones.

Aim 2: To understand the molecular mechanism through which HIF2α promotes tumour maintenance in ccRCC

Objective 1. Molecular characterisation of the responses to HIF2α withdrawal

The system generated was used to study the role of HIF2α in ccRCC *in vivo*. DOX inducible HIF2α was expressed and subsequently inhibited, in order to observe the effects of HIF2α loss in established ccRCC tumours.

Objective 2. Functional characterisation of the mechanisms through which HIF2α mediates ccRCC growth

The inducible HIF2α genetic model served to elucidate the molecular mechanisms involved in ccRCC tumour maintenance. Tumours before and after HIF2α loss were analysed by RNA-seq to identify any differences. The list of significantly altered genes was studied to elucidate the pathways through which HIF2α drives tumour progression. The identified HIF2α downstream targets were functionally validated using CRISPRi.

Chapter 2. Materials and Methods

2.1 Cell lines and cell culture

The following human ccRCC adherent cell lines were used: OSLM1B cells, a metastatic clone of OS-RC2 (obtained from RIKEN Cell Bank, Japan), RFX631 (obtained from National Cancer Institute), 786-M1A/M2D both metastatic clones of 786-O cells, 769-P and RCCMF (obtained from the ATCC). Cells were cultured in a RPMI-1640 medium (Sigma R8758) supplemented with 10% (v/v) fetal bovine serum (FBS) and 1% (v/v) penicillin-streptomycin (P/S). Cells were split every 3-4 days and cell line stocks were created by freezing cells in FBS supplemented with 10% (v/v) dimethyl sulfoxide (DMSO). All the renal cell lines were validated by detecting known unique homozygous VHL mutations by Sanger sequencing: 786-M1A/M2D- deletion of G at position 310, OSLM1B- deletion of G at position 173, RCCMF- C to T point mutation at position 256, 769-P- T to A point mutation at position 539. Cells were tested biannually for mycoplasma using MycoAlert^{TM} Mycoplasma Detection Kit (Lonza, LT07-318). Human embryonic kidney HEK293T cells (obtained from the ATCC) were used for lentivirus production. These were cultured in a DMEM medium (Invitrogen) supplemented with 10% (v/v) FBS and 1% (v/v) P/S.

2.2 Cloning

2.2.1 DOX-inducible HIF2α

A DOX-inducible LT3GEPIR plasmid (courtesy of the Zuber laboratory[116]) was used as a backbone to construct a DOX-inducible HIF2α plasmid. GFP was digested out of LT3GEPIR and was substituted by dsRED obtained from the LT3REVIR[116] plasmid. HIF2α wild type (WT) was PCR-amplified from pBABE-HA-HIF2α WT (Addgene plasmid #26055) and was ligated to the constructed LT3-dsRed backbone.

2.2.2 CRISPRi constructs

The pHR-SFFV-KRAB-dCas9-P2A-mCherry plasmid was obtained from Jonathan Weissman (Addgene plasmid #60954). The sgRNA expression vector pKLV-U6-gRNA(BbsI)-PGKpuro2ABFP, was obtained from Kosuke Yusa (Addgene plasmid #50946). This plasmid was modified in our lab to generate the following variants: pKLV-U6-gRNA(BbsI)-PGKpuro2AGFP and pKLV-U6-gRNA(BbsI)-PGKhygro2AeGFP. The CRISPRi sgRNA sequences were obtained from either the genome-scale CRISPRi sgRNA library designed by Gilbert *et al*., or from the Broad Institute online sgRNA design tool (https://portals.broadinstitute.org/gpp/public/).

Tandem sgRNA cloning

The tandem shRNA constructs were designed to express two individual sgRNAs. The cloning strategy was designed by a postdoc in the lab. The strategy involves designing an oligo template which include BbsI restriction side on both ends and two sgRNAs separated by a spacer DNA containing AarI sites. The oligo template was first serially diluted to 1:1000 and then PCR amplified using standard PRC protocol. PRC product was purified using Qiagen's Mini Elute PCR purification kit and digested with BbsI restriction enzyme (NEB, R0539S). The digested product was purified using Quick Clean II Gel Extraction Kit (Genescript, L00418). The sgRNA expression vector pKLV-U6-gRNA(BbsI)-PGKpuro2ABFP was also digested by BbsI and the tandem oligo was ligated in. Competent *E. coli* were transformed with the ligation product and colonies were picked, grown over night and mini-prepped. Plasmids that incorporated the tandem oligo were positively selected by digestion with AarI restriction enzyme. An additional sgRNA scaffold-U6 promoter fragment present in the pBigT plasmid (available in the lab) was digested out using AarI and ligated into AarI digested pKLV plasmid containing the sgRNA tandem oligo. The ligation product was transformed into competent *E.coli* and the

presence of sgRNAs and ligated U6 promoter was confirmed by Sanger sequencing.

2.2.3 VHL reintroduction

pLVX-puro (Clontech #632164) was used to express HA-VHL (Addgene #19234) for the VHL reintroduction experiments. The empty vector (EV) of pLVX-puro was used as the control. This cloning was performed by a member of the lab.

2.2.4 Enhancer reporter vectors

Individual constituents of each enhancer comprising approximately 700bp was PCR- amplified from 786-M2D genomic DNA. The primer3 online tool was used to generate appropriate primers (https://primer3plus.com/primer3web/primer3web_input.htm). Suitable restriction sites were added to the PCR-amplified enhancer regions via primer tails. The same restriction enzymes were used to digest pNL1.1[Nluc] plasmid (Promega, N1001). Each enhancer region was ligated upstream of the minimal promoter which drives the expression of the Nanoluc luciferase gene.

All primers, oligos and sgRNA constructs were ordered from Sigma-Aldrich. Sequences are listed in **table I**:

Table I. Sequences of primers and sgRNAs

	Name	Sequence (5'-3')
1	dsRed-BamHI Forward primer	GTTGGATCCACCATGGCCTCCTCC
2	dsRed-T2A-XhoI Reverse primer	CGATCTCGAGGACCATGGTCCCGGGTTCTCTTCCA CATCACCACAGGTCAGCAGGGAGCCTCTCCCTTCT CCGGACCCGCCGCCCAGGAACAGGTGGTGGCGGC
3	HIF2α-SalI Forward primer	CTGCGTCGACTATGGCCTACCCCTACGACGTGCC
4	HIF2α-MfeI Reverse primer	TATCAATTGTCAGGTGGCCTGGTCCAGGGCTC
5	iMYC 1 tandem sgRNA	TGGATGATATTAGCATTACC and CAATTTGGACTTACCCAGAA
6	iMYC 2 tandem sgRNA	CCGTGGCGCTTGGGTGACAG and GCGTGACTTGAGTAGAGACC
7	iMYC 3 tandem sgRNA	ACAGGTTTAGCAGAGTGGCG and GCGTGACTTGAGTAGAGACC
8	iCCND1 1 tandem sgRNA	ACGGACACTGAGGTGCTCAG and CGGCAGTGCCAGCTCCCACA
9	iCCND1 2 tandem sgRNA	CTCCACAGTCACGGACACTG and TCCGGCTGTGACAACCTCAG
10	MYC and TGFa (MT1) tandem sgRNA	ACAGGTTTAGCAGAGTGGCG and TGACACGCTGTGGTGAACTC
11	MYC and TGFa (MT2) tandem sgRNA (iMT)	GCGTGACTTGAGTAGAGACC and CCCACAGTAATTACTAGGGC
12	double CCND1 (CC1) tandem sgRNA (iCC)	ACGGACACTGAGGTGCTCAG and ACGTGCATGTGCATGCGTGT
13	double CCND1 (CC2) tandem sgRNA	CGGCAGTGCCAGCTCCCACA and CGGTTAGCAACAAGGAACGT
14	Scramble tandem sgRNA	GAGTGTCGTCGTTGCTCCTA and GGAGATGCATCGAAGTCGAT
15	MYC enhancer gDNA- NheI Forward primer	CTACGCTAGCCCCGCTTTCGTCCTTTACCT
16	MYC enhancer gDNA-XhoI Reverse primer	CACTGAGCTCCAACCCCACAGACAGGTCTC
17	CCND1-1 enhancer gDNA- NheI Forward primer	CTACGCTAGCAGATTCAGACCCTTCCAGAGC
18	CCND1-1 enhancer gDNA-XhoI Reverse primer	CACTGAGCTCGGCAGACGTATCTGCATGTG
19	CCND1-2 enhancer gDNA- NheI Forward primer	CTACGCTAGCGGGGCAAATGCTGACTCC
20	CCND1-2 enhancer gDNA-XhoI Reverse primer	CACTGAGCTCCTCCGTATGCTGGGTCCTGT
21	TGFa enhancer gDNA- NheI Forward primer	CTACGCTAGCTACTGCCATCGGTTCATTCA
22	TGFa enhancer gDNA-XhoI Reverse primer	CACTGAGCTCGGCTAAGGAAGCCTTTCTGC

2.2.5 PCR Amplification

PRC amplification was carried out using Accuzyme™ DNA polymerase (Bioline, Bio-25028). A standard reaction consisted of a total of 25µl. The reaction mix was made up of 2xAccuzyme, 1µleach of the Forward and Reverse primers (10µM), 10ng of DNA and water up to 25µl in total volume. PCR conditions are shown in **table II**.

Table II. PCR conditions.

1	Initial denaturation	95°C	5min
2	Denaturation	95°C	15sec
3	Annealing	55-65°C*	30sec
4	Extension	72°C	1min/kbp
5	Final extension	72°C	10min

*The annealing temperature was selected based on the SnapGene software

2.2.6 Site directed mutagenesis (SDM)

Primers for SDM were generated as follows: forward and reverse primers were made up of 15bp upstream and downstream of the region to be mutated, including the mutated sequence of interest. Standard PRC amplification was performed as described above, but AccuPrime™ Pfx DNA Polymerase (Thermo, 12344040) was used instead of Accuzyme and 3% DMSO was added. 1µl of Dpnl enzyme was subsequently added and incubated for 1h at 37°C. The entire reaction mixture was transformed following a standard protocol into competent E. coli and plated overnight. Colonies were picked and grown overnight in LB Broth supplemented with Ampicillin. Plasmid DNA was extracted using the QuickClean II Plasmid

Miniprep kit (GeneSript, L00420-100). Plasmids were validated by sequencing. Primers used for SDR are listed **table III** (mutated sites are highlighted in red):

Table III. Primer sequences used for SDR.

Name	Sequence (5'-3')
SDM MYC- HIF2α F	CAGAGCAGAGCCGATAAACCTGCTCCTGGTCAT
SDM MYC- HIF2α R	ATGACCAGGAGCAGGTTTATCGGCTCTGCTCTG
SDM CCND1-1a HIF2α F1	GAGCTGGTTCTGCACAAACCTCCGCTCCACAG
SDM CCND1-1a HIF2α R1	CTGTGGAGCGGAGGTTTGTGCAGAACCAGCTC
SDM CCND1-1b HIF2α F2	ACTGGGCAGCCGTACAAATCCCAGGCAGCGGGA
SDM CCND1-1b HIF2α R2	TCCCGCTGCCTGGGATTTGTACGGCTGCCCAGT
SDM CCND1-2 HIF2α F	TGACTGTGGGCCGACAAACATAAACATGCGTGTGCATGT
SDM CCND1-2 HIF2α R	ACATGCACACGCATGTTTATGTTTGTCGGCCCACAGTCA
SDM TGFa- HIF2α F	TCTGAATTCCAGCACAAATCCACTCTGCTGTAG
SDM TGFa- HIF2α R	CTACAGCAGAGTGGATTTGTGCTGGAATTCAGA

2.2.7 Bacterial transformation

Plasmids were transformed into chemically competent E. coli (made in-house). Plasmids were added to the bacteria and mixed gently by flicking. The mix was incubated on ice for 30 mins, heat shocked at 42°C for 1 min and incubated on ice for 2 mins. SOC recovery media (made in-house) was added into the mixture and incubated on shaking incubator at 37°C for 1h. Transformed bacteria was then plated on LB-Ampicillin plates and incubated overnight at 37°C.

2.2.8 Sanger sequencing

All purified samples were verified by sequencing using the MIX2Seq Kit (Eurofins Genomics). Each sample consisted of 50-100ng/µL of purified DNA, 2µl of primer (10µM) and was made up to 15µL with water. Sequencing analysis was undertaken using SnapGene software.

2.3 Nucleofection

CRISPR/Cas9 engineering of HIF2α KO cell lines was performed by electroporating each cell line with the constructs of interest as follows using the Amaxa Cell Line Optimisation Nucleofector Kit by Lonza). Cells were counted using the ViCell XR viability analyser (Beckman Coulter) to determine the volume of medium required for 2 million cells per reaction. Cells were spun down and resuspended in 100µL of Nucleofector solution and respective plasmids were added for co-nucleofection: pcDNA3.1 (transient expression of RFP for selection) and pX330-U6-Chimeric_BB-CBh-hSpCas9 (Addgene plasmid #42230). pX330 contains two expression cassettes, one for Cas9 and one for the sgRNA targeting regions of the gene to be mutated. The sgRNA is made of two annealed oligos and can be inserted into pX330 by vector digestion and sgRNA ligation. The following sgRNAs targeting HIF2α were used:

sgEPAS1_1

5’ – **CACCG**GAGTAGCTCGGAGAGGAGGA – 3’

3’ – **C**CTCATCGAGCCTCTCCTCCT**CAAA** – 5’

sgEPAS1_5

5’ – **CACCG**TGAGATTGAGAAGAATGACG – 3’

3’ – **C**ACTCTAACTCTTCTTACTGC**CAAA** – 5’

The cell/DNA mix was transferred to a dedicated cuvette and nucleofected applying program T-020. Immediately following this, 500µl of pre-warmed culture medium was added into the cuvette and incubated for 5 min at 37°C. Cells were then plated in 6-well plates containing 1.5mL of fresh pre-warmed medium. Fresh medium was added the day after nucleofection. On the second day after nucleofection cells were analysed and RFP positive single cells were sorted into 96-well plates using FACS. Cells were expanded from single cells up to 15cm plates prior to being frozen for storage and/or used for subsequent experiments.

2.4 Evaluation of generated cells

Cells were trypsinised and spun down at 1200 rpm for 5 min. Cell pellets were collected and stored in -80°C for use in the following analysis.

2.4.1 qPCR

RNA was extracted with RNAzol RT (Sigma-Aldrich R4533) according to the manufacturers protocol for total RNA isolation. RNA concentration was measured using a Nanodrop (ND 1000- Spectrophotometer) and 500ng of RNA was used to prepare cDNA by reverse transcription-PCR using the High-Capacity cDNA Reverse Transcription Kit (Thermo #4368814). The cDNA generated was used for qPCR analysis (as listed in **table IV**).

Table IV. Protocol for qPCR.

Taqman probe (10x)	0.5uL
FAST Master mix (2x)	5uL
Nuclease-free H_2O	4uL
cDNA	0.5uL
Total	10uL

qPCR plates were analysed using the StepOne Plus Real-Time PCR machine (ThermoFisher Scientific). The gene of interest Ct value were normalised to the Ct value of the housekeeping gene, *TBP*. The gene expression fold change was calculated using the $2^{-\Delta\Delta Ct}$ method as described previously[117]. Probes used included: EPAS1 (Hs01026149_m1), CXCR4 (Hs00607978_s1), LTBP1 (Hs00386448_m1), MYC (Hs00153408_m1), CCND1 (Hs00765553_m1), TGFa (Hs00608187_m1) and house-keeping gene TBP (Hs00427620_m1)-Taqman (ThermoFisher Scientific).

2.4.2 Western blot

Cell pellets were washed in PBS and resuspended in 100µL RIPA buffer (Sigma-Aldrich R0278) supplemented with 1µL of Protease Inhibitor Cocktail (Sigma-Aldrich) and lysed on ice for 30 min. Lysates were centrifuged (1,000 rpm at 4°C for 15 min) and supernatants were collected. The Pierce™ BCA Assay Kit (ThermoFisher Scientific, 23225) was used to determine protein concentration. 50µg of extracted protein was mixed with 5µL of 4x TruePAGE LDS loading buffer (Sigma-Aldrich PCG3009), 1µL β-mercaptoethanol (Sigma, M6250) and made up to 20µL with H_2O. Samples were boiled at 95°C for 5 min, loaded onto the gel and run at 60V for 15min and then at 100V for around 2h. The Precision Plus Protein Kaleidoscope Pre-Stained Protein Standards (BioRad #1610375) was used as the molecular weight marker. Proteins were transferred into a PVDF membrane (Millipore) at 150V for 2h. The membrane was blocked for 1h in blocking buffer (5% milk in 0.1% PBS-Tween), washed three times for 5 min in PBS-Tween and blotted with primary antibody overnight. The membrane was washed three times for 5 min in PBS-Tween and a secondary antibody was added for 1h at room temperature (RT), followed by three 5min PBS-Tween washes. β-actin blotting was used as a loading control. Membranes were incubated with Luminata™ Classico Western HRP Substrate

(Millipore WBLUC0500) for 5min and films were then exposed for 30 min for HIF2α/VHL proteins and for a few seconds for β-actin prior to being developed.

Antibodies used (**Table V**):

Table V. Antibodies, their dilution and condition used for western blots.

Rabbit anti-HIF2α primary antibody	Novus NB100-122	1:1000	overnight at 4°C
Mouse anti-VHL primary antibody	BD Pharmingen 564183	1:500	overnight at 4°C
Mouse anti-Actin primary antibody	Abcam ab8227	1:20000	1h at RT
HRP-conjugated anti-mouse secondary antibody	Dako P0447	1:10000	1h at RT
HRP-conjugated anti-rabbit secondary antibody	Dako P0448	1:5000	1h at RT

2.4.3 Genomic analysis - TOPO cloning

Genomic DNA was extracted using the QIAamp DNA Mini Kit (Qiagen). The region of interest was PCR amplified, run on a 1% agarose gel and gel extracted. "A" overhangs were added by a Biotaq^{TM} DNA Polymerase (Bioline, BIO-21040) reaction according to the following protocol (**Table VI**).

Table VI. Biotaq DNA polymerase reaction conditions.

Biotaq buffer (10x)	5µL
dNTPs (100mM)	0.5µL
Biotaq enzyme	0.5µL
PCR product	44µL

The reaction was incubated at 72°C for 30 min. For TOPO cloning, the TOPO TA Cloning Kit for Sequencing (Thermo, 450071) was used according to the following protocol (**Table VII**).

Table VII. TOPO TA cloning reaction conditions.

Biotaq reaction product	4µL
dH_2O	1µL
Salt solution	0.5µL
TOPO vector	0.5µL

The TOPO reaction (6µL) was used for transformation of 100µL of competent bacteria (made in-house) following the standard protocol for bacterial transformation. DNA from 10 colonies was extracted using the QIAGEN miniprep kit and sequenced by Sanger sequencing.

2.4.4 Flow cytometry

Cells were analysed by flow cytometry on an LSR Fortessa (BD Biosciences). dsRed fluorescence was measured with 561nm excitation and was detected at 582nm. GFP was measured with 488nm excitation and was detected at 530nm. BFP fluorescence was measured with 383nm excitation and was detected at 445nm. mCherry was measured with 561nm excitation and was detected at 610nm. Cell sorting was provided by Cambridge Institute for Medical Research (CIMR) core facility services.

2.5 Lentiviral cellular transduction

2.5.1 Lentiviral production

10µL of Fugene 6 (Promega, E269A) and 160µL of Opti-MEM medium (Gibco, LS31985062) were mixed. In a separate tube, envelope and packaging vectors (0.5µg of pMD2G (Addgene #12259), 1.3µg of psPAX2 (Addgene #12260)), and 1.5µg of plasmid of interest were diluted in 160µL of Opti-MEM medium and incubated at RT for 5 min. The Fugene 6-Opti-MEM mix

was added into the plasmid mix in a dropwise manner, mixed gently by flicking and incubated for 30 min at RT. The mix was used to transfect one well of the 6-well plate with HEK293T cells, seeded at $6x10^5$ 24h before transfection. 48h post transfection, viral supernatants were collected, filtered, aliquoted and stored at -80°C.

2.5.2 Lentiviral transduction of mammalian cells

Cells were plated in 6-well plates ($3x10^5$ per well) 24h before transduction. For transduction, fresh medium supplemented with 8µg/mL of polybrene transfection reagent (Merck Millipore, TR-1003) and 100-500µL of the lentiviral titre was added per well. Viral titration was undertaken to determine the virus efficiency. The medium was changed, and fresh medium was added 24h after transduction. Selection antibiotics were added 48h after transduction: 4µg/mL of puromycin (Invivogen, ant-pr), 900µg/mL of hygromycin (Invivogen, ant-hg) were added for selection of resistant cells containing the plasmid of interest. Positive cells were then expanded and used for further experimentation.

2.6 Luciferase reporter assay

One million cells were counted by the ViCell XR viability analyser (Beckman Coulter) and co-nucleofected with 3.6ug pNL1.1[Nluc] (Promega, N1001) Empty or pNL1.1[Nluc] carrying the enhancer sequence of interest and 0.4µg pRL-TK Renilla plasmid (Promega, E2241) in 100µl of nucleofection solution, using program T-020 (as described above). Once nucleofected, 550µl of pre-warmed medium was added into the nucelofection cuvette and incubated for 10 min at 37°C. The nucleofection mix was seeded into 6 wells of a white clear-bottom 96-well plate. 100µl of fresh medium was added to each well. Luciferase activity was measured 48h

post nucleofection using a plate reader (Tecan infinite M200 pro). Three wells were used to measure Renilla luciferase and the remaining three wells were used for the NanoLuc luciferase assay.

Renilla luciferase assay (Promega, E2810) was performed as follows: cells were washed with 1xPBS and lysed in 20µl/well of lysis buffer (5x lysis buffer diluted in water) for 15 mins at RT on a shaker. 100µl of Renilla reagent (100x diluted in water) was added to each well and mixed. The reading was taken immediately.

Nano-Glo Luciferase assay (Promega, N1110) was performed as follows: media was removed and 50µl of fresh media was added into each well, 50µl of NanoLuc reagent (diluted 1:50 in buffer provided) was added into each well and mixed. The plate was incubated for 3 minutes before readings were taken.

Analysis was performed by normalising the NanoLuc activity to the average Renilla activity and the resulting value was normalized to that of the empty vector.

2.7 In vivo studies

All animal studies were approved by Home Office UK. Athymic nude and NSG mice were injected subcutaneously into the left and right flanks, $1x10^5$-$5x10^5$ cells per flank in 100µL PBS/Matrigel (Corning, cat. no. 356231) 1:1 mixture. For the metastasis assay, athymic nude mice were injected intra-cardially with $1x10^5$ cells/100µL. When applicable, cells were pre-treated with 0.3µg/mL of DOX for 3 days prior injecting. Doxycycline was administered through food (200PPM). Tumours were monitored by weekly bioluminescence imaging using the IVIS Spectrum Xenogen machine (Caliper Life Sciences). Before imaging, mice were injected with 100µl D-luciferin (D-Luciferin - K+ Salt; Perkin Elmer LAS (UK), Cat. No: 122796)

via intra-peritoneal/ subcutaneous injection, put under anaesthesia using isofluorane, and imaged in the IVIS 10mins after injection. Data was analysed using the Living Image software (Caliper Life Sciences). Tumour volume was also measured by calipers once tumours were palpable. Tumour volume was calculated using the equation $V = (L \times W2) \times 0.5$, where L is the length and W is the width of the tumour.

2.8 RNA-seq

Tumour RNA was extracted using RNeasy Mini Kit (Qiagen, 74104) as per the manufacturer's protocol. RNA quality was measured using the RNA Nano 6000 kit (Agilent, 5067-1511) run on Agilent Bioanalyser 2100. Library preparation and quantification was performed by Paulo Rodrigues and Saiful Effendi Bin Syafruddin . The RNA-Seq libraries were prepared using the SENSE mRNA-Seq Library Prep Kit V2 (Lexogen) by following the manufacturer's recommendations. 1µg of total RNA was used as the starting material. The size and quality of the final library products were determined using the Agilent High Sensitivity DNA Kit (Agilent #5067-4626) on the Agilent Bioanalyzer 2100 instrument. The library concentration was determined using the KAPA Library Quantification Kit (KR0405) according to manufacturer's recommendations.

The RNA-Seq data was analysed by other members of the lab. Gene set enrichment analysis and pathway analysis were performed by Dora Bihary and Shamith Samarajiwa using the analysed RNA-Seq data.

2.9 ChIP-seq

H3K27ac and HIF2α ChIP-seq were performed by Paulo Rodrigues of the lab as previously described[118]. Cells were cross-linked for 10 minutes at room temperature in 1% formaldehyde in growth media, followed by 5 minutes of quenching with 0.125M glycine. Cells were washed twice with PBS, the supernatant was aspirated, and the cell pellets were frozen in liquid nitrogen and stored at −80°C. For tumour ChIP-seq, samples were homogenized in PBS using a Precellys instrument (Bertin) before cross-linking. Protein A/G magnetic beads (100 µL; Thermo Scientific, 26162) were blocked with 0.5% BSA in PBS, then incubated with antibody at 4°C for at least 4 hours. The antibodies used were H3K27ac (Abcam, ab4729) and HIF2α (Abcam, ab199). Cross-linked cells were resuspended and sonicated in lysis buffer (20 mmol/L Tris–HCl pH 8.0, 150 mmol/L NaCl, 2 mmol/L EDTA pH 8.0, 0.1% SDS, and 1% Triton X-100). Sonication was performed in a Bioruptor (Diagenode) for 14 cycles (30 sec on/30 sec off) at max output to obtain fragments of 100 to 500 bp. Sonicated lysates were cleared and incubated overnight at 4°C with antibody-bound magnetic beads. Beads were sequentially washed three times with low-salt buffer (50 mmol/L HEPES pH7.5, 140 mmol/L NaCl, 1% Triton) and once with high-salt buffer (50 mmol/L HEPES pH7.5, 500 mmol/L NaCl, 1% Triton). DNA was eluted in elution buffer (50 mmol/L NaHCO3, 1% SDS) and cross-links were reversed for 3 hours (65°C, 1,000 rpm shaking). DNA was purified using the QuickClean II PCR Extraction Kit (Genescript L00419- 100) according to the manufacturer's recommendations and eluted with 100ul H_2O. Purified ChIP DNA was used to prepare Illumina multiplexed sequencing libraries with the KAPA Hyper Prep Kit (KR0961) Illumina platforms sample preparation protocol (v1.14). After adapter ligation, libraries were size-selected to 150 to 350 bp using Agencourt AMPure XP beads (Beckman Coulter, A63880) as per protocol. Size-selected

libraries were amplified for 15 cycles using the KAPA HiFi HotStart ReadyMix. PCR libraries were then pooled in equimolar concentrations and sequenced.

ChIP-seq data was analysed by other members of the lab. Raw ChIP seq data was aligned to hg38 using bowtie[119], generating sam files which were converted into bam files using samtools[120]. Peaks were then called using MACSC2 with the option –q 5e-2[121]. The corresponding input samples from the ChIP experiment for each cell line were used as controls.

2.10 Immunohistochemistry

Tumours were collected and fixed overnight at 4% paraformaldehyde, washed with PBS and stored in 70% ethanol before being embedded in paraffin and sectioned. H&E staining was performed using a standard technique. Bond-Max instrument (Leica) IHC protocol F was used to stain for Human Vimentin (Cell signalling, 5741, 1:100), HIF2α (Santa Cruz, 46691, 1:200), Ki67 (Bethyl, 00375, 1:100) and CCND1 (ab134175, 1:100).

Staining for MYC (Ab32072, 1:500) and Cleaved Caspase 3 (NEB 9664, 1:1000) was performed manually as follows. Tissue slides were de-waxed and re-hydrated by performing three 5min xylene waxes followed by three 5min 70% EtOH washes and then placed in water. Antigen retrieval in citrate buffer (pH 6, 1:100 dilution in water, Vector laboratories #H-3300) was performed in the microwave (10min). Slides were then blocked with 5% NGS in PBST with 2%BSA for 1h at room temperature. Primary antibody was incubated overnight at 4°C in a humid chamber. Slides were then blocked with 2.5% Normal Horse Serum (ImmPress™ Vector, MP-7401) followed by incubation with the ImmPress™ (Peroxidase) Polymer Anti-

Rabbit IgG Reagent. DAB mix (SK-4100) was then added to each sample and left on slides until staining was observed. Slides were then dehydrated by placing them in an increasing ethanol gradient and then placed in xylene. Coverslips were then mounted using DPX glue. Stained slides were then scanned with a Zeiss AxioScan machine. The Halo software was used for quantification, using the Cytonuclear module, and images were collected at 10X magnification.

Results

Chapter 3. Generating and characterising the DOX-inducible HIF2α system

Introduction

Previous observations suggest that HIF2α has oncogenic effects in ccRCC and is required for tumour initiation and progression[46–48]. A genetic model allowing for control of HIF2α expression has not been reported. I developed genetic models that allow for temporal control of HIF2α expression in VHL mutant ccRCC cell lines. Using CRISPR-Cas9 genome engineering, I developed HIF2α KO clones where I have then re-introduced HIF2α under the control of DOX-inducible element allowing for precise control of HIF2α expression *in vitro* and *in vivo* (**Figure 3.1**).

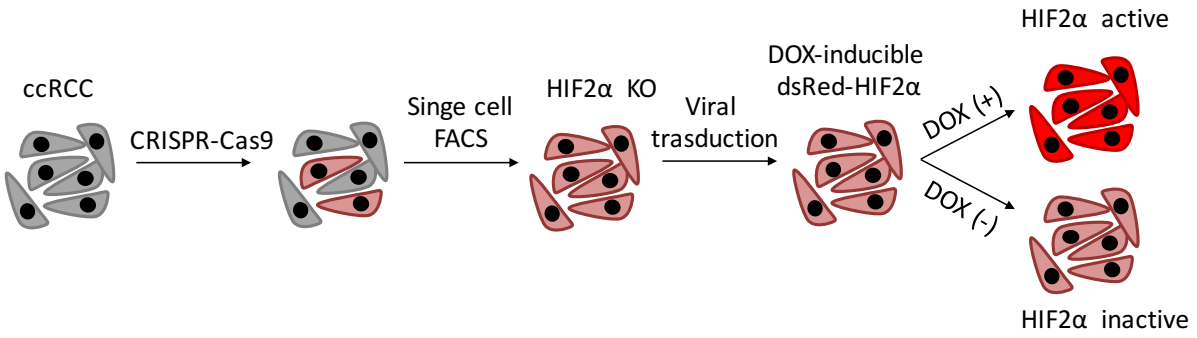

Figure 3.1 Schematic diagram showing the approach to study the role of HIF2α in ccRCC. HIF2α KO clones were generated by CRISPR/Cas9 and sorted using FACS. Sorted clones with HIF2α KO were then virally transduced to express a DOX-inducible dsRed-HIF2α.

3.1 Generating HIF2α KO clones

Five human ccRCC cell lines were chosen for this experiment; three highly metastatic cell lines, namely RFX631, 786-M2D and OSLM1B, and two primary ccRCC cell lines with high expression of HIF2α, 769-P and RCCMF. Each of these cell lines has a known unique homologous VHL mutation which was confirmed by Sanger sequencing (performed by another member of the lab). CRISPR-Cas9 targeted genome editing was used to generate HIF2α KO clones. CRISPR-Cas9 is a novel tool based on a bacterial adaptive immune system, which enables bacteria to

recognise and eliminate invading genomic material. The system relies on RNA-guided Cas9 endonuclease to cleave complementary DNA sequences. Cas9 activity also requires a short conserved sequence, known as protospacer-associated motif (PAM). The double-stranded DNA cleavage is in most cases repaired by a non-homologous end joining, resulting in insertions and/or deletions which disrupt the targeted sequence. Alternatively, if a donor template with homology to the targeted locus is supplied, homology directed repair takes place, allowing for precise mutations so be made[122].

HIF2α is not necessary for cell survival *in vitro*, based on studies showing that shRNA-mediated HIF2α knockdown does not affect cell survival and proliferation in culture[47,48]. Moreover, using molecular antagonists of HIF2α also did not show any effect on the proliferation of ccRCC cell lines in culture[75]. Altogether, this observation suggests that generation of HIF2α KO clones is possible. HIF2α KO clones were generated using the CRISPR-Cas9 system, *via* electroporation as described in the Chapter 2. Two sgRNAs targeting *EPAS1* exons 2 and 9 were used (**Figure 3.2**). A total of 143 clones were generated: 75 single cell clones were isolated from 786-M2D, 16 from OSLM1B, 26 from RFX-631, 17 from 769-P and 9 from the RCCMF cell line after transfection.

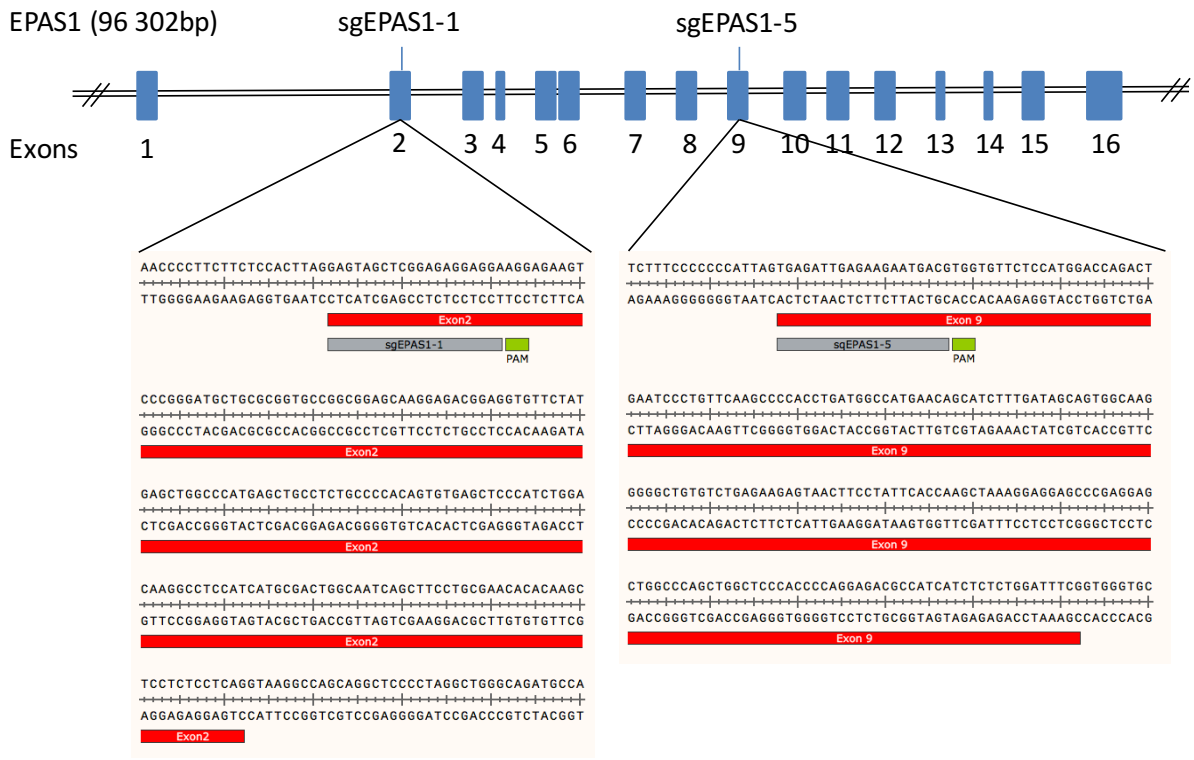

Figure 3.2 Position of sgRNAs in the EPAS1 gene body. Single guide RNAs- sgEPAS 1-1 and sgEPAS 1-5 cloned into pX330 allow for Cas9 cleavage of *EPAS1 (HIF2α*).

To evaluate whether the clones obtained were HIF2α KO, HIF2α expression and activity was measured by Western blot and qPCR. Only a small number of clones was confirmed to be HIF2α KO, specifically, three 786-M2D clones, two OSLM1B clones, eight RFX-631 clones, five 769-P clones and two RCCMF clones. To further study the lack of HIF2α functional activity in the HIF2α KO clones, qPCR analysis was performed to look at expression of the HIF2α downstream target gene *CXCR4*. High expression of CXCR4 (chemokine (C-X-C motif) receptor 4) has been linked to poor patient prognosis in ccRCC; CXCR4 was also shown to have a critical role in metastatic colonization in renal cancer[14,123]. The expression of CXCR4 was significantly lower in 786-M2D and OSLM1B HIF2α KO clones, but in the case of the RCCMF,769-P and RFX-631 clones, *CXCR4* expression was variable independent of HIF2α expression (**Figure 3.3**).

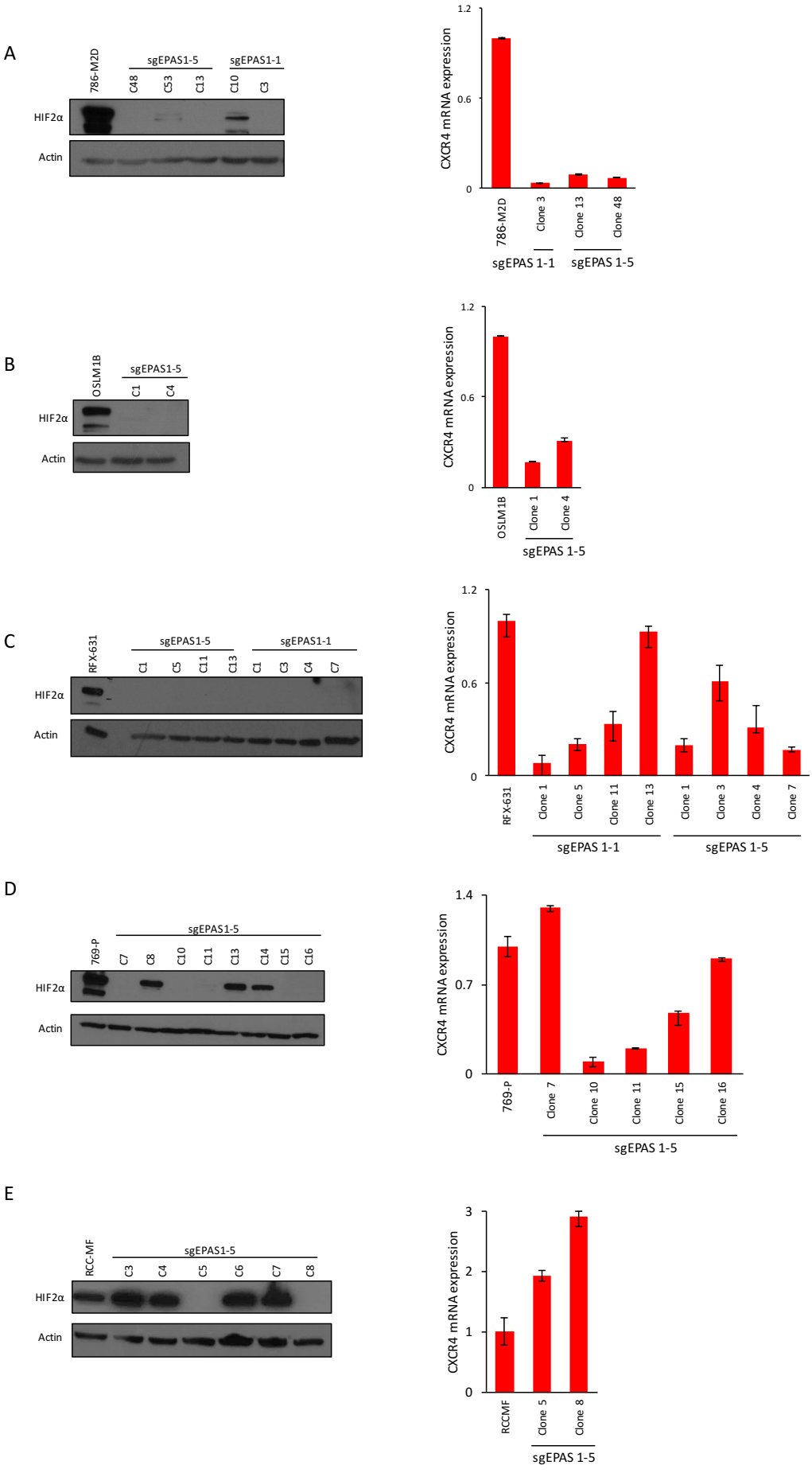
A
786-M2D
sgEPAS1-5
sgEPAS1-1
C48
C53
C13
C10
C3
HIF2α
Actin
CXCR4 mRNA expression
1.2
0.6
0
786-M2D
Clone 3
Clone 13
Clone 48
sgEPAS 1-1
sgEPAS 1-5
B
OSLM1B
sgEPAS1-5
C1
C4
HIF2α
Actin
CXCR4 mRNA expression
1.2
0.6
0
OSLM1B
Clone 1
Clone 4
sgEPAS 1-5
C
RFX-631
sgEPAS1-5
sgEPAS1-1
C1
C5
C11
C13
C1
C3
C4
C7
HIF2α
Actin
CXCR4 mRNA expression
1.2
0.6
0
RFX-631
Clone 1
Clone 5
Clone 11
Clone 13
Clone 1
Clone 3
Clone 4
Clone 7
sgEPAS 1-1
sgEPAS 1-5
D
769-P
sgEPAS1-5
C7
C8
C10
C11
C13
C14
C15
C16
HIF2α
Actin
CXCR4 mRNA expression
1.4
0.7
0
769-P
Clone 7
Clone 10
Clone 11
Clone 15
Clone 16
sgEPAS 1-5
E
RCC-MF
sgEPAS1-5
C3
C4
C5
C6
C7
C8
HIF2α
Actin
CXCR4 mRNA expression
3
2
1
0
RCCMF
Clone 5
Clone 8
sgEPAS 1-5

Figure 3.3 Western blots and qPCR analysis of HIF2α obtained by CRISPR-Cas9 engineering of ccRCC cell lines. (A-E) Western blots (left) of HIF2α KO clones. Parental cell lines were used as positive controls to compare the expression level of HIF2α. β- actin was used as a loading control. qPCRs (right) show the expression of the HIF2α target gene *CXCR4* normalised to the expression of the house-keeping gene *TBP*. Data are presented relative to parental cell line control. Error bars show 95% confidence intervals based on three technical triplicates.

Two clones from each cell line were further analysed by PCR amplification of the genetically engineered region, followed by TOPO cloning and Sanger sequencing to identify the mutations introduced by CRISPR-Cas9 editing. No WT copies of HIF2α have been detected in the clones analysed. Furthermore, most of the mutations detected were frameshift mutations caused by indels within the *HIF2α* gene sequence (**Figure 3.4**).

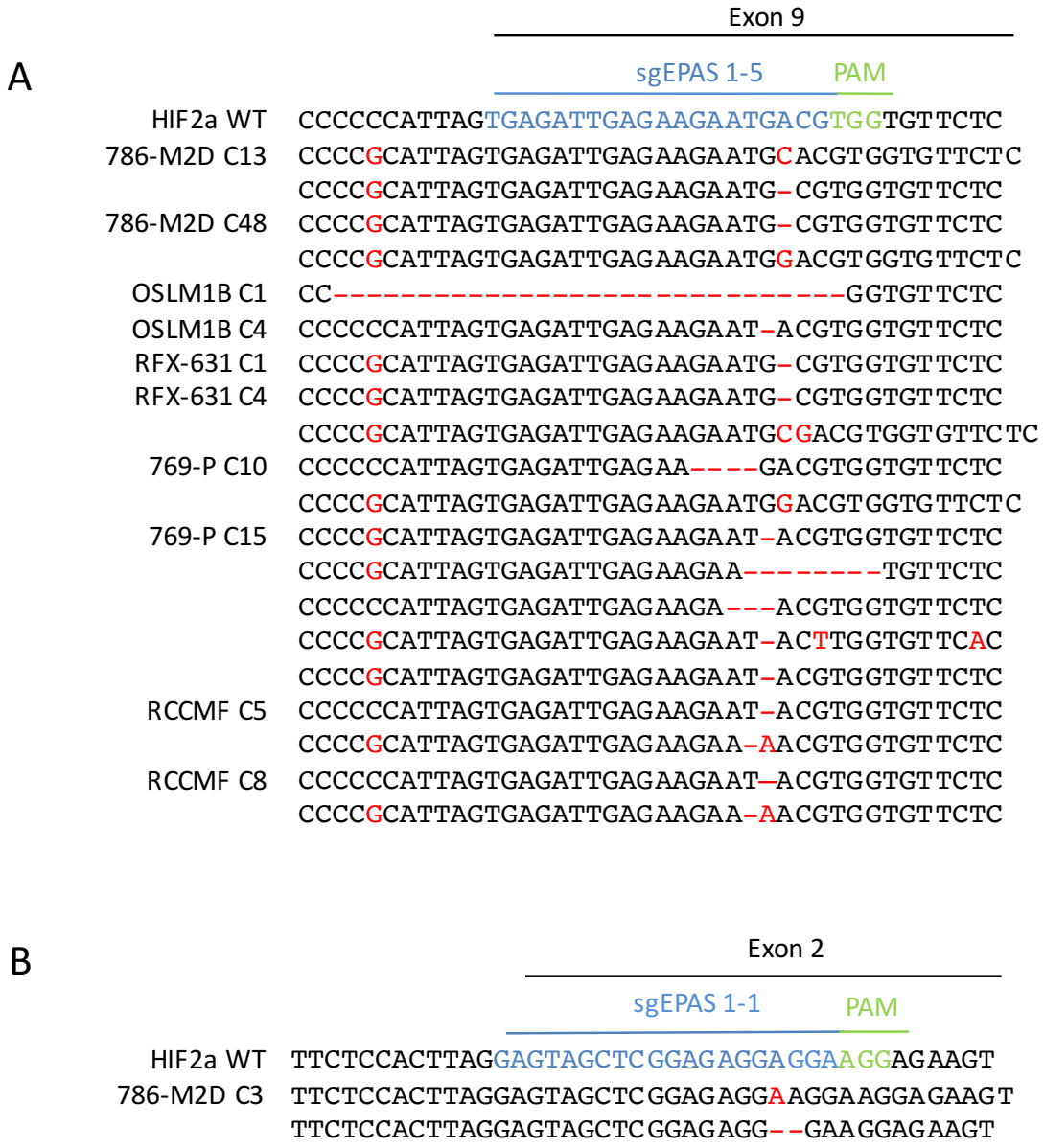

Figure 3.4 Mutation profiling of cell lines generated by CRISPR-Cas9 genome editing. Mutations, shown in red, were detected by Sanger sequencing of TOPO cloned PCR fragments. Protospacer adjacent motif (PAM) sequence is shown in green and single guide RNAs, sgEPAS 1-5 (A) and sgEPAS 1-1 (B), are shown in blue.

3.2 Constructing a DOX inducible HIF2α vector

Cloning a DOX inducible HIF2α plasmid involves a number of requirements essential to facilitate selection and characterisation of cells that will integrate the construct into their genome. In this regard, it is desirable to have a fluorescent marker and antibiotic resistance gene. We selected dsRed (as GFP-luciferase reporter is already integrated in the cells' genomes for the purposes of *in vivo* assays and imaging) and puromycin as a fluorescent marker and antibiotic resistance gene, respectively.

To make a controllable HIF2α expression construct a third-generation version of DOX-inducible plasmids (TET ON 3G) was selected as a suitable plasmid backbone type. TET ON 3G, compared to previous DOX-inducible systems, has a lower background expression and increased sensitivity to DOX[124]. It contains a mutated version of the tetracycline repressor (TetR) expressed under the PGK promoter, rTetR, which relies on tetracycline/doxycycline for gene induction, instead of gene repression. Once induced, it binds to a Tet responsive element (TRE) and drives the expression of its downstream genes (**Figure 3.5**)[124].

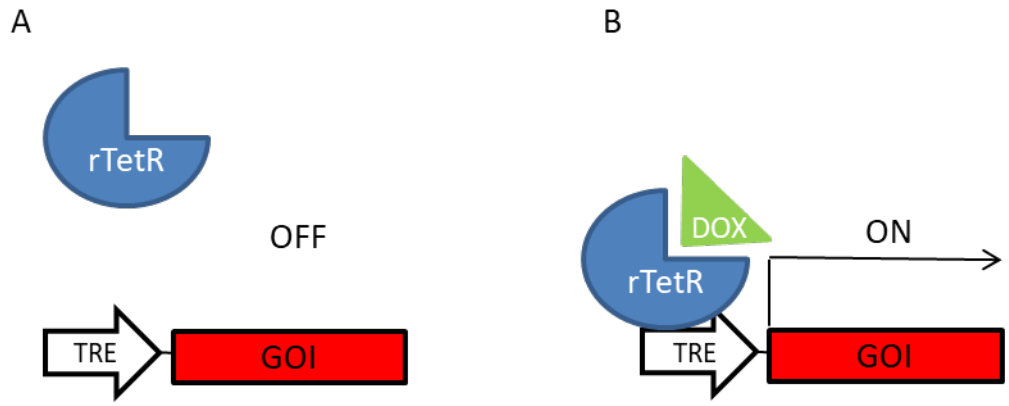

Figure 3.5 TET ON 3G DOX-inducible system. Tetracyclin responsive element (rTetR) stays inactive in absence of doxycycline (DOX) (A). In presence of doxycycline, DOX binds tetR and together they bind to tet responsive element within the tetracyclin responsive promoter which then drives the expression of its downstream genes of interest (B).

The cloning strategy to generate the DOX-inducible HIF2α gene is illustrated in Figure 3.6. LT3GEPIR, a TET ON 3G plasmid, generated and validated by Fellmann and colleagues[116], was chosen as a plasmid backbone to construct a DOX-inducible HIF2α plasmid. This plasmid carries a phosphoglycerate kinase (PGK) promoter which drives the expression of puromycin (Puro) resistance gene linked to rTetR via an internal ribosome entry site (IRES) allowing translation of the two separate proteins. Following viral transduction of ccRCC clones, cells containing the DOX-inducible HIF2α construct are selected by puromycin treatment. GFP under the TRE3G promoter within LT3GEPIR plasmid was removed by restriction enzyme digestion and substituted with dsRed-T2A, where T2A was added to dsRed via PCR amplification. T2A is a self-cleaving peptide used for producing multiple polypeptides from a single transcript by "ribosome skipping", which leads to cleavage between the T2A peptide and its downstream peptide[125]. HIF2α cDNA was ligated downstream of dsRed-T2A, allowing it to be equally expressed under the TRE3G promoter. Once the plasmid was generated, it was sequence verified by Sanger sequencing, which confirmed that the correct sequences were cloned in.

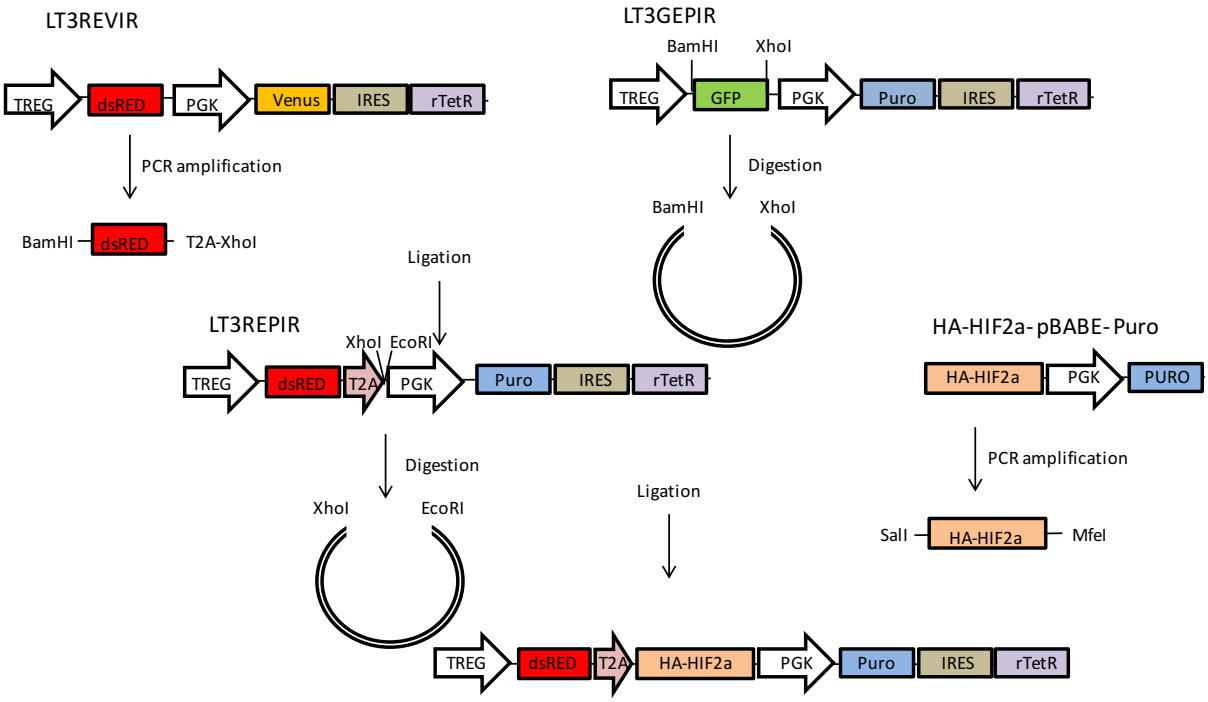

Figure 3.6 Cloning strategy to generate the DOX-inducible HIF2α gene. LT3GEPIR was chosen as a plasmid backbone, it was digested by BamHI and XhoI to remove GFP. dsRED was PCR amplified from LT3REVIR, BamHI and T2A-XhoI sites were added as primer tails to be added to dsRED by PCR amplification. dsRed-T2A was ligated to the digested LT3GEPIR. This newly generated plasmid was digested by XhoI and EcoRI. HA-HIF2α was PCR amplified from HA-HIF2α-pBABE-Puro plasmid and restriction sites for SalI and MfeI were added as primer tails. SalI and XhoI, EcoRI and MfeI create compatible sticky ends. HA-HIF2α was ligated into digested LT3REPIR to generate the DOX-inducible dsRed-T2A-HIF2α plasmid.

3.3 Characterising DOX inducible HIF2α system *in vitro*

DOX- inducible HIF2α reintroduction

HIF2α KO clones were virally transduced with a lentivirus carrying the DOX-inducible *dsRed-T2A-HIF2α* construct. After puromycin treatment, which selected for cells that were successfully transduced with the plasmid construct, cells were expanded and treated with 0.3ug/ml DOX to evaluate and characterise the DOX-inducible HIF2α system. Approximately 50-70% of cells were dsRed positive after 3 days of DOX treatment. The expression of dsRed dropped completely within ten days after DOX withdrawal. As a control, DOX-inducible dsRed-*T2A- empty vector* (EV) construct was used to transduce the same HIF2α KO clones. The same trend was observed in both, dsRed- HIF2α and dsRed-EV where dsRed population increased followed by DOX treatment and decrease when DOX was withdrawn (**Figure 3.7**).

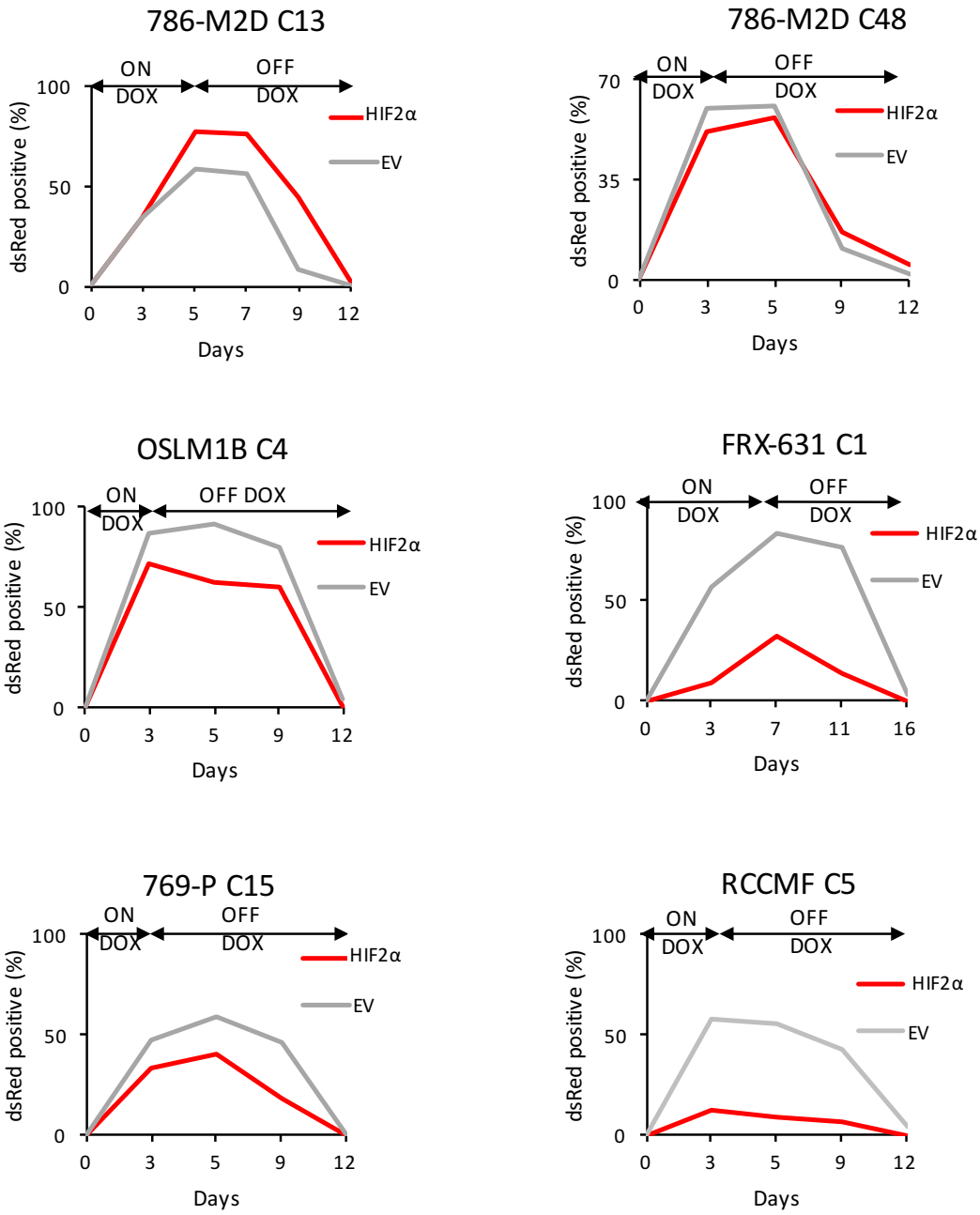

Figure 3.7 Analysis of dsRed expression by FACS. The induction of dsRed expression in cells transduced with either HIF2α or empty vector (EV) control is shown. The percentage of dsRed positive cells increased following DOX administration and decreased after DOX withdrawal.

To confirm the activation of HIF2α followed by the DOX treatment, I performed qPCR and western blot analysis that confirmed the presence of HIF2α at the mRNA and protein level, respectively. As expected, no HIF2α was observed in cells in the absence of DOX and in the cells transfected with empty vector control. Functional activity of DOX-inducible HIF2α was further assessed by looking at expression of HIF2α and its regulated gene *CXCR4*. The expression is only upregulated after DOX treatment compared to untreated cells and empty vector controls (**Figure 3.8**).

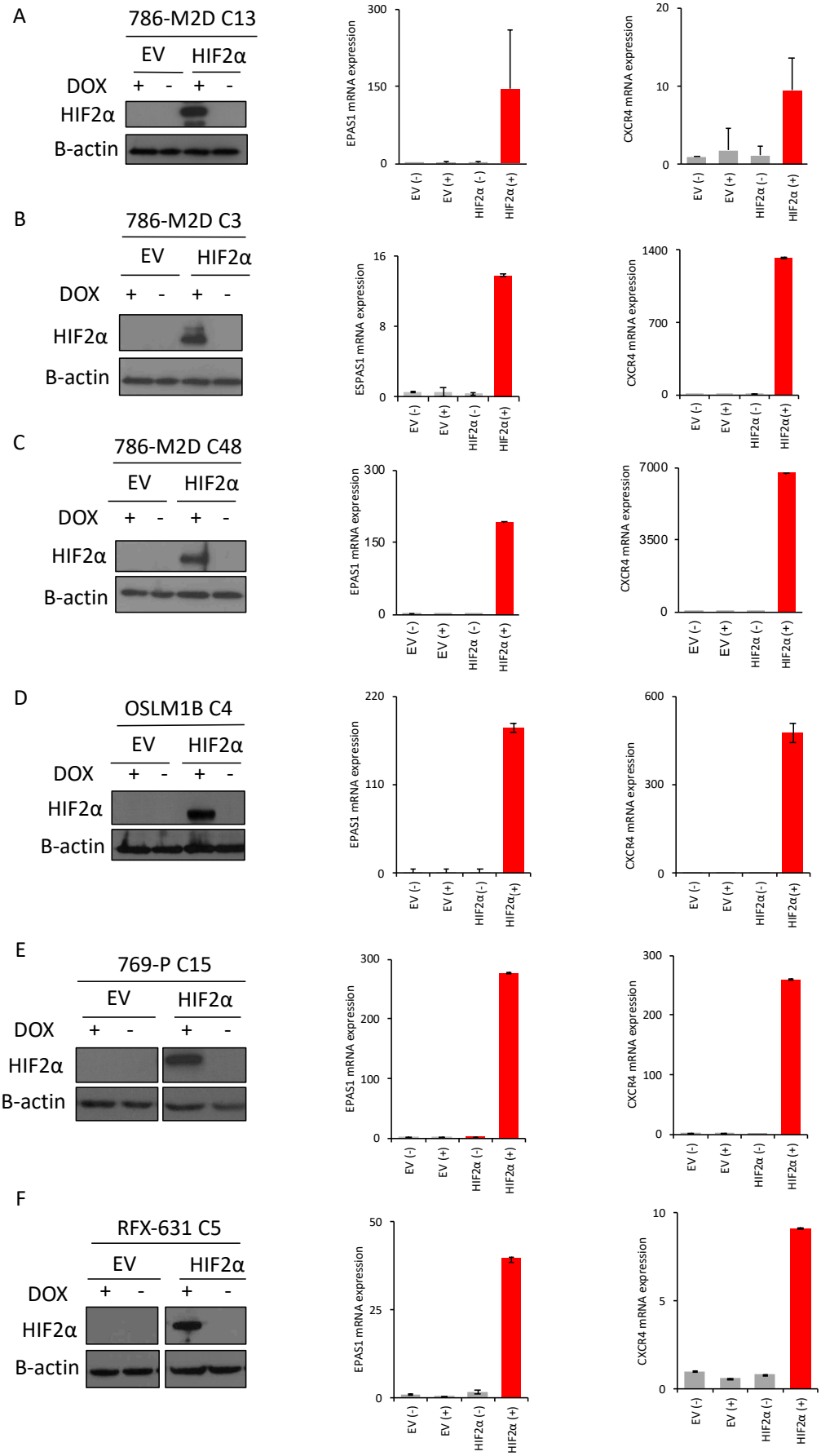
A
786-M2D C13
EV
HIF2α
DOX
+ - + -
HIF2α
B-actin
EPAS1 mRNA expression
300
150
0
CXCR4 mRNA expression
20
10
0
EV (-)
EV (+)
HIF2α (-)
HIF2α (+)
B
786-M2D C3
ESPAS1 mRNA expression
16
8
1400
700
C
786-M2D C48
7000
3500
D
OSLM1B C4
220
110
600
E
769-P C15
200
100
F
RFX-631 C5
50
25
10
5

Figure 3.8 Western blot and qPCR analysis of HIF2α KO clones transduced with either HIF2α or empty vector (EV) constructs. Cells were cultured in presence and absence of DOX. Western blots (left) show the expression of HIF2α. β-actin was used as a loading control. qPCRs (right) shows the expression of *EPAS1* (HIF2α) and its target gene *CXCR4* in HIF2α KO clones transduced with either HIF2α or empty vector (EV) constructs, grown in the presence or absence of DOX. Data was normalised to the expression of the housekeeping gene *TBP* and presented relative to EV cells cultured in absence of DOX. Error bars show 95% confidence interval based on biological triplicates (A) and technical triplicates (B-F).

Furthermore, proliferation assays were performed to assess the importance of HIF2α *in vitro*. No difference in growth has been observed between cells expressing inducible HIF2α and controls under standard tissue culture conditions, suggesting that HIF2α activity *in vitro* does not confer any growth advantage to the cells (**Figure 3.9**). This is in agreement with previous studies where HIF2α inhibition by shRNA and by HIF2α antagonist did not show any effect on cell proliferation *in vitro*[47,48,75].

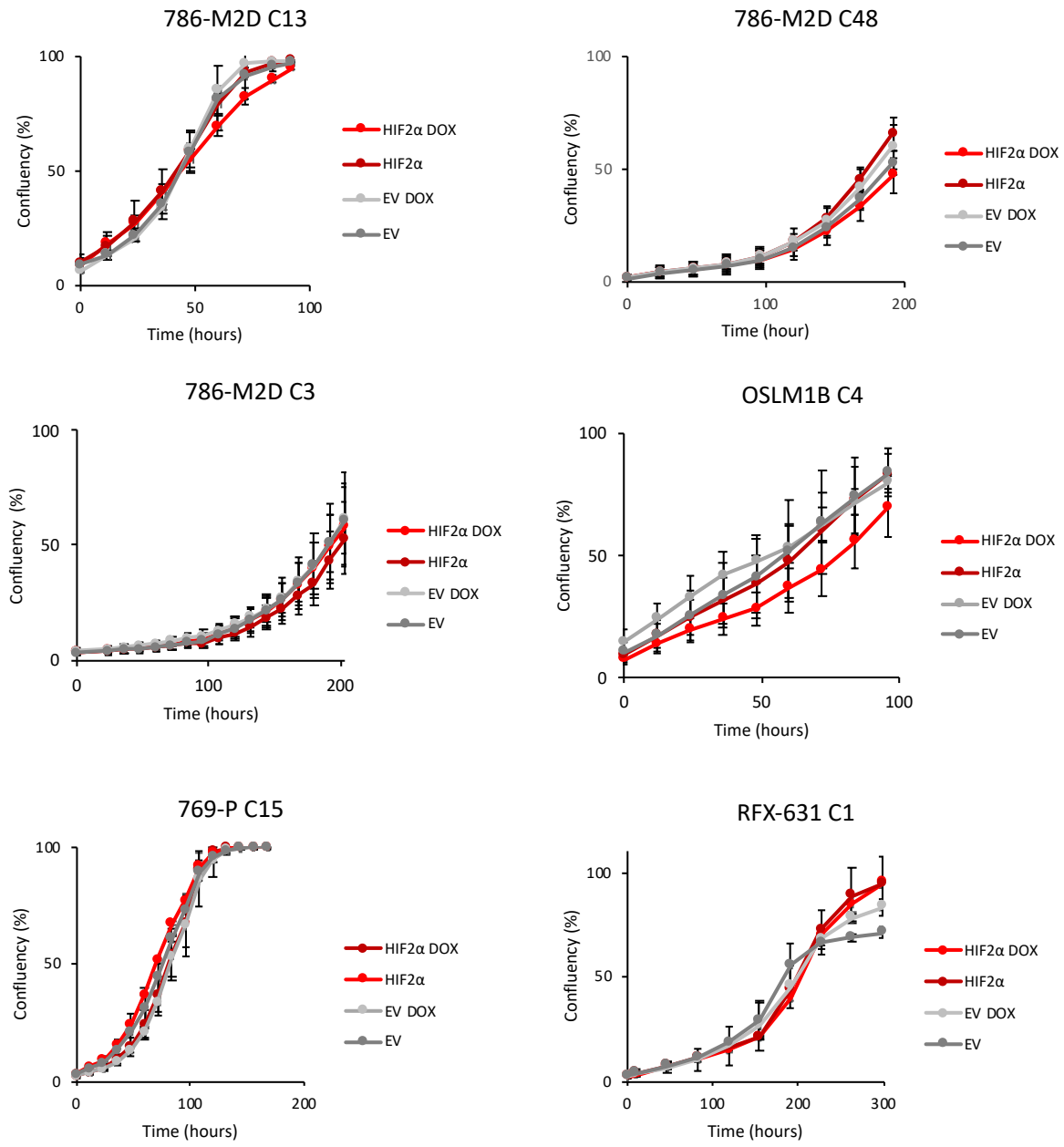

Figure 3.9 Proliferation assays in ccRCC HIF2α KO cells with re-introduced DOX inducible HIF2α. The confluency of HIF2α KO clones expressing either DOX-inducible HIF2α or empty vector (EV) control in presence and absence of DOX treatment was determined using the Incucyte.

The kinetics of HIF2α expression in response to DOX treatment was analysed by performing an *in vitro* experiment to study HIF2α degradation following DOX withdrawal using the 786-M2D clone 13 (7513). HIF2α levels were determined by qPCR. A significant loss of HIF2α expression was observed after 4 hours and no detectable HIF2α protein was observed after 12 hours (**Figure 3.10**). The intensity of HIF2α bands was quantified using ImageJ and plotted, resulting in an exponential equation suggesting that the half-life of HIF2α is 3 hours.

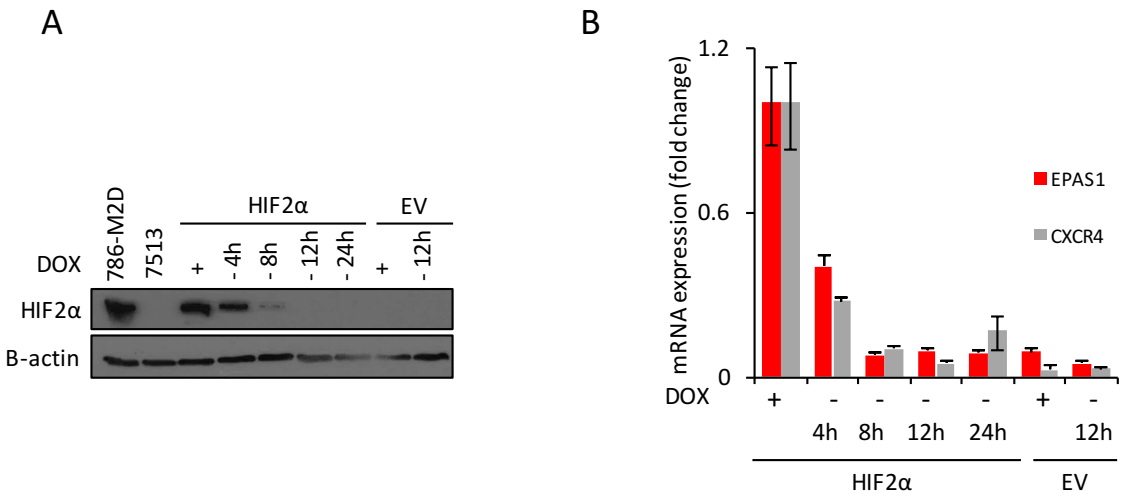

Figure 3.10 Kinetics of HIF2α degradation. (A) Western blot of HIF2α before and after DOX withdrawal. Parental cell line was used as positive controls to compare the expression level of HIF2α. Empty vector (EV) control cells were used as a negative control. β- actin was used as a loading control. (B) qPCR shows the expression of HIF2α and its target gene *CXCR4* normalised to *TBP* housekeeping gene expression. Data are presented relative to "ON DOX" HIF2α expressing cells. Error bars show 95% confidence interval based on technical triplicates.

Summary

To study the role of HIF2α in ccRCC maintenance, a controllable HIF2α construct and HIF2α KO cell lines were developed. I observed great differences in number of HIF2α clones generated by CRISPR Cas9. This could be due to the high ccRCC heterogeneity and individual cells fail to survive on their own. There was great variability in the *CXCR4* expression in HIF2α single cell clones. This could be explained by the fact that not all cells within the parental population express *CXCR4*. Also, *CXCR4* expression can be upregulated by other mechanisms in these cells apart from the presence/absence of HIF2α. Therefore, other more suitable HIF2α regulated genes should be used in future for validation of HIF2α activity.

The FACS experiments outlined in figure 3.7 prove that the DOX-inducible system provides temporal control over the expression of HIF2α. However, the DOX-inducible system is not perfect and approximately 30% of cells did not respond to DOX treatment in this study. Thus, for further experiments, these cells were excluded by sorting only DOX responsive, dsRed positive cells. HIF2α loss *in vitro* did not show any growth disadvantage under standard tissue culture conditions, consistent with previous studies[47,48,75], therefore the role of HIF2α in ccRCC maintenance will be tested *in vivo*.

Chapter 4. Molecular characterisation of the responses to HIF2α withdrawal

Introduction

HIF2α overexpression is a known critical driver of ccRCC tumorigenesis, nevertheless, the role of HIF2α in ccRCC maintenance is less well characterised. Consistent with previous studies, the experiments described in Chapter 3 demonstrated that loss of HIF2α *in vitro* did not show any phenotype[47,48,75]. Therefore, the inducible HIF2α genetic model was tested *in vivo*. To do The role of HIF2α in ccRCC maintenance was investigated by introducing and subsequently inhibiting the DOX-inducible HIF2α in HIF2α KO clones *in vivo*. Cells were implanted subcutaneously on immunocompromised mice and the effects of HIF2α inhibition on tumour growth were determined.

4.1 DOX inducible reintroduction of HIF2α *in vivo*

Proliferation assays showed no difference in growth between the cells expressing inducible HIF2α and controls cells (**Figure 3.9**). Therefore, I tested the DOX-inducible HIF2α system *in vivo*. The characterised HIF2α KO clones were injected subcutaneously into athymic nude mice. All the HIF2α KO clones tested *in vitro* did not show any growth advantage regardless of expressing *EPAS1* or not. OSLM1B clone 1, RFX631 clone 1 and 769-P clone 15 followed the same trend *in vivo* and overall, neither HIF2α nor EV expressing cells resulted in tumour formation (**Figure 4.1**).

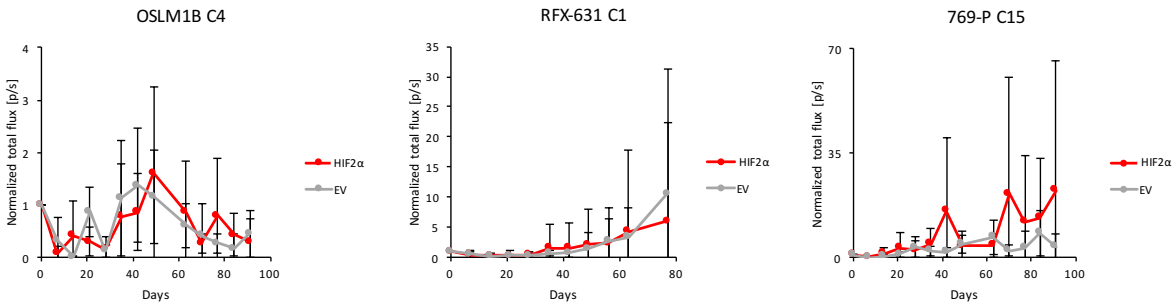

Figure 4.1 Tumour growth in mice injected with HIF2α KO clones expressing DOX-inducible exogenous HIF2α. Athymic nude mice were injected subcutaneously with OSLM1B clone 4, RFX631 clone 1 and 769-P clone 15 expressing either empty vector control cells (EV) or the DOX-inducible HIF2α cells (HIF2α). $5x10^5$ cells per flank were injected. Error bars represent Standard Error of the mean (SEM). N= 5 for EV, N=5 for HIF2α for each clone. P value was calculated by Greham-Breslow-Wilcoxon one tailed test. P>0.05

Both HIF2α expressing 786-M2D clones, clone 13 (7513) and clone 48 (7548), formed tumours *in vivo*. In both cases palpable tumours formed within 8 weeks whereas the control cells transduced with an empty vector did not grow throughout the whole experiment (**Figure 4.2**).

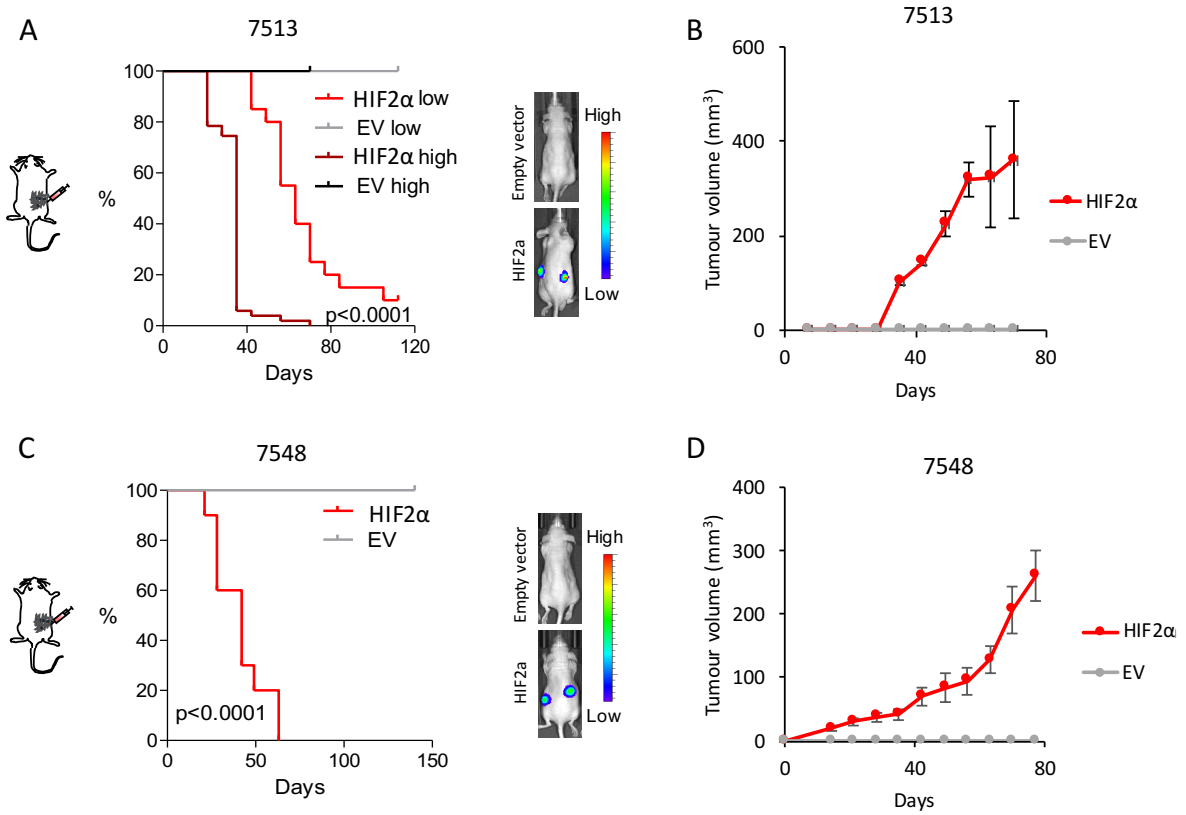

Figure 4.2 Tumour formation and growth in mice injected with 786-M2D HIF2α KO clones. Athymic nude mice were injected subcutaneously with empty vector control cells (EV) and the DOX-inducible HIF2α cells (HIF2α). Tumour-free survival in mice injected with 7513 (A) and 7548 (C). Low and high refer to the number of 7513 cells injected, $3x10^5$ and $5x10^5$ per flank, respectively. Clone 7548 was injected at $5x10^5$ cells per flank. Tumour growth measured by caliper for mice injected with 7513 (B) and 7548 (D). Error bars represent standard error of the mean (SEM). P value was calculated by Logrank test. N=5 for 7513 EV low, N= 3 for EV high, N=10 for 7513 HIF2α low, N=27 for 7513 HIF2α high, N=5 for 7548 EV, N= 5 for 7548 HIF2α.

When tumours became palpable, mice were split into two groups: with and without DOX diet. Tumours of mice kept on the DOX diet (HIF2α active) continued to grow, while tumours of mice withdrawn from the DOX diet regressed rapidly (**Figure 4.3 A, C**). None of the control mice (injected with cells expressing an empty vector construct) formed tumours. In order to understand the importance of HIF2α in tumour maintenance and why tumours regressed so rapidly following DOX withdrawal, the mice in the "HIF2α activated" group were split into 2

further groups: Half of the mice were sacrificed while still on DOX (expressing HIF2α) and the other half was kept off DOX diet for three days before being sacrificed. Tumours regressed significantly following HIF2α inactivation (**Figure 4.3 B, D**).

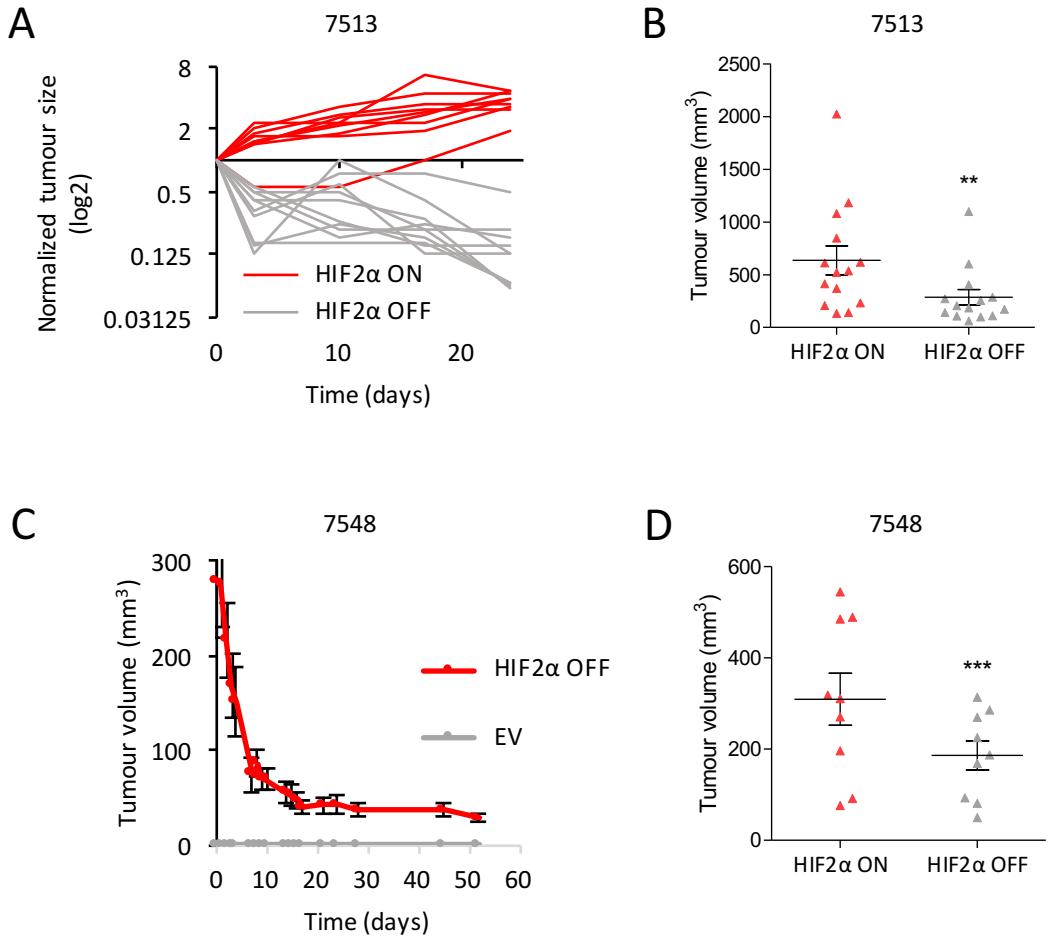

Figure 4.3 Long term tumour regression following HIF2α inactivation. Tumours were measured by bioluminescent imaging for 7513 cells (A) and by caliper for 7548 (C). Difference in tumour volumes before (DOX+) and 3 days after (DOX-) inactivation of HIF2α measured by caliper in 7513 (B) and 7548 (D). P value was calculated based on two-tailed paired T-test. **= P<0.01

All the tumours were collected and used for immunohistochemistry (IHC) and gene expression analysis. Paraffin-embedded tumours were processed and analysed for HIF2α and vimentin expression by IHC (**Figure 4.4**). As expected, only the "HIF2α ON" tumour group expressed HIF2α. Regressing tumours did not express any HIF2α. Control cells expressing the empty vector did not form tumours *in vivo*, neither express HIF2α. Vimentin staining was used to

confirm that the cells forming tumours were of human origin.

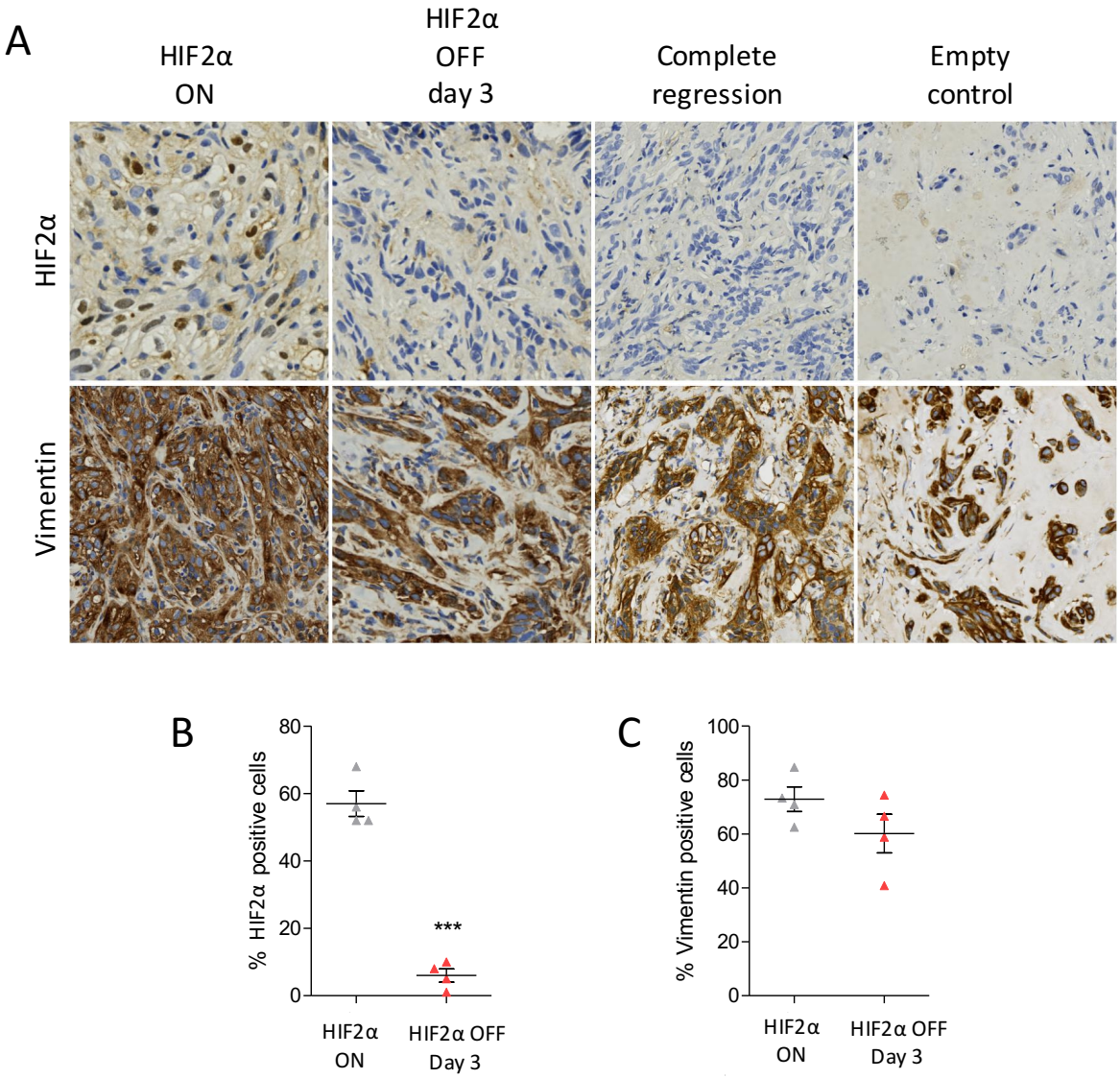

Figure 4.4 Immunohistochemical analysis of subcutaneous tumours. (A) IHC staining for HIF2α and Vimentin in cells with activated and inactivated HIF2α, in completely regressed tumours and control tumours. Quantification of HIF2α (B) and Vimentin (C) expression was performed using the Halo software. P value was calculated based on Student's T-test. ***= P<0.0001

To further characterize the "HIF2α activated" and "HIF2α inactivated" tumours, I performed Ki67 and Cleaved Caspase 3 (Cas3) staining. Ki67 is a widely used proliferation marker. Ki67 is expressed during all active phases of the cell cycle (G1, S, G2, M), but absent in resting cells (G0)[126]. Cas3 activation is an indicator of apoptosis. This protease has been implicated as an "effector" caspase associated with the initiation of the "death cascade"[127]. As expected, "HIF2α activated" tumours expressed Ki67, and its expression is lost when HIF2α is inactivated and tumours regress (**Figure 4.5 A, B**). Cas3 did not stain within proliferating "HIF2α activated" tumours, but some Cas3 activation was detected by IHC in "HIF2α inactivated" regressing tumours (**Figure 4.5 A, C**).

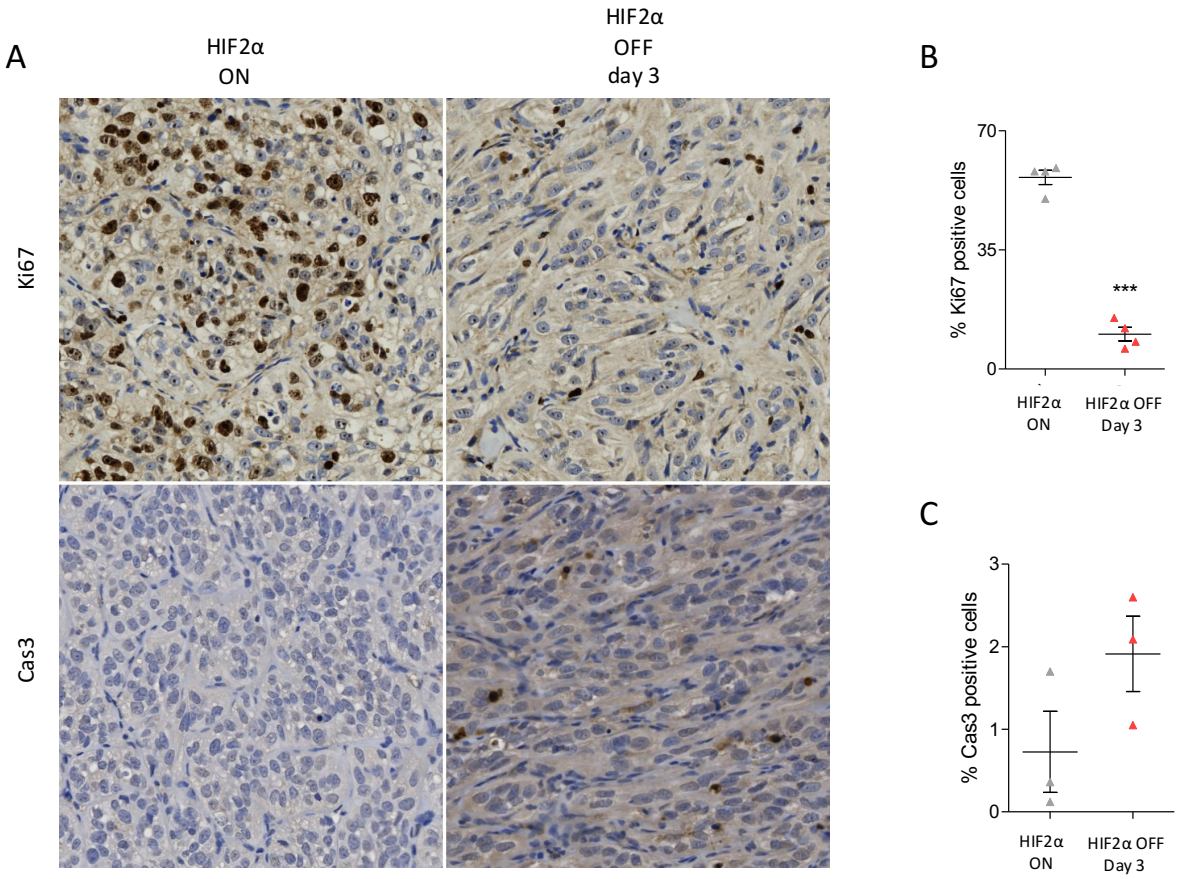

Figure 4.5 Ki67 and caspase 3 staining in subcutaneous tumours. (A) Immunohistochemistry staining for Ki67 and Caspase3 in cells with activated and inactivated HIF2α. Quantification for Ki67 (B) and Cas3 (C) was performed using Halo software. P value was calculated based on

Student's T-test. ***= P<0.0001

Half of each tumour collected was snap-frozen and used to extract RNA. Samples were analysed using qPCR to validate the *in vivo* DOX inducible system by looking at the expression of *HIF2α* and its known downstream target genes *CXCR4, EGLN3 and ADM*. Significant downregulation of *HIF2α* mRNA and the downstream target genes was observed 3 days after DOX withdrawal (**Figure 4.6**).

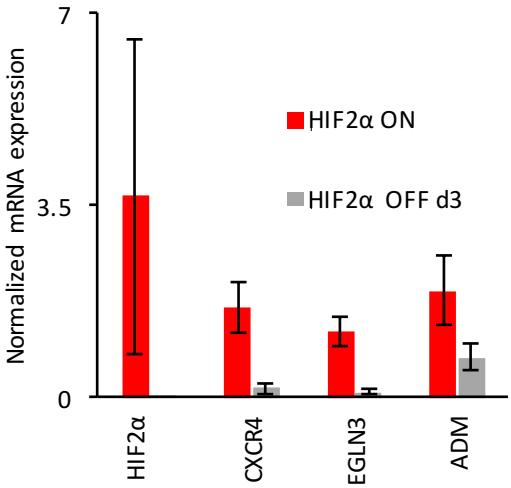

Figure 4.6 mRNA expression of HIF2α and its downstream target genes CXCR4, EGLN3 and ADM before and after HIF2α inactivation. Gene expression was normalised to the expression of the housekeeping gene TBP. Data is normalised to one of the "HIF2α ON" sample for each gene. Error bars show standard deviation between the tumour samples. N=4 for HIF2α ON, N= 4 for HIF2α OFF day 3

Oncogene inactivation can result in a state of tumour dormancy. This phenomenon has been observed while studying the *MYC* oncogene. *MYC* inactivation in epithelial tumours (hepatocellular and breast cancer) results in a proliferative arrest, differentiation and apoptosis of most tumour cells, but some "normal-like" tumour cells remain and may regain tumorigenic properties upon *MYC* reactivation[128,129]. In the HIF2α inducible system, I observed complete tumour regression when HIF2α was inactivated, however, a weak

bioluminescence signal remained in all animals. To test whether the remaining cells are capable of forming a tumour, HIF2α was reactivated by the DOX diet. Indeed, HIF2α reactivation led to tumour formation (**Figure 4.7**).

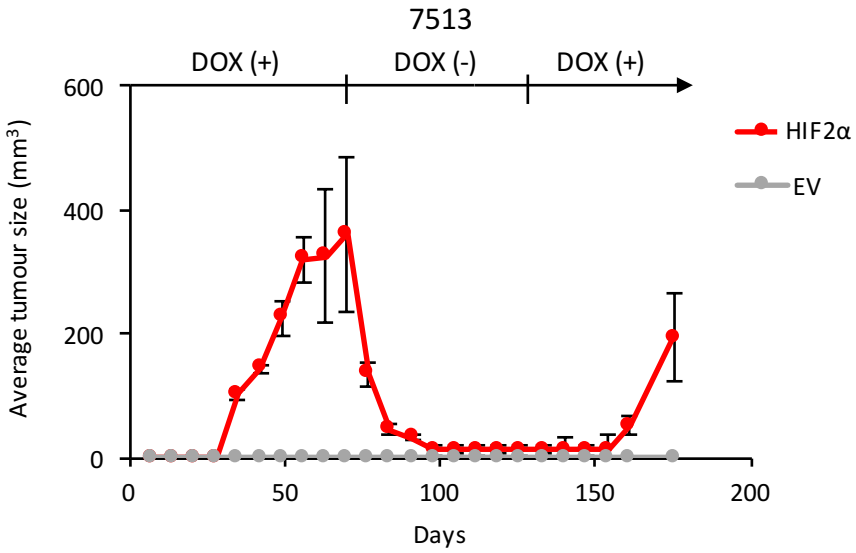

Figure 4.7 Effects of HIF2α re-activation on tumour growth. Tumour growth and regression measured by caliper. Tumour growth was initiated by DOX administration until day 70. Tumours regressed completely following DOX withdrawal. DOX was re-administered at day 126. Error bars represent Standard Error of the mean (SEM). N=5 for EV, N= 2 for HIF2α.

4.2 Metastatic potential of 7513

ccRCC is usually asymptomatic and patients often present with metastasis. To evaluate the metastatic potential of the 7513 clone, the cells were injected intra-cardially in athymic nude mice. As expected, the empty vector control cells did not form any metastasis. However, 60% of the HIF2α activated cells formed metastasis mostly in the lower limbs (**Figure 4.8 A**). Upon DOX withdrawal, the signal from all the metastasis dropped significantly within the first 3 days and remained low until the end of experiment (**Figure 4.8 B, C**) suggesting that HIF2α expression is important for metastatic growth in ccRCC.

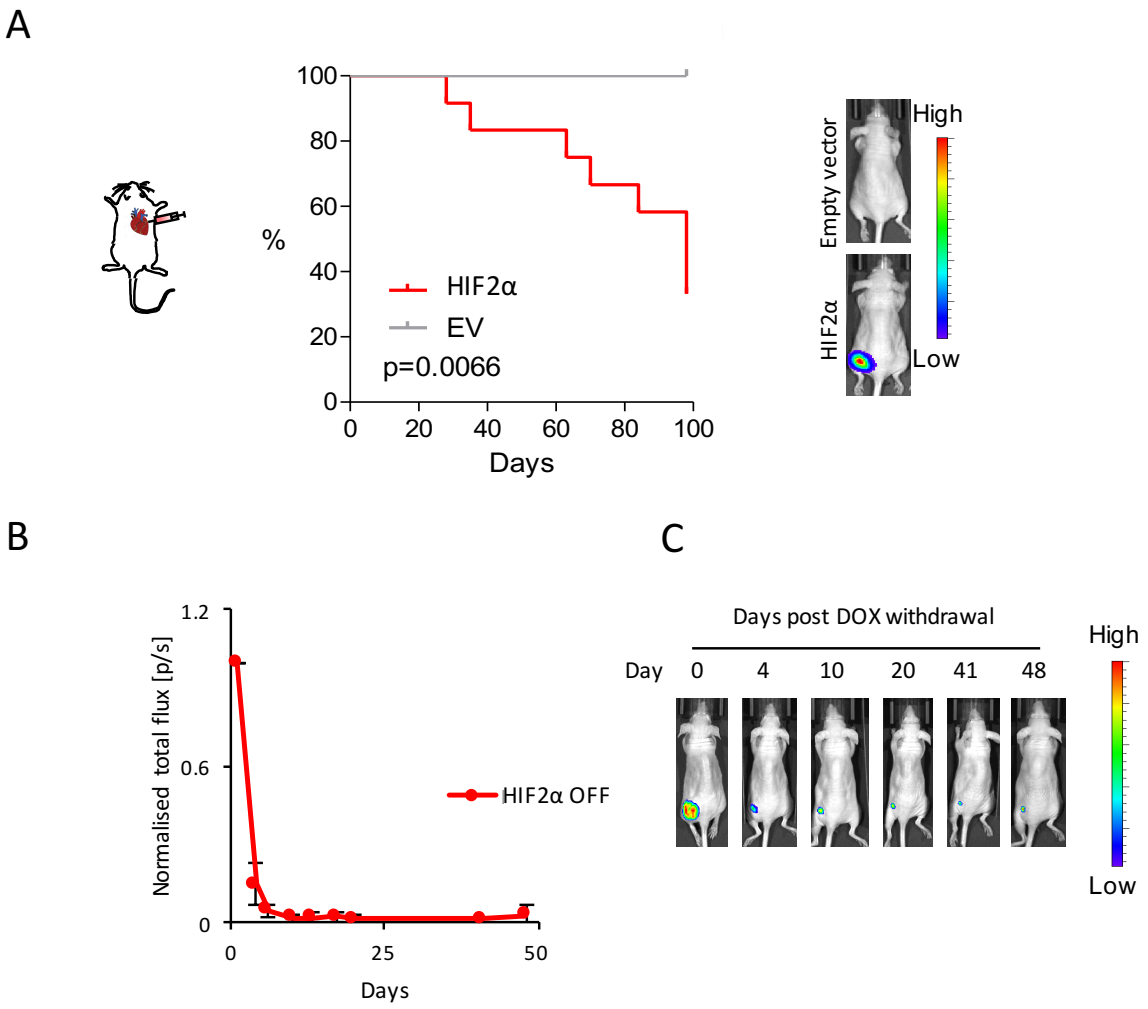

Figure 4.8 Tumour formation and regression in metastasis mouse assay. (A) Metastasis-free survival in mice injected with the 7513 clone. Athymic nude mice were injected intra-cardially with empty vector control cells (EV) and the DOX-inducible HIF2α cells (HIF2α), 1x 10^5 cells were injected. P value was calculated by Logrank test. N= 8 for EV, N= 12 for HIF2α. (B) Long term tumour regression following HIF2α inactivation measure by bioluminescent imaging. (C) Representative bioluminescence images showing tumour regression after DOX withdrawal (HIF2α inactivation).

4.3 Involvement of the Immune system in ccRCC regression

The importance of the Immune system for tumour regression was discussed in Chapter 1. Oncogene inactivation usually leads to tumour regression, which is in many cases dependent on various constituents of the immune system[97,101]. We hypothesized whether this would be the case in tumour regression initiated by the loss of HIF2α in our HIF2α-inducible system. The experiments performed so far used the athymic nude mice which lack T cells, but still have robust B cell and NK cell responses[130]. To understand the involvement of the adaptive immune system in tumour regression in our system, the experiment using the 7513 clone was repeated, however, the cells were injected subcutaneously into NSG mice. NSG mouse are severely immune deficient, they lack mature T cells, B cells, functional NK cells and are also deficient in cytokine signalling[131]. The immune cells detected in the NSG mouse include mostly neutrophils and monocytes. Some dendritic cells and macrophages are also present but they are defective because of the non-obese diabetic (NOD) genetic background[131]. Following the injection of HIF2α expressing and EV cells, tumours were formed within 6 weeks only by the cells expressing HIF2α (**Figure 4.9**).

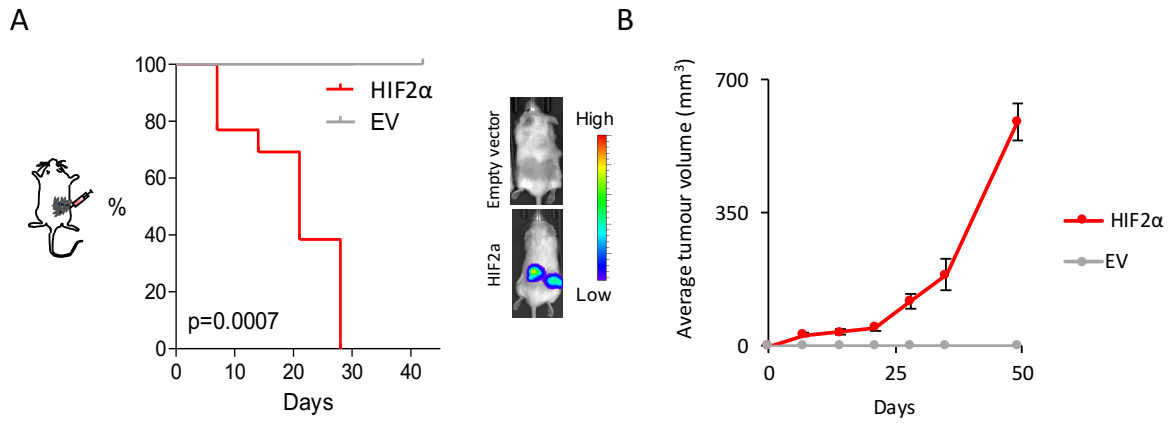

Figure 4.9 Tumour formation and progression in NSG mouse models. (A) Tumour-free survival in mice injected with the 7513 clone. NSG mice were injected subcutaneously with empty vector control cells (EV) and the DOX-inducible HIF2α cells (HIF2α), 5x 10^5 cells were injected. P value was calculated by Logrank test. (B) Tumour growth measured by caliper. Error bars represent Standard Error of the mean (SEM). N= 3 for EV, N= 7 for HIF2α.

When all the tumours became palpable, HIF2α was inactivated by removing DOX from the diet. Rapid tumour regression was observed, as observed in athymic nude mouse model. Tumours regressed completely and did not relapse (**Figure 4.10**). Importantly, the speed of regression was again significant. This data suggests that the adaptive immune system does not seem to contribute significantly to tumour regression in this ccRCC model.

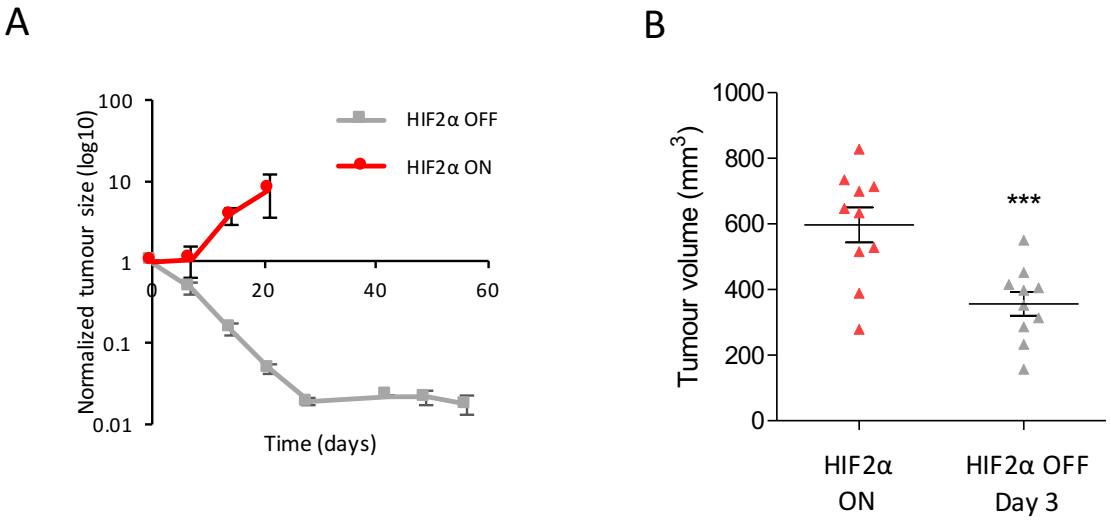

Figure 4.10 Tumour regression in NSG mice. (A) Long term tumour regression following HIF2α inactivation measure by bioluminescent imaging. (B) Difference in tumour volumes before (DOX+) and 3 days after (DOX-) inactivation of HIF2α measured by caliper. Error bars represent standard deviation between the tumour sizes. P value was calculated based on two-tailed paired T-test. ***= P<0.0001

Summary

The role of HIF2α was studied using the HIF2α DOX-inducible system *in vivo*. The oncogenic effect of HIF2α and its importance in tumour initiation and progression have been previously observed[46–48] and are consistent with our *in vivo* observations. Some of the clones tested, namely OSLM1B clone 4, RFX-631 clone 1 and 769-P clone 15 did not form tumours regardless of expressing HIF2α or not. This may be because ccRCC is a very heterogeneous disease and the single cell HIF2α KO clones that survived the sorting process may have lost their tumorigenic potential. Other systems, such as using DOX-inducible shRNA targeting HIF2α may be more suitable alternative.

Both 786-M2D clones expressing HIF2α developed tumours and furthermore, tumours regressed significantly after HIF2α expression was inhibited. Importantly, no tumour relapse was observed in absence of HIF2α. However, we observed that some ccRCC cells remained at the site of injections and were capable of re-initiating the tumour growth upon HIF2α reintroduction. This suggest that not all ccRCC cells die when the tumour regressed, and some cells remain in dormant state.

Metastasis assays confirmed the HIF2α dependency not only for tumour formation, but also for metastatic progression. Cells with activated HIF2α readily formed metastasis *in vivo* and, metastatic nodules rapidly regressed rapidly when HIF2α was inhibited. This is of great clinical importance since the principal cause of death in ccRCC patients is due to the development of metastatic lesions in distant organs.

Recent studies have shown the importance of the immune system in tumour regression[97,101], however, experiments performed using severely immunocompromised mouse model suggest

that the adaptive immune system does not seem to contribute significantly to tumour regression observed in our model.

To understand the molecular mechanisms through which HIF2α drives tumorigenesis, further experiments were performed.

Chapter 5. Functional characterisation of the mechanisms through which HIF2α mediates ccRCC growth

Introduction

I studied the role of HIF2α in tumour maintenance by using the novel inducible HIF2α isogenic cell line described in Chapter 3. Using this genetic model, I discovered that established ccRCC tumours are very dependent on HIF2α and when HIF2α expression is lost, tumours regress and do not relapse. In this chapter, I will determine the mechanisms by which HIF2α drives ccRCC progression.

5.1 HIF2α promotes tumorigenesis through upregulation of canonical oncogenic signalling pathways

The characterisation of the inducible HIF2α model *in vivo* was described in Chapter 4. Gene expression in fully grown 786-M2D clone 13 (7513) "HIF2α activated" tumours and regressing "HIF2α inactivated after 3 days" tumours was compared through RNA-seq. This analysis revealed several differentially expressed genes between the two groups (**Figure 5.1 A**). As expected, *HIF2α* and its target genes were significantly downregulated following DOX withdrawal from the diet. Interestingly, *TGFα* and *MYC* were also shown to be significantly downregulated while *Cyclin D1* (*CCND1*) came up as the most significantly downregulated gene. Next, Ingenuity pathway analysis (IPA) was performed in the RNA-seq data. IPA is a web-based software application for the analysis, integration and interpretation of 'omics data[132]. IPA analysis showed that pathways involved in cell cycle control, DNA replication and DNA repair were indeed significantly downregulated after *HIF2α* expression was lost (**Figure 5.1 B**).

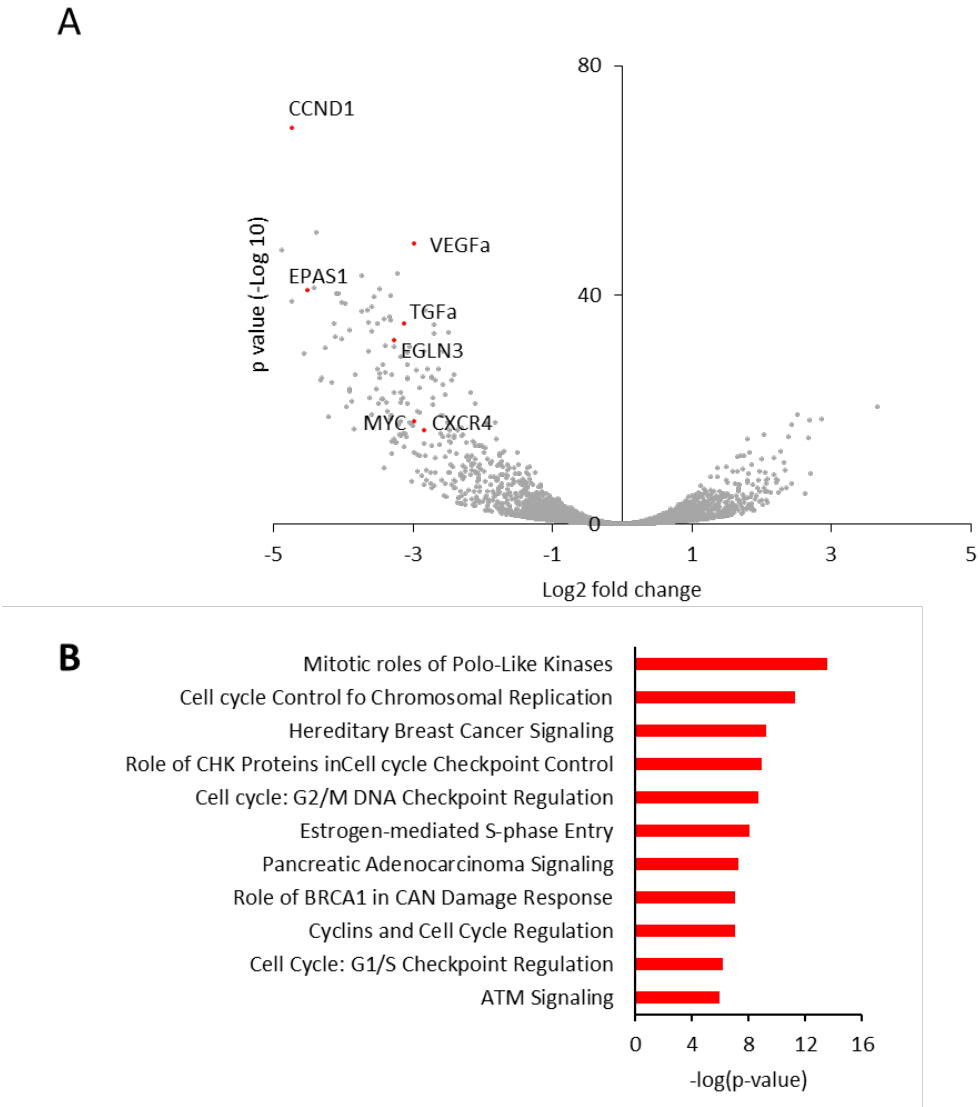

Figure 5.1 Differential gene expression determined by RNA-seq analysis of 7513 tumours. (A) Genes differentially expressed following DOX withdrawal are shown in grey. *HIF2α (EPAS1)* and its downstream target genes *VEGFA, EGLN3, CXCR4* as well as *MYC*, *TGFα* and the top downregulated gene C*yclin D1* (*CCND1*) are shown in red. (B) List of pathways most significantly downregulated 3 days after loss of HIF2α*,* generated by Ingenuity pathway analysis (IPA).

Gene set enrichment analysis (GSEA) was undertaken to further validate our findings. GSEA is a computational method that determines whether a *a priori* defined set of genes shows statistically significant, concordant differences between two biological states[133]. Similar to what was observed through the IPA analysis, GSEA confirmed that cell cycle, DNA replication and homologous recombination gene clusters were significantly downregulated when HIF2α expression was lost (**Figure 5.2**).

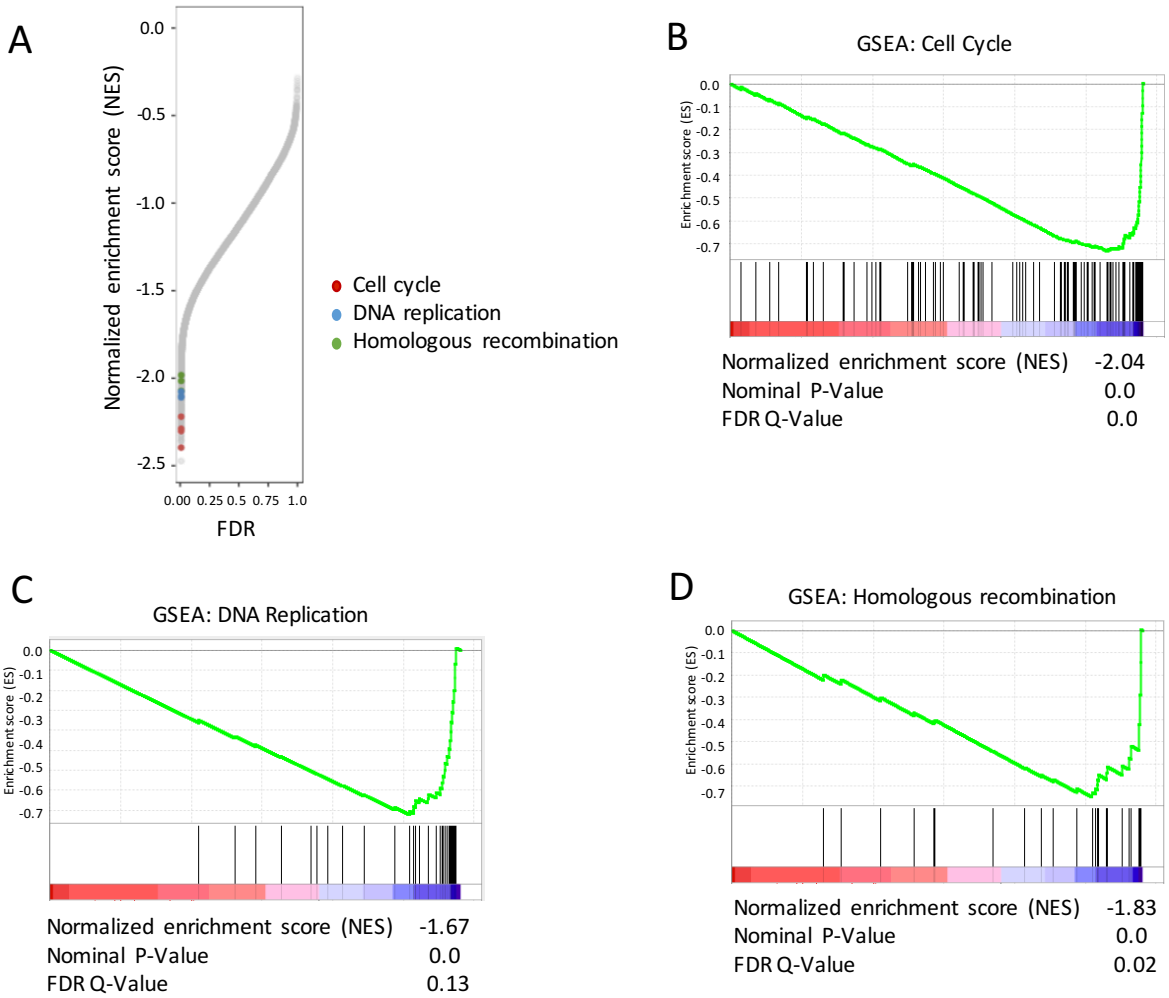

Figure 5.2 Gene set enrichment analysis in 7513 tumours. (A) Normalized GSEA of RNA-seq data showing the significantly downregulated pathways. (B-D) GSEA showing the enrichment scores of differentially expressed genes within Cell cycle, DNA replication and Homologous recombination gene clusters 3 days after loss of HIF2α expression.

Moreover, RNA-seq analysis comparing 7513 HIF2α expressing cells and 7513 control EV cells grown *in vitro* confirmed that HIF2α KO clones do not depend on HIF2α to maintain cell proliferation. Loss of HIF2α resulted in downregulation of some of the known HIF2α target genes such as *CCND1, CXCR4* and *EGLN3* (**Figure 5.3 A**). However, the expression of *MYC* stayed unchanged, suggesting that MYC *in vitro* is regulated by other mechanisms. GSEA further confirmed these finding by demonstrating that cell cycle, DNA replication and homologous recombination gene clusters are not downregulated in absence of HIF2α *in vitro* (**Figure 5.3 B**).

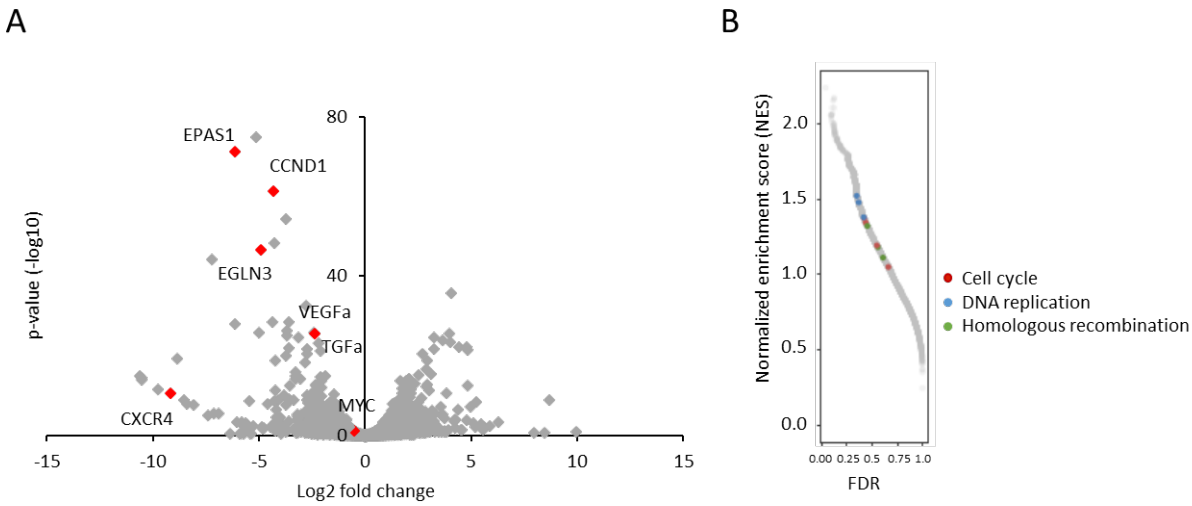

Figure 5.3 *In vitro* RNA-seq analysis of the 7513 clone upon HIF2α inactivation. (A) Genes differentially expressed in HIF2α expressing cells versus EV controls are shown in grey. *HIF2α (EPAS1)* and its downstream target genes *VEGFA, EGLN3, CXCR4* and *MYC*, *TGFα* and *CCND1* are shown in red. (B) Gene set enrichment analysis. Normalized GSEA of RNA-seq data highlighting the pathways of interest.

In agreement with the RNA-seq data, IHC was performed to confirm the presence and absence of MYC and CCND1 in 7513 "HIF2α activated" and "HIF2α inactivated" tumours (**Figure 5.4**). As expected, both MYC and CCND1 were only expressed when HIF2α is activated and their expression dropped significantly upon HIF2α inactivation.

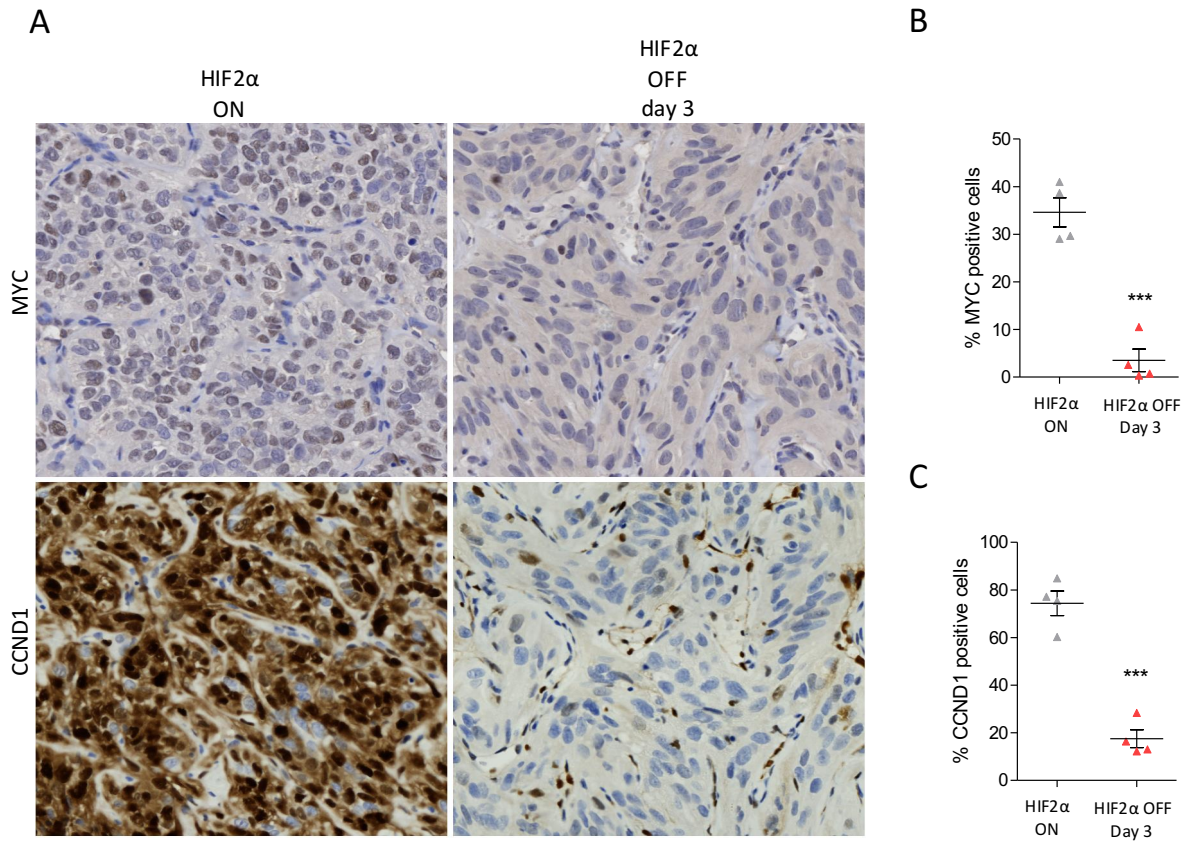

Figure 5.4 Expression of MYC and CCND1 in subcutaneous 7513 tumours. (A) Immunohistochemistry staining for MYC and CCND1 in cells with activated and inactivated HIF2α. Quantification for MYC (B) and CCND1 (C) was performed using Halo software. P value was calculated based on two-tailed paired T-test. ***= P<0.0001

Next, I hypothesized that the downregulation of these pathways can either be caused by loss of HIF2α directly, or it can be a secondary effect due to ongoing tumour regression. To address this question, I repeated the subcutaneous tumour growth experiment using clone 7153 but, following tumour formation and HIF2α inactivation by DOX withdrawal, tumours were collected at different time points post-DOX withdrawal (0h, 8h, 24h, 28h and 32h). Tumour tissue was then analysed via western blot, qPCR and IHC. No significant difference in HIF2α expression between HIF2α expressing 0h control samples and the tumours from the 8h post DOX-withdrawal time point (**Figure 5.5**). However, expression of HIF2α was shown to

disappear in the 24h after DOX withdrawal samples. Expression of downstream targets of HIF2α was still observed 24 hours post DOX withdrawal and a significant decrease was only observed in 32h post DOX withdrawal tumours (**Figure 5.5**). Since tumours have not started to regress after 32h of HIF2α inactivation, this time point was selected for further analysis.

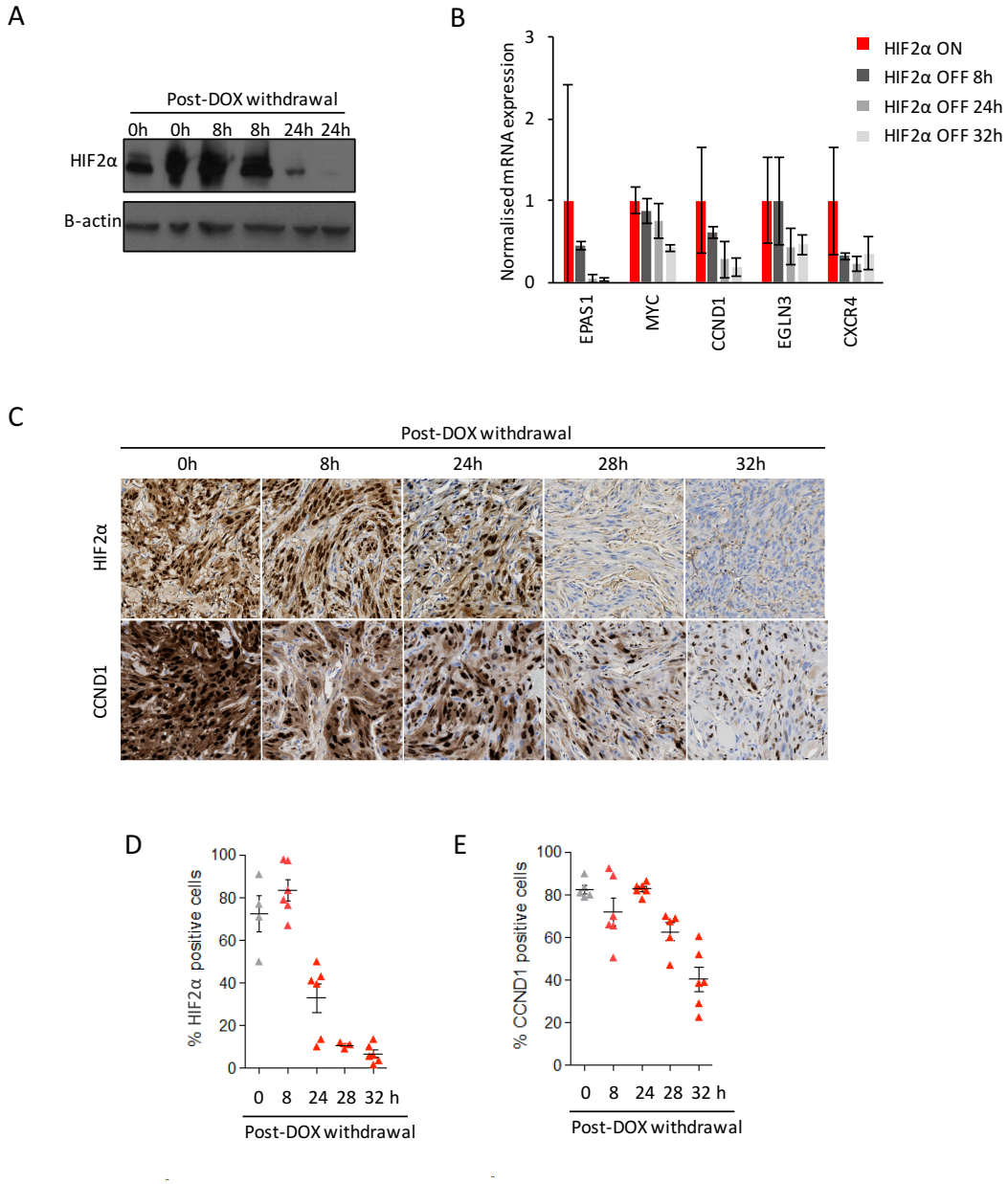

Figure 5.5 *In vivo* expression of HIF2α target genes at different times post-HIF2α inactivation. (A) Western blot of HIF2α showing loss of HIF2α after DOX withdrawal. Tumour

samples with activated HIF2α (0h) were used as positive controls. β- actin was used as a loading control. (B) mRNA expression of HIF2α and its target genes *CXCR4, EGLN3, MYC* and *CCND1* before and after HIF2α inactivation. Gene expression was normalised to TBP housekeeping gene. Data is normalised to one of the "HIF2α ON" sample for each gene. Error bars show the standard deviation between the tumour samples. N= 3 for each time point (C) Immunohistochemistry staining for HIF2α and CCND1 in cells with activated and inactivated HIF2α. Quantification for HIF2α (D) and CCND1 (D) was performed using Halo software.

Interestingly, RNA-seq analysis comparing "HIF2α activated" versus "HIF2α inactivated after 32h" tumours revealed several differentially expressed genes (**Figure 5.6 A**). As previously observed, *EPAS1* and its downstream target genes are significantly downregulated when expression of HIF2α is lost. Importantly, *CCND1* is again one of the most significantly downregulated genes. Moreover, IPA analysis in these tumours once again highlighted the downregulation of pathways involved in cell cycle control and DNA damage response (**Figure 5.6 B**).

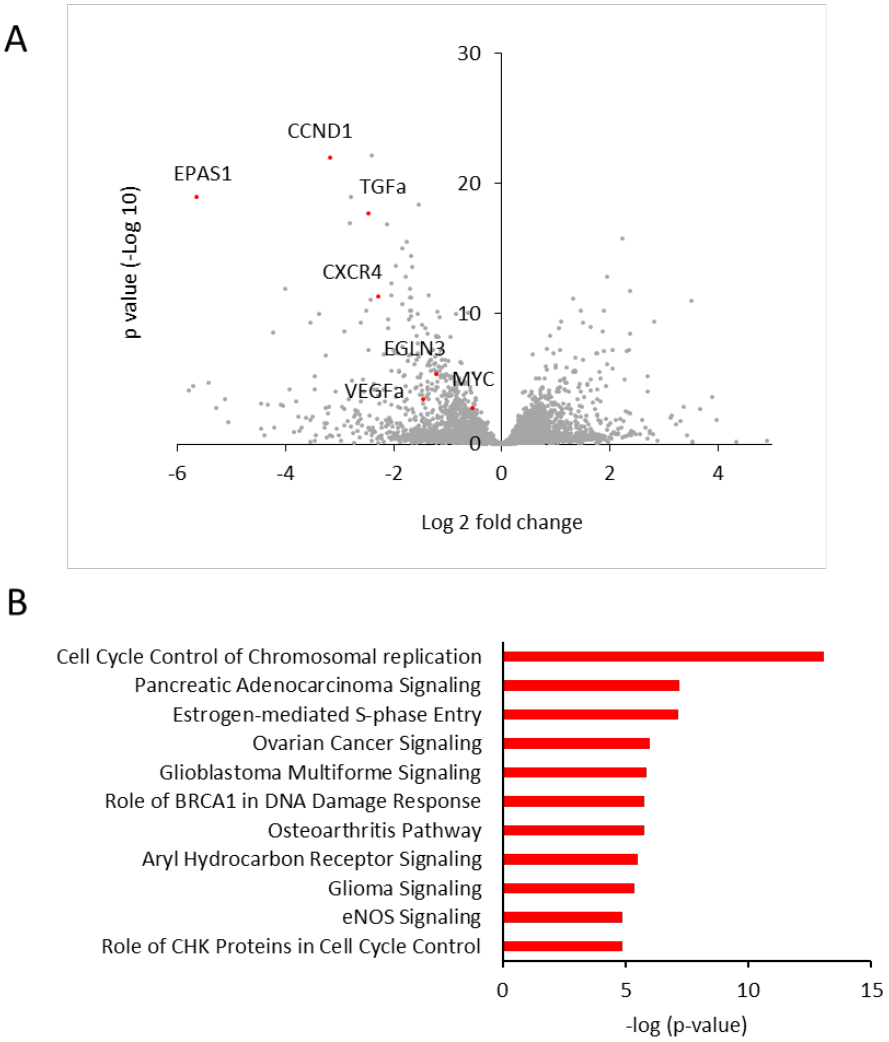

Figure 5.6 RNA seq and IPA analysis in 32h post-HIF2*α* inactivation tumours. (A) Differential gene expression by RNA-seq analysis. Genes differentially expressed after 32 hours following DOX withdrawal are shown in grey. *HIF2α (EPAS1)* and its downstream target genes *VEGFA, EGLN3, CXCR4* and *MYC*, *TGFα* and top downregulated *Cyclin D1* (*CCND1*) are shown in red. (B) List of pathways most significantly downregulated 32 hours after loss of HIF2α, generated by Ingenuity pathway analysis (IPA).

GSEA further confirmed downregulation of cell cycle, DNA replication and homologous recombination gene clusters in HIF2α inactivated tumours (**Figure 5.7**).

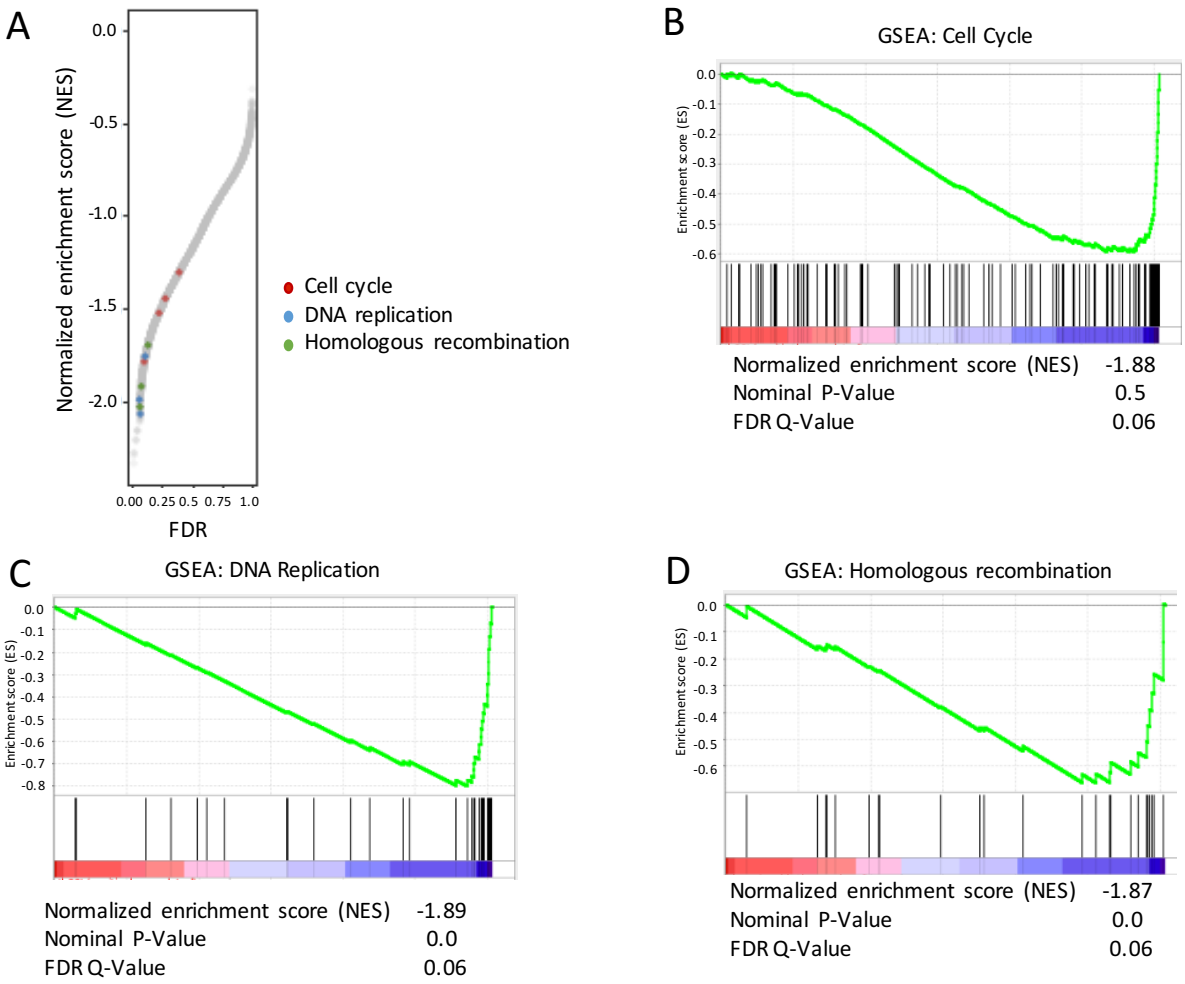

Figure 5.7 Gene set enrichment analysis in 32h post DOX withdrawal tumours. (A) Normalized GSEA of RNA-seq data showing the significantly downregulated pathways. (B-D) GSEA showing the enrichment scores of differentially expressed genes within Cell cycle, DNA replication and Homologous recombination gene clusters 32 hours after loss of HIF2α expression.

Altogether, the GSEA and IPA analysis showed that genes involved in the regulation of cell cycle progression, DNA replication and homologous recombination are significantly downregulated when HIF2α expression is lost. Within the list of differentially expressed genes, I found that *MYC, CCND1* and *TGFα* were some of the most significantly downregulated. *MYC, CCND1* and *TGFα* play an important role in cell cycle progression and were shown to be deregulated in many other cancer types (Discussed in more detail in

Chapter 6). Therefore, I next investigated the link between HIF2α and regulation of *MYC, CCND1* and *TGFα* in ccRCC.

5.2 HIF2α drives activation of cell cycle regulators via binding to their enhancers

To better understand the role of HIF2α and its importance in the activation of pro-tumorigenic signalling pathways, HIF2α and H3K27ac ChIP-seq was used to determine the HIF2α binding sites in the genome and the transcriptionally active chromatins regions in ccRCC, respectively. ChIP was performed in ccRCC cell lines 786-M1A (786-M1A and 786-M2D are both metastatic clones of 786-O) and OS-LM1B as well as in mouse tumour xenografts derived from ccRCC cell lines. All ChIP-seq experiments and data analysis were done by others in the lab. In agreement with our RNA-seq data, ChIP experiments revealed HIF2α binding and enrichment of H3K27ac signal in the *MYC, CCND1* and *TGFα* genes locus. H3K27ac activity was detected in close vicinity of these genes in patterns that suggested the presence of active enhancers. Within these active enhancer regions, I also detected very prominent peaks containing HIF2α binding motifs (**Figure 5.8**). Furthermore, single nucleotide polymorphism (SNP) associated with ccRCC susceptibility have been previously identified within the same enhancer region of *MYC* and *CCND1*[134,135]. Altogether, the ChIP seq data suggest that HIF2α activates the expression of *CCND1, MYC* and *TGFα* through binding and activating their enhancers.

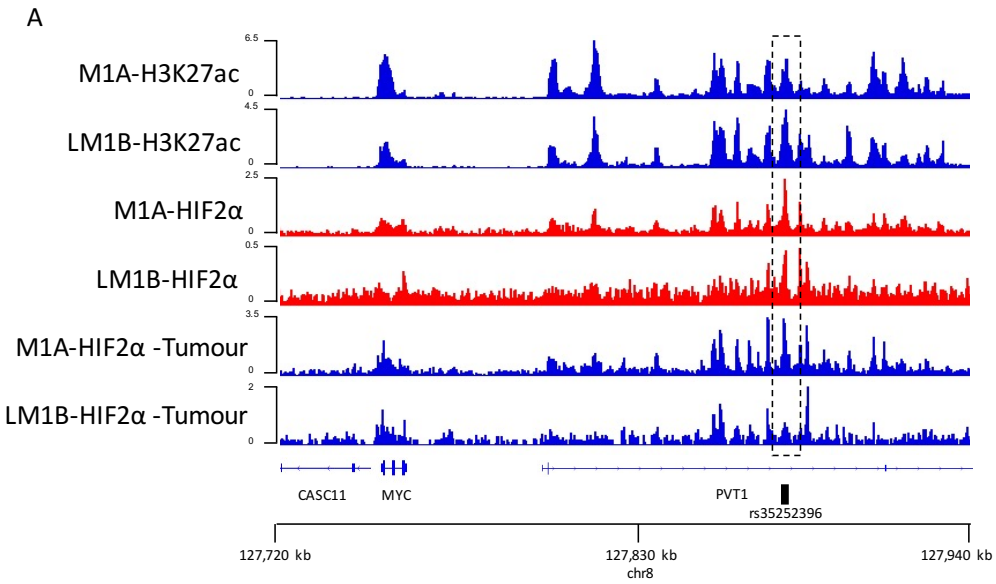
A
M1A-H3K27ac
LM1B-H3K27ac
M1A-HIF2α
LM1B-HIF2α
M1A-HIF2α -Tumour
LM1B-HIF2α -Tumour
CASC11
MYC
PVT1
rs35252396
127,720 kb
127,830 kb
chr8
127,940 kb

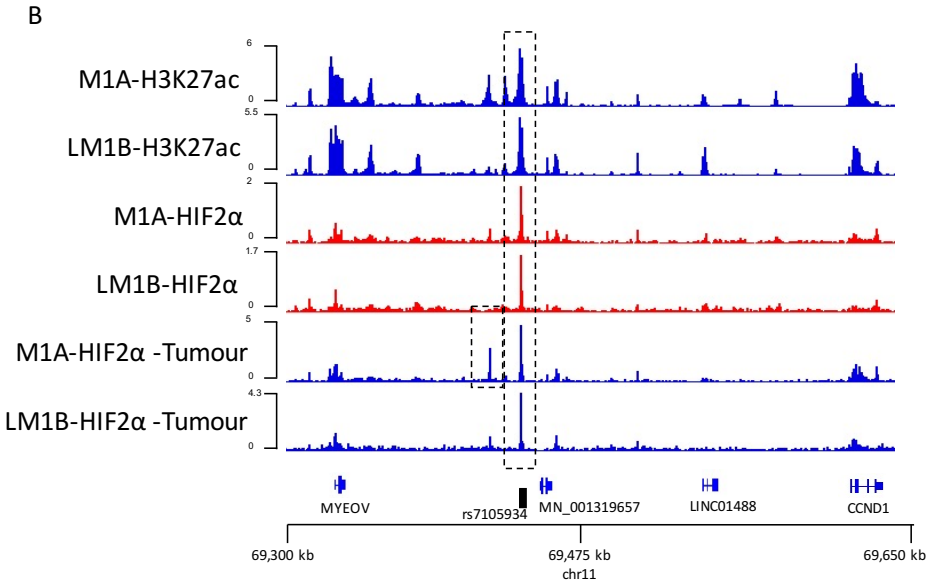
B
M1A-H3K27ac
LM1B-H3K27ac
M1A-HIF2α
LM1B-HIF2α
M1A-HIF2α -Tumour
LM1B-HIF2α -Tumour
MYEOV
rs7105934
MN_001319657
LINC01488
CCND1
69,300 kb
69,475 kb
chr11
69,650 kb

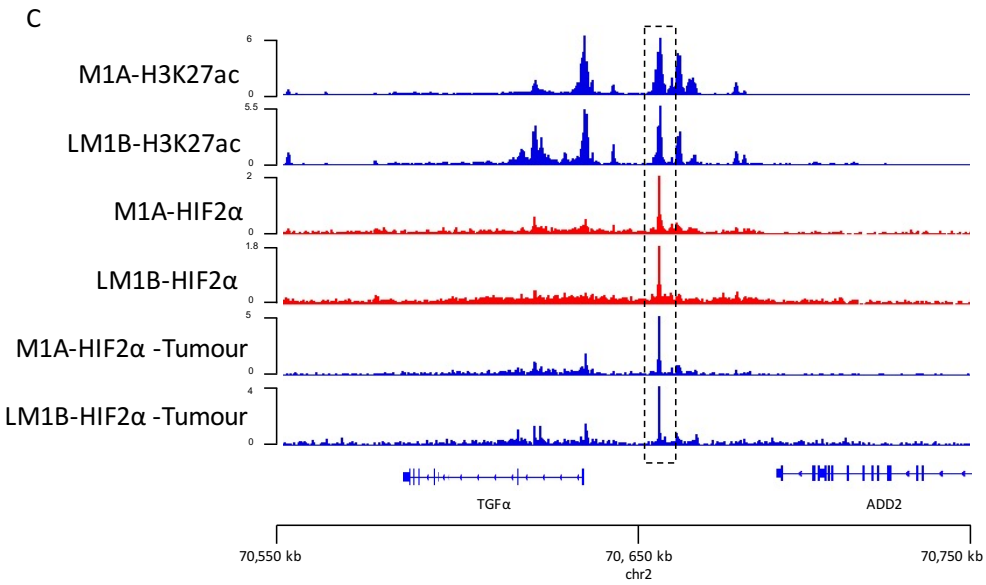
C
M1A-H3K27ac
LM1B-H3K27ac
M1A-HIF2α
LM1B-HIF2α
M1A-HIF2α -Tumour
LM1B-HIF2α -Tumour
TGFα
ADD2
70,550 kb
70, 650 kb
chr2
70,750 kb

Figure 5.8 H3K27ac and HIF2α signal in the *MYC, CCND1* and *TGFα* locus. 786-M1A and OSLM1B cells as well as mouse tumours were analysed. The regions corresponding to the MYC (A), CCND1 (B) and TGFα (C) locus are shown. Dashed boxes highlight HIF2α prominent peaks identified in the vicinity of these three genes. Other genes present in the close vicinity of *MYC, CCND1* and *TGFα* and known genetic variants within the *MYC* and *CCND1* enhancers are shown.

Other genes apart from MYC, CCND1 and TGFα are present near their enhancer regions. HIF2α bound MYC enhancer and SNP predisposing for ccRCC sit within the *PVT1* gene[134] (**Figure 5.8 A**). *PVT1* is an oncogenic long non-coding RNA which was shown to be co-amplified with MYC across many cancers (>98%) and seem to be necessary for MYC stabilisation and tumour growth[136]. Grampp and colleagues suggested that the MYC enhancer locus is likely to be regulating the expression of both genes, *MYC* and *PVT1*[134]. The transcriptional enhancer of *CCND1* was previously described by Schodel *et al* who discovered a protective SNP which prevented HIF2α from binding to this region[135]. *MYEOV* and *LINC01488* are present upstream and downstream of the *CCND1* enhancer respectively (**Figure 5.8 B**). *LINC01488* is a long intergenic non-coding RNA and *MYEOV- Myeloma overexpressed* gene that has been shown to be co-amplified with *CCND1* in various cancers such as leukaemia, oesophageal and breast cancer [137–139]. *Adducin 2 (ADD2)* gene is located upstream of TGFα enhancer. *ADD2* is a membrane skeletal protein which promotes assembly of a spectrin-actin network in erythrocytes and in epithelial tissues at sites of cell-to-cell contact[140].

5.3 Functional validation of cell cycle enhancers *in vitro*

In order to validate whether the binding of HIF2α to enhancer regions of *CCND1, MYC* and *TGFα* is necessary for their activation, I performed a luciferase reporter assay. Luciferase reporter assay is a commonly used genetic tool to study gene expression at the transcriptional level. Enhancer regions of *CCND1, MYC* and *TGFα* (peaks highlighted in **figure 5.8**) were cloned

individually upstream of a mini-promoter which sits upstream of a luciferase gene generating enhancer reporter plasmids. These constructs, as well as the empty control (EV), were introduced into 7513 HIF2α cells via nucleofection alongside with a Renilla expressing plasmid which serves as an internal control. Luciferase activity was measured and normalised to the Renilla luminescence. The reporter assay showed non-significant increase in activation of *MYC, TGFα* and one of the *CCND1* peaks and no activation in the other *CCND1* peak (**Figure 5.9 A**). This may be because the HIF2α binding is chromatin context dependent.

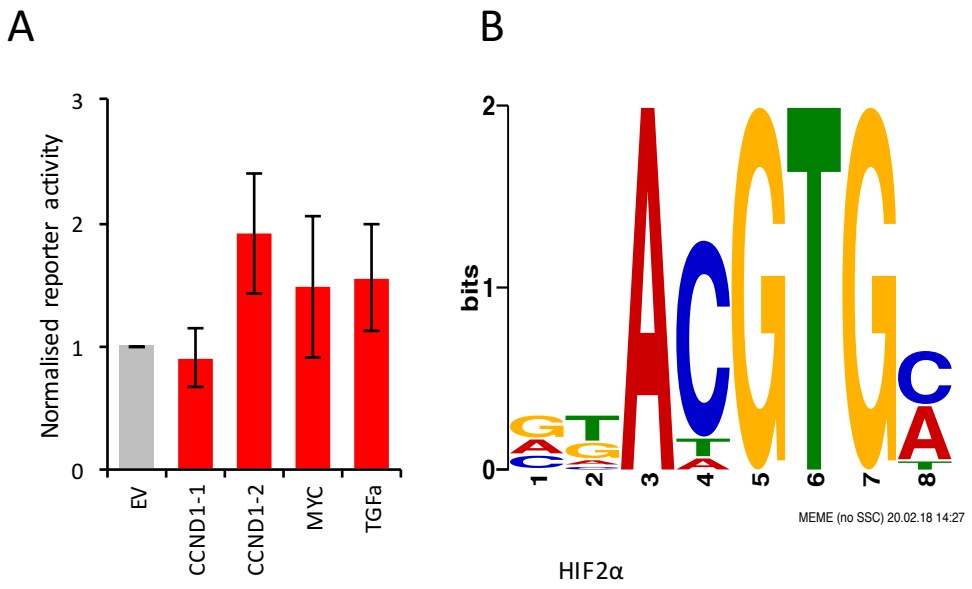

Figure 5.9 Enhancer reporter plasmids. (A) Luciferase reporter assay showing the effects of presence and absence (EV) of the enhancers of interest. Error bars represent standard deviation of two independent experiments. P value was calculated based on two-tailed paired T-test. P>0.05 (B) Conserved HIF2α binding motif. Obtained from MEME (http://meme-suite.org/).

Next, I used FIMO tool to identify the conserved HIF2α binding motifs (5'–ACGTG-3') within the enhancer regions of *CCND1, MYC* and *TGFα* (**Figure 5.9 B**)[141]. Once identified, I mutated the HIF2α in these regions 5'-ACAAA-3' using site directed mutagenesis within the enhancer reporter plasmids. Then, I performed luciferase reporter assay to find out whether mutating

the HIF2α motif would prevent its binding to the enhancer region and therefore prevent its activity. No difference in luciferase activity was observed (**Figure 5.10**).

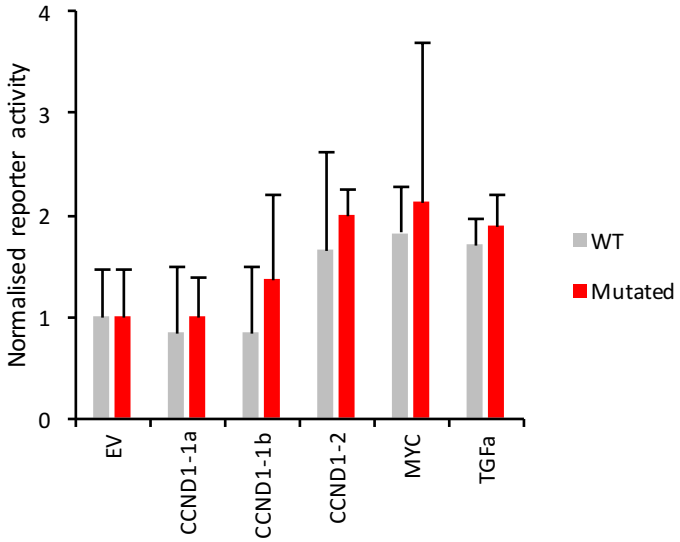

Figure 5.10 Luciferase reporter activity showing the effects of mutated HIF2α motif compared to the wild type. Error bars based on standard deviation of technical triplicate. P value was calculated based on Student's T-test. P>0.05

5.4 CRISPRi targeting of HIF2α bound enhancer elements

To determine whether the activity of this HIF2α bound enhancer elements was important for the expression of MYC and CCND1 I used CRISPR interference (CRISPRi) to inactivate those regions. CRISPRi uses a catalytically dead Cas9 protein (dCas9) fused to a KRAB domain. dCas9 is guided to a specific genomic region by sgRNA, but its unable to create a double stranded break. Instead, it binds to DNA and the attached KRAB mediates transcriptional repression[142,143].

786-M1A ccRCC cells were used. Firstly, I stably transduced this cell line with a dCas9-KRAB-mCherry construct. Multiple sgRNA sequences to target the area of HIF2α binding within the

enhancer regions of *MYC* and *CCND1* were selected. For better targeting efficiency and specificity of dCas9, each HIF2α was targeted with a pair of sgRNAs cloned in tandem[144]. Each tandem construct contains a two sgRNAs, each flanked by a U6 promoter and sgRNA scaffold (see materials and methods). I generated three tandem sgRNA constructs for *MYC* enhancer (iMYC1-3) and two tandem sgRNA constructs for *CCND1* enhancers (iCCND1 1-2) were already available in the lab. As a control, I used a tandem sgRNA construct carrying two non-targeting scramble sgRNAs (SCR) which was also available in the lab. All of these tandem constructs were generated using the pKLV-U6-gRNA(BbsI)-PGKpuro2ABFP plasmid. Once cloned, I transduced the 786-M1A dCas9-KRAB-mCherry cells with the iMYC, iCCND1 and SCR tandem construct. Puromycin treatment selected for the cells transduced with the tandem constructs and sorting for mCherry and BFP double positive cells ensured that only the cells expressing the dCas9-KRAB and the tandem sgRNA were being tested. I firstly validated these cells by qPCR looking at the mRNA expression of *MYC* and *CCND*1. I found that none of the iMYC constructs significantly downregulated the *MYC* expression, but both of the iCCND1 constructs downregulated the mRNA expression of *CCND1* (**Figure 5.11**).

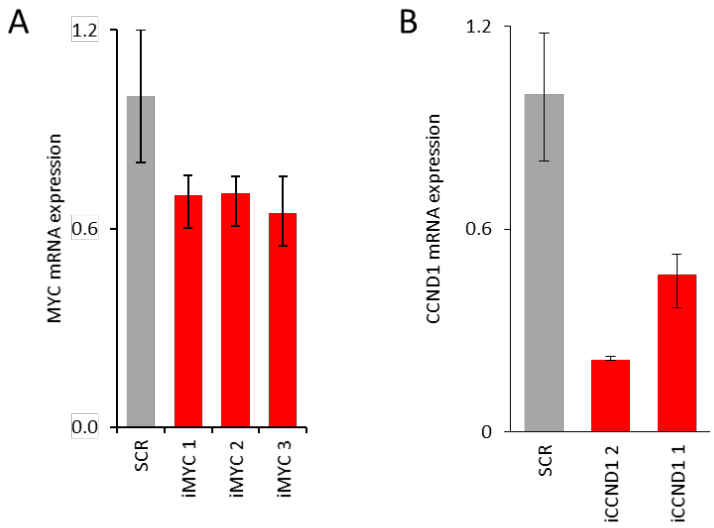

Figure 5.11 CRISPRi targeting of the *MYC* and *CCND1* enhancers. qPCRs show the mRNA expression of MYC and CCND1 normalised to *TBP* housekeeping gene expression. Data are presented relative to non-targeting scramble (SCR) control. Error bars show 95% confidence interval based on technical triplicates.

Next, I was interested to find out whether the inhibition of these enhancer sites would affect cell growth. Proliferation assay did not show any significant differences in cell growth *in vitro* (**Figure 5.12 A-B**). This was as expected, because previously I did not observe any growth advantage in cells expressing HIF2α compared to HIF2α KO cells. Therefore, the tumorigenic potential of these cells was tested *in vivo*. Two tandem sgRNA and SCR control cells were injected subcutaneously in athymic nude mice. Tumours started to form after 2 weeks and continued growing until the end of experiment. No significant difference in tumour size was observed between the SCR control and the iMYC/iCCND1 (**Figure 5.12 C-D**).

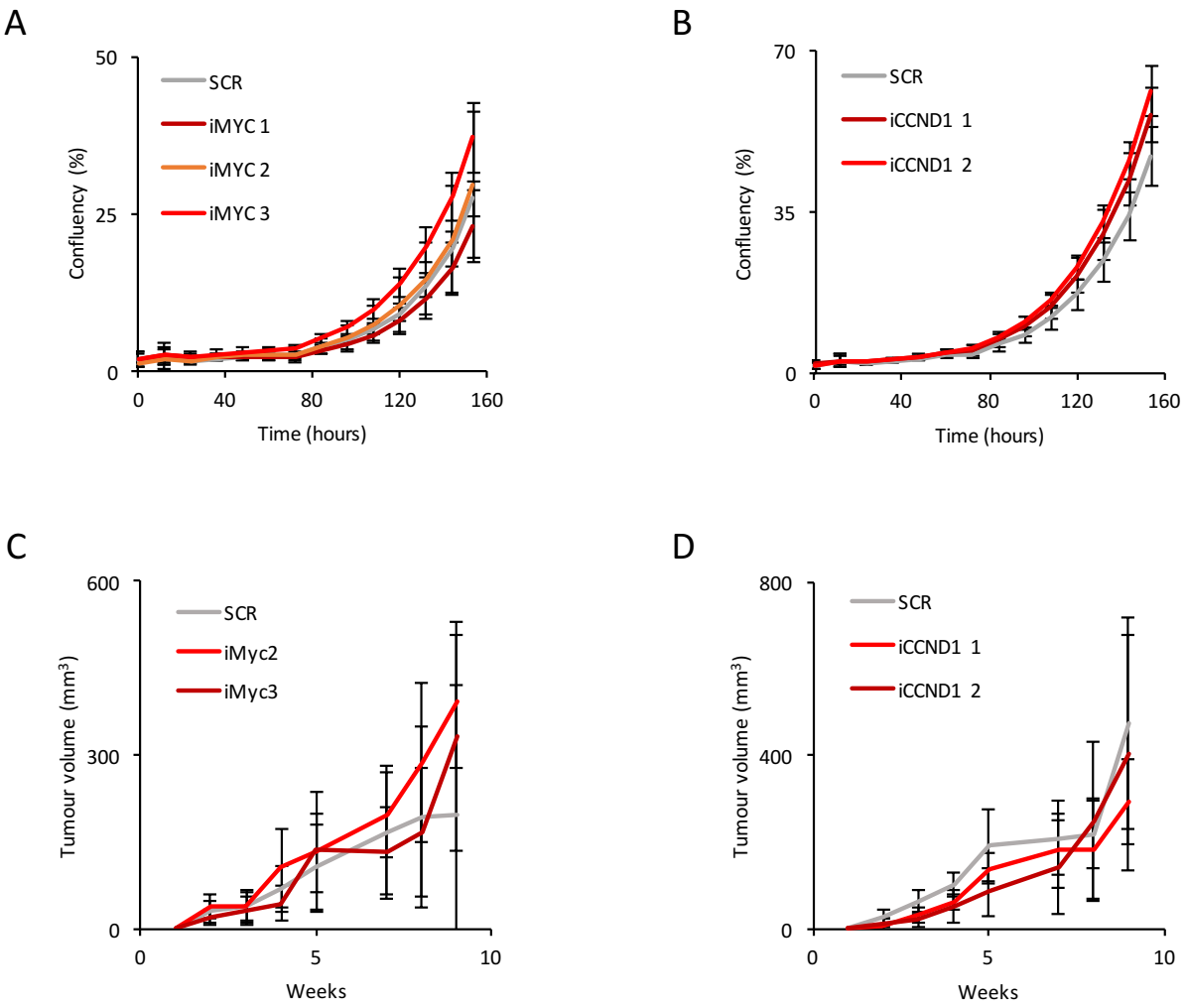

Figure 5.12 *In vitro* and *in vivo* growth of ccRCC cells with CRISPRi targeted *MYC* and *CCND1* enhancers. (A-B) *in vitro* Proliferation assays measured by Incucyte. The confluency of CRISPRi cells targeting MYC enhancer (A) and CCND1 enhancer (B) relative to non-targeting scramble control (SCR) was analysed. Error bars represent standard deviation based on technical triplicates. (C-D) Tumour volume measured by Caliper comparing the tumour size formed by CRISPRi cells targeting MYC enhancer (C) and CCND1 enhancer (D) relative to non-targeting scramble control (SCR). $0.1x10^6$ cells per flank were injected. Error bars represent standard deviation between the tumour sizes. N= 7 for SCR, N= 3 for iMYC2, N= 3 for iMYC3, N= 3 for iCCND1 1, N= 3 for CCND1 2. P value was calculated based on Student's T-test. P>0.05

5.5 Combinatorial downregulation of HIF2α bound enhancer elements *in vivo* slows down tumorigenesis

I speculated what could be the reasons for the failure of the previous *in vivo* experiment. One of the hypotheses is that clones are more sensitive compared to cell lines or simply, targeting a single gene/enhancer is not sufficient to slow down/prevent tumour growth. Furthermore, I discovered that the VHL-reintroduced M1A cell line is not sensitive to loss of HIF2α *in vivo* (unpublished data from the Vanharanta lab). To address these concerns, I decided to generate single cell clones from the M2D cell line (used for generating 7513 and 7548 clones). These clones were not genetically modified in any way and hence will have endogenous expression of HIF2α. Clones were cultured, expanded and tested. Western blot analysis confirmed that all the clones expressed endogenous HIF2α at comparable level to the parental M2D cell line (**Figure 5.13 A**).

The dependency of M2D single cell clones on HIF2α for tumorigenesis is not known. I suspect it is highly dependent on HIF2α expression, as 7513 and 7548 clones. To test whether it is true, I chose one of the clones- M2D clone 2 (C2) and I introduced VHL into it via viral transduction using the pLVX-HA-VHL-puro plasmid available in the lab. As a control I used pLVX-puro-EV (Empty vector). After the puromycin selection, I validated the cells by performing western blot which confirmed the presence of VHL in the VHL reintroduced cells. The VHL reintroduced cells lost expression of HIF2α, as expected (**Figure 5.13 B**). Proliferation assay comparing the VHL reintroduced cells compared to the EV controls did not show any growth disadvantage (**Figure 5.13 C**). To test the HIF2α dependency in M2D C2, these cells were injected subcutaneously in athymic nude mice. VHL reintroduced cells which lost expression of HIF2α did not form tumours whereas the EV control did (**Figure 5.13 D**).

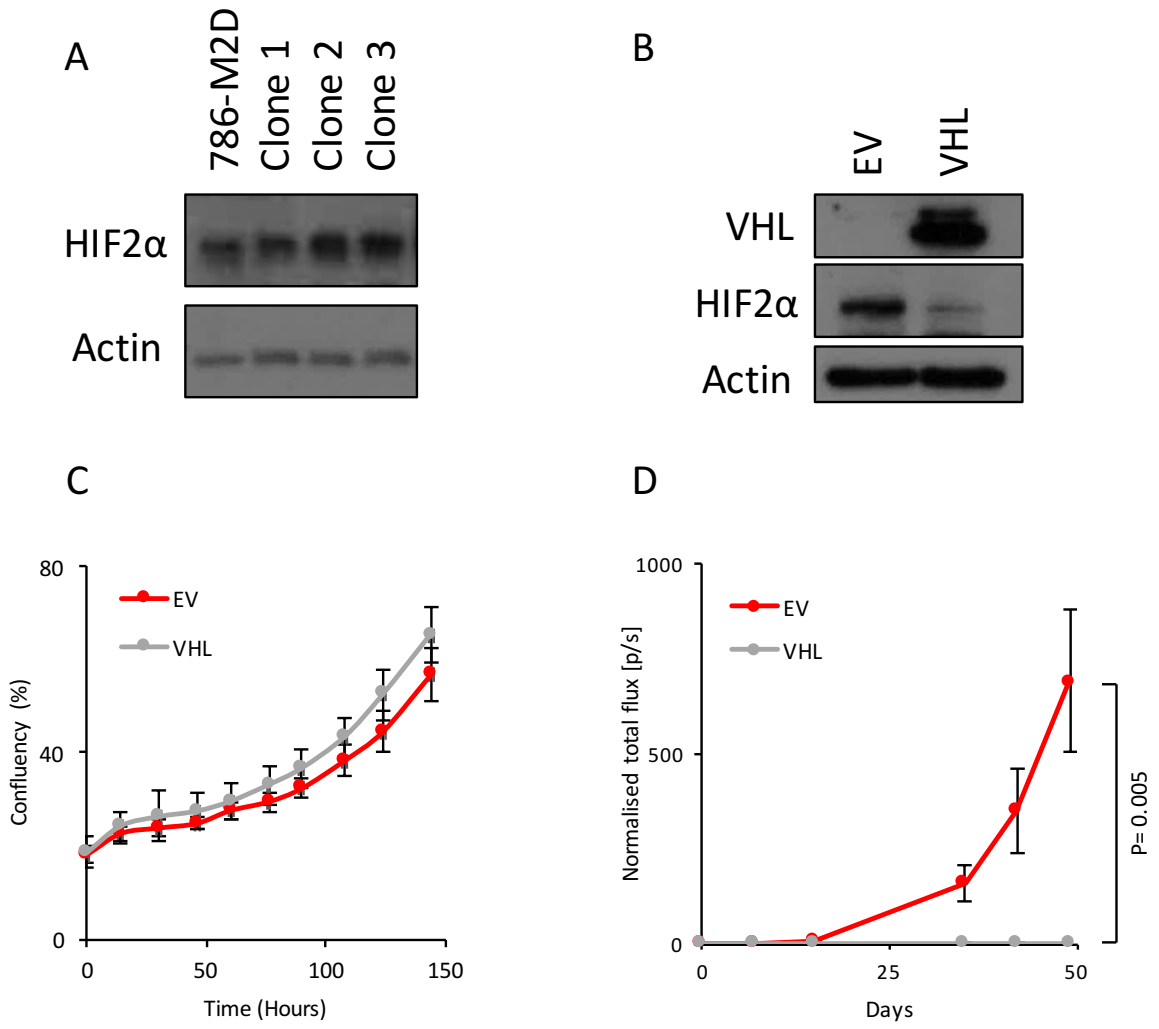

Figure 5.13 *In vivo* and *in vitro* growth of VHL re-introduced cells. (A) Western blot of HIF2α expression in 786-M2D single cell clones compared to the 786-M2D parental population. (B) Western blot of VHL and HIF2α in VHL reintroduced cells and empty vector control. β- actin was used as a loading control. (C) Proliferation assay measured by Incucyte showing the confluency of VHL reintroduced M2D C2 clone compared to control cells. Error bars represent standard deviation based on technical triplicates. (D) Tumour size measured by bioluminescence in mice injected with VHL-reintroduced and Empty vector (EV) control M2D C2 cells. Error bars represent Standard Error of the mean (SEM). P value calculated based on Student's T test. N=5 for EV, N= 5 for VHL.

This experiment confirmed the dependency of M2D C2 clone on HIF2α for tumorigenesis and therefore this clone was used for the simultaneous targeting of *MYC, CCND1* and *TGFα* enhancer regions bound by HIF2α. M2D (C2) was stably transduced with a dCas9-KRAB-mCherry construct. The tandem sgRNA approach was used, however, this time, each construct carried two sgRNA targeting different HIF2α bound enhancer region (**Figure 5.14**). A combination of sgMYC and sgTGFα was cloned in pKLV-U6-gRNA(BbsI)-PGKpuro2ABFP plasmid and a combination of two different sgCCND1 (targeting two different HIF2α bound peaks within the *CCND1* enhancer show in in **Figure 5.8 B**) were cloned in pKLV-U6-gRNA(BbsI)-PGKhygro2AeGFP. M2D C2 dCas9-KRAB-mCherry cells were transduced with tandem construct targeting HIF2α bound *MYC* and *TGFα* enhancer regions (iMT). Puromycin treatment selected for the transduced cells. These cells were then further transduced by the double *CCND1* tandem construct targeting two different HIF2α bound *CCND1* enhancer regions (iCC). Hygromycin treatment selected for positive cells. As a control, the non-targeting scramble construct (SCR) was used twice (cloned in pKLV-U6-gRNA(BbsI)-PGKpuro2ABFP and cloned in pKLV-U6-gRNA(BbsI)-PGKhygro2AeGFP). Finally, cells were triple sorted for mCherry, BFP and GFP positive cells to only include cells that express dCas9-KRAB and both tandem constructs.

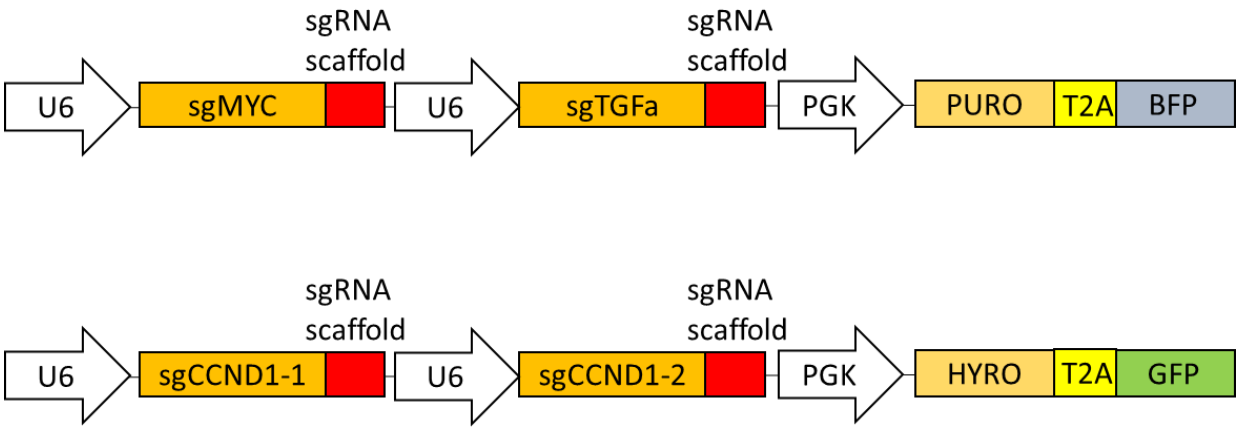

Figure 5.14 Combinatorial enhancer targeting strategy. Each tandem construct contains two sgRNAs, each flanked by a U6 promoter and sgRNA scaffold. Both constructs contain an antibiotic resistance (puromycin/hygromycin) and fluorescent marker (BFP/GFP).

I tested the CRIPSRi cells by qPCR to determine the mRNA levels of *MYC, CCND1* and *TGFα in vitro*. One of the combinations of sgRNA constructs demonstrated better result compared to others. sgMYC, sgCCND1 and sgTGFα moderately downregulated the expression of *MYC, CCND1* and *TGFα*, respectively (**Figure 5.15**).

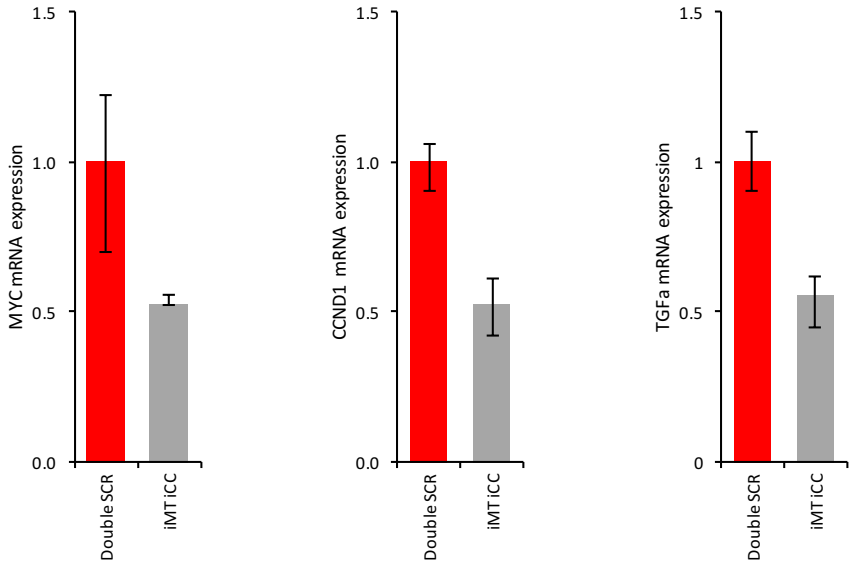

Figure 5.15 Expression of HIF2α enhancer target genes. mRNA expression of *MYC, CCND1* and *TGFα* in CRIPSRi tandem cells simultaneously targeting MYC and TGFα (iMT) and two peaks of CCND1 (iCC). Data was normalised to *TBP* housekeeping gene expression. Data are presented relative to non-targeting double scramble (SCR) control. Error bars show 95% confidence interval based on technical triplicates.

M2D C2 transduced with the iMT and iCC constructs, alongside with double non-targeting scramble control (SCR), were injected subcutaneously in athymic nude mice (**Figure 5.16**). Simultaneous downregulation of enhancer regions of *MYC, CCND1 and TGFα* slowed down tumour formation and progression.

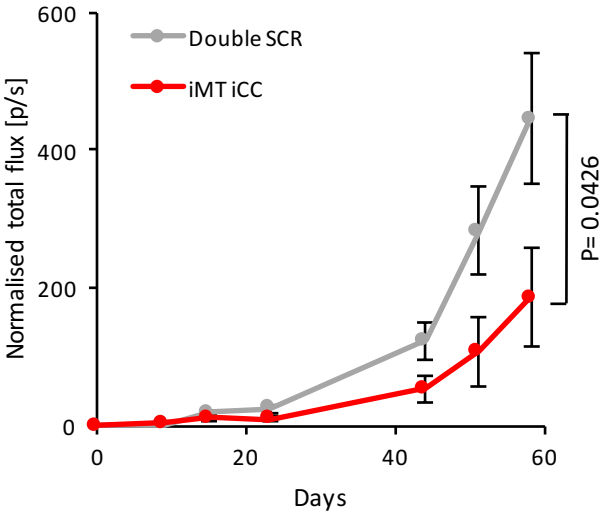

Figure 5.16 Tumour formation in cells with combinatorial enhancer targeting. Tumour size measured by bioluminescence in mice injected with iMT/iCC (targeting *MYC, CCND1 and TGFα* enhancers) and double scramble (SCR) control in M2D C2 cells. Error bars represent Standard Error of the mean (SEM). P value calculated based on Student's T test. N=5 for iMT iCC, N= 5 for SCR.

Summary

To understand the molecular mechanisms through which HIF2α drives tumorigenesis in 786-M2D clones, I compared the RNA-seq data pre- and post- HIF2α loss which revealed that genes involved in processes such as cell cycle control, homologous recombination and DNA repair are significantly downregulated following HIF2α inhibition.

H3K27ac and HIF2α ChIP-seq data suggest that HIF2α promotes tumour initiation and progression via binding the enhancer regions of genes involved in canonical oncogenic signalling and in cell cycle progression such as *MYC, CCND1* and *TGFα*.

I tested this hypothesis by performing Luciferase reporter assay *in vitro*. The assay chosen to perform this experiment was not optimal because of a Renilla luciferase leaking which interfered with NanoLuc luciferase. This assay needs more optimisation, such as using LacZ as an internal control instead of Renilla luciferase. Another reason for failure of the enhancer reporter assay could be that it is context dependent and even if HIF2α bound to the enhancer, it wouldn't activate it because it is placed out of the chromatin context.

The hypothesis that HIF2α promotes tumour growth by upregulating *MYC, CCND1* and *TGFα* via binding to their enhancers was tested using CRISPRi. Indeed, combinatorial silencing of *MYC, CCND1* and *TGFα* enhancers slowed down tumour growth, but did not prevent tumour initiation. This data suggests that *MYC, CCND1* and *TGFα* are important HIF2α downstream targets, but their transcriptional silencing was not sufficient to prevent tumorigenesis or there are another HIF2α regulated genes important for tumour maintenance. Performing a ChIP-seq after the experiment could determine to what extent were sgRNAs effective in inactivation of *MYC*, *CCND1* and *TGFα* enhancers.

Chapter 6. Conclusions and discussion

Introduction

The purpose of this study was to understand how HIF2α regulates tumour progression in ccRCC. This is of particular interest because current treatments are insufficient, and patients often develop resistance to treatment. Recently, HIF2α inhibitors were developed and early clinical studies show variable results in patient outcomes. Better understanding of ccRCC molecular dependencies and the mechanisms behind HIF2α-regulated pathways may help to understand differences in patient outcome and offer new therapeutic avenues to improve patient survival.

6.1 Generating a HIF2α-inducible genetic model to study the role of HIF2α in ccRCC progression

The importance of HIF2α in ccRCC initiation is well established. Previous studies have demonstrated that tumour suppression by pVHL can be overridden by a HIF2α variant that evades recognition by pVHL, proving that HIF2α stabilisation is necessary for tumour formation[46]. Moreover, inhibition of HIF2α using shRNA supressed tumour growth *in vivo*[47,48]. However, there are no studies investigating the importance of HIF2α in tumour maintenance. In this study, I developed a novel DOX-inducible HIF2α system which allows for studying of HIF2α and its role in ccRCC maintenance. To prevent any endogenous HIF2α expression, HIF2α KO single cell clones were generated using CRIPSR-Cas9 genome editing. Similar studies where HIF2α expression has been downregulated by shRNA[48] showed that HIF2α loss did not affect cell growth *in vitro* under standard tissue culture conditions, but prevented tumour formation *in vivo*. This is in agreement with our data where knocking out HIF2α by CRISPR-Cas9 did not affect cell growth *in vitro*, but impaired tumour formation *in vivo*. It is currently not well understood what are the molecular mechanisms leading to adaptation to loss of

HIF2α in ccRCC cells, however, these unknown compensatory events allow them to maintain cell proliferation *in vitro*, most likely by *MYC* upregulation. It is still unclear why this is not the case *in vivo*, where cells require HIF2α expression to sustain *MYC* and form tumours. The HIF2α-*MYC* correlation needs to be determined. Another possibly explanation could be the difference in cell to cell interactions. It would be interesting to perform the HIF2α activation and depletion experiments in ccRCC 3D culture or organoids. Previous studies showed that there is no detectable HIF1α present in the 786-M2D and 769-P cells[145]. The DOX-inducible HIF2α system was introduced into HIF2α KO ccRCC clones. Multiple ccRCC cell lines were tested *in vitro* and demonstrated a favourable DOX responsiveness profile. Though antibiotic treatment selected for cells that expressed the DOX-inducible HIF2α construct, not all cells were expressing it. To account for that, cells of interest were sorted by FACS. Upon DOX introduction, increased expression of *HIF2α* and its downstream target gene *CXCR4* was observed. Both, HIF2α and CXCR4 expression were variable following treatment with DOX. Differences in HIF2α expression could be due to variability in number and site of exogenous HIF2α integration, which could also contribute to variable *CXCR4* expression. Variability in *CXCR4* expression could also be due to differences in individual clones. Not all clones have the same basal level of *CXCR4* expression. Subsequent activation of HIF2α further upregulates the *CXCR4* expression. Another limitation of this system is the level of exogenous HIF2α expression which was constantly higher in clones compared to the respective parental cell lines. DOX was also demonstrated to alter metabolism towards more glycolytic phenotype and slower proliferation[146]. To account for that, I experimentally determined the lowest amount of DOX that would still induce the expression of HIF2α (0.3 μg/mL rather than the standard 1μg/mL). Regardless of the amount of DOX treatment used, the system was effective in turning the expression of HIF2α on and off, but it did not allow for controlling of the HIF2α

levels that were being expressed. Overall, the *in vitro* characterisation performed in six clones showed that the inducible HIF2α system generated in this study is variable, but reproducible.

Clones from five ccRCC cell lines were characterised *in vitro*, but only clones from the 786-M2D cell line were capable of forming tumours *in vivo* when HIF2α was activated. ccRCC is a highly heterogenous disease[13] which may account for the observed differences in the cells ability to form tumours. It is possible that certain single cell clones may not have expressed tumorigenic potential, but the heterogenous population of cells enabled tumour growth. To demonstrate the role of HIF2α in ccRCC maintenance in these cell lines, an alternative approach such as DOX-inducible shEPAS1 could be used in future work.

6.2 HIF2α addiction, tumour microenvironment and tumour dormancy

Generally, tumorigenesis is caused by activation of oncogenes or inactivation of tumour suppressor genes. Some cancers respond to targeted inactivation of oncogenes, a phenomenon called oncogene addiction[80]. In some cases, oncogene inactivation results in complete tumour regression, but in other cases, some cells remain, convert to dormant latent tumour cells and can regain the ability to self-renew upon oncogene reactivation[147]. In these cases, tumour cell autonomous and host dependent programs are both regulating the balance between self-renewal and cell death or senescence. Tumour microenvironment (TME) also plays an important role in tumour initiation, progression and regression. Thus, the interplay between these factors and their regulation of cell renewal programs defines the future of the regressing tumour.

In *VHL*$^{-/-}$ ccRCC, HIF2α stabilisation is the main driver of tumour initiation based on studies demonstrating that activation of HIF2α leads to tumorigenesis in VHL-reintroduced cells[46]. Using the DOX-inducible HIF2α model, HIF2α activation resulted in tumour growth *in vivo*. HIF2α inactivation resulted in decreased expression of HIF2α downstream target genes and sustained tumour regression. Within the first three days, tumours regressed significantly, cells underwent proliferative arrest associated with loss of cell renewal (decrease in Ki67 staining) and apoptosis (increase in Cas3 staining). Tumours regressed completely within thirty days post HIF2α inactivation. However, as observed by bioluminescent imaging, some signal remained for up to six weeks. This suggests that the loss of HIF2α has an anti-proliferative effect and in a small subset of cells it has cytostatic, rather than cytotoxic effect. Cho *et al.*[148] also observed a similar response to HIF2α antagonist where a drug washout led to an increase in HIF2α activity followed by an decrease in HIF2α activity after drug rechallenge. A similar observation has been shown in a study of *MYC* dependency in a pancreatic cancer mouse model[149]. In fact, dormant cancer cells were found to remain in the tumour site upon *MYC* inactivation. A significant number of these residual cells expressed cancer stem cell markers, and re-activation of *MYC* in these cells led to rapid cancer recurrence. This suggests that some tumour cells remained in a state of dormancy. In fact, in our system, when HIF2α expression was re-induced, these dormant tumour cells regained the ability to self-renew and formed tumours. However, it is unclear whether these cells would eventually be able to activate HIF2α or overcome HIF2α addiction and start proliferating without induced HIF2α activation. It would be interesting to see if these tumours would regress again upon HIF2α inactivation. An additional control could be added to these set of experiments where DOX-inducible HIF2α ccRCC cells *in vivo* would be maintained without the DOX throughout the experiment to see if they would acquire the potential to form tumours without DOX-induced HIF2α activation.

Regarding resistance to HIF2α inhibition, data from preclinical studies using HIF2α inhibitors only showed that prolonged treatment led to resistance due to alterations of the drug target (mutation in HIF2α/HIF1β binding sites)[77,78]. Interestingly, in other tumour types, tumours could not regrow once they regressed following oncogene inactivation. Studies by Jain *et al*.[150] and Flores *et al*.[151] demonstrated that a brief inactivation of *MYC* in osteosarcoma cells and keratinocytes led to a growth arrest and a spontaneous differentiation which made the cells insensitive to subsequent *MYC*-induced tumorigenesis. In the case of osteosarcoma cells, MYC reactivation led to induced apoptosis, however, MYC reactivation in keratinocytes led to terminal differentiation and shedding. These examples demonstrate that the same oncogene plays many different roles that are greatly dependent on the specific cell type. Given that in ccRCC HIF2α promotes MYC activity[43] and MYC expression is downregulated following HIF2α inactivation, it would be interesting to know whether the phenotype I observed is due to loss of HIF2α or MYC, or the combination of both. This could be addressed by an experiment where tumorigenesis would be induced by HIF2α activation, followed by HIF2α inactivation and activation of MYC (using an alternative conditional system such as MYC-ERT). This experiment would confirm whether MYC activation is sufficient to form tumours in cells that previously showed oncogenic potential.

Host immune cells generally serve as a barrier against tumour formation[152]. Activation of the immune host response can contribute to tumour regression through both adaptive and innate immune effectors[102,103,153]. In fact, tumour-infiltrating cells can demonstrate either tumour suppressive or tumour promoting effects, depending on cancer type and model used. For example, regulatory T cells and tumour-associated macrophages (TAM) have been previously associated with a pro-tumour function[154,155], whereas $CD8^+$ T cells have been associated with

improved clinical outcomes and response to immunotherapy[156]. In ccRCC, HIF2α inactivation led to rapid tumour regression in athymic nude mice. To investigate the role of the host immune system in the DOX-inducible HIF2α model, a severely immunodeficient NSG mouse strain was used. After tumours were fully formed, HIF2α inactivation led to sustained tumour regression which occurred despite the lack of T cells, B cells, NK cells and cytokine signalling. This suggests that in the ccRCC model presented in this study, HIF2α inactivation leads to sustained tumour regression despite the lack of an adaptive immune system.

Nonetheless, TME in ccRCC patients' tumours seems to play an important role. A study comparing an immune infiltration score and a T cell infiltration score across 19 cancer types showed that ccRCC scores highly in both[157]. They characterized three groups of ccRCC tumours: T cell enriched, heterogeneously infiltrated, and non-infiltrated. Despite a high level of T cell infiltration and effector molecules associated with it (granzyme B and interferon γ), patients in the T cell enriched class exhibited poorer outcomes compared to the non-infiltrated group. Distinct subsets of T cells also showed variable prognostic values, such as Th17 which was strongly associated with a positive outcome or Th2 and Treg cells which were associated with a negative outcome. Another study evaluated the immune landscape of ccRCC patients based on a mass cytometry[158]. They revealed a phenotypic complexity in TME and identified well-defined subsets of T cells and TAM that are present within ccRCC TME. The concurrence of M-11 and M-13 TAM clusters was associated with more positive outcomes compared to the concurrence of T cells and M-5 TAM clusters which was associated with a poorer clinical outcome. These observations demonstrate that the immune system does plays an important role in tumour progression and regression in ccRCC patients and highlights the need for a better more reliable mouse models of ccRCC.

6.3 Modelling the response to HIF2α inhibition in ccRCC

The inducible HIF2α genetic model serves to investigate the molecular mechanisms involved in ccRCC maintenance. This is of particular interest because HIF2α inhibitors are currently in early clinical trials and understanding the mechanisms through which HIF2α maintains tumour progression can help to predict patient outcome and guide patient therapy.

RNA-seq was performed using tumours with activated HIF2α and tumours with inactivated HIF2α. IPA and GSEA demonstrated that cell cycle progression, homologous recombination and DNA replication pathways are significantly downregulated following HIF2α inhibition. This observation is consistent with the study by Chen and colleagues[77] where they treated patient-derived xenografts (PDX) models with the HIF2α antagonist. They observed that tumours sensitive to the treatment exhibited a distinguishing gene expression signature, such as downregulation of cell cycle, DNA replication and DNA repair processes (**Figure 6.1**).

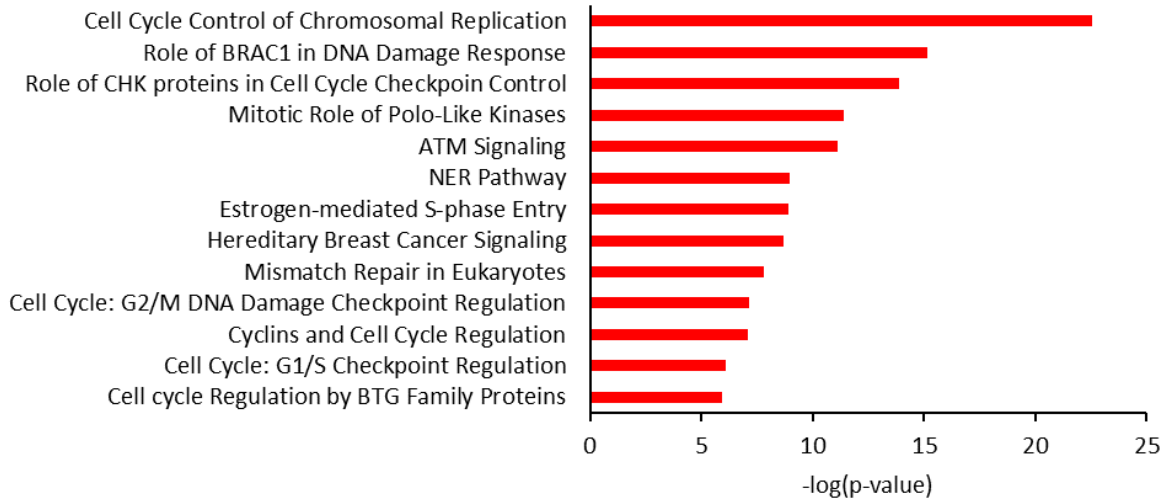

Figure 6.1 RNA-seq analysis of tumours sensitive to HIF2α antagonist. List of pathways most significantly downregulated following the HIF2α antagonist treatment, generated by Ingenuity pathway analysis (IPA).

The correlation of RNA-seq data presented in this study and the one generated by Chen *et al.*[77] demonstrates that the HIF2α inducible system recapitulates the phenotype observed in PDX following HIF2α inhibition.

The HIF2α inducible system allows for temporal control of HIF2α expression *in vivo*. Therefore, to study the immediate effects of HIF2α inhibition, we collected tumour samples immediately after HIF2α inactivation (when there were no detectable traces of HIF2α and before tumours started to regress) and performed RNA-seq. Cell cycle and DNA damage response signature were within the top downregulated pathways, suggesting that HIF2α may be directly regulating these processes. Interestingly, HIF2α has been previously associated with regulation of DNA repair genes, which may explain the resistance to radiotherapy often seen in ccRCC patients[159]. Studying the differentially expressed genes, we found that *CCND1* was consistently the most significantly downregulated gene. *TGFα* and *MYC* were also very significantly downregulated compared to other known HIF2α regulated genes.

6.4 Role of *MYC, CCND1* and *TGFα* in ccRCC

Role of MYC in ccRCC

MYC is a proto-oncogene encoding for a nuclear phosphoprotein which plays a role in G1-S cell cycle progression, apoptosis and cellular transformation[160]. MYC forms a heterodimer with its binding partner MAX. The MYC/MAX complex binds E-box DNA consensus sequences and regulates the transcription of genes involved in cell cycle progression (*Cyclin D1* and *E2F1*), ribosome biogenesis and biomass accumulation[161]. MYC also inhibits the expression of genes such as *p21* and *p27,* by binding to their transcription initiator element in a complex with MAX and SP1/MIZ1[162,163]. Importantly, *MYC* has been identified as one of the most

commonly deregulated oncogenes in a wide range of cancers[164]. The most commonly observed *MYC* deregulation is via gene amplification. *MYC* amplification was first identified in the human leukaemia cell line HL60[165] but as since then been observed in many cancers, such as neuroblastoma, lung cancer and breast cancer to list a few[166–168]. *MYC* mutations and translocations, such as those observed in multiple myeloma, have been associated with multiple cancers[164,169]. The Cancer Genome Atlas (TCGA) data further supports that *MYC* is mutated across many cancers. However, in ccRCC *MYC* is very rarely mutated (**Figure 6.2**)[170].

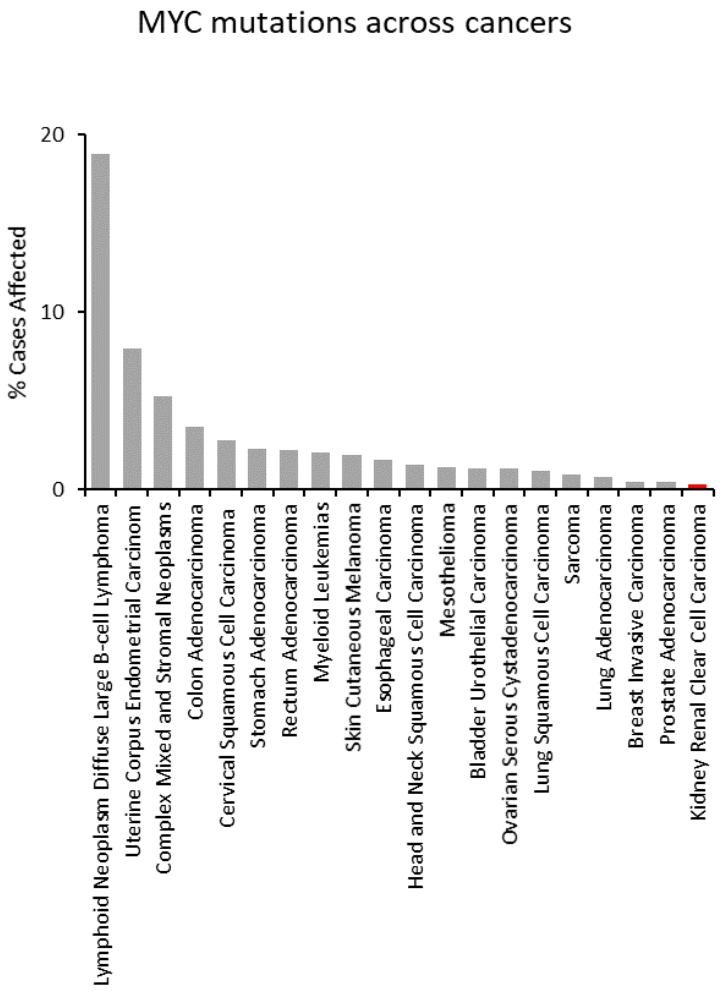

Figure 6.2 *MYC* mutations across cancers. Source: TCGA

Studies by Gordan and colleagues[43] have previously suggested that HIF2α enhances MYC expression in ccRCC. They generated a *HIF2α* knockdown and a *MYC* knockdown and showed that *MYC* regulated genes such as *CCND1* and *p28* are equally deregulated in the absence of either HIF2α or MYC [43].

Our H3K27 and HIF2α ChIP-seq analysis revealed strong binding within the MYC promoter and within a set of prominent peaks downstream of the *MYC* gene, suggesting the presence of a *MYC* enhancer. In fact, a renal cancer susceptibility locus was identified within this *MYC* enhancer[134]. Differential HIF2α binding was associated with this Single Nucleotide Polymorphism (SNP) which affected accessibility and activity of this site.

Role of CCND1 in ccRCC

The most significantly downregulated gene based on our RNA-seq data analysis was *CCND1*. *CCND1* belongs to the family of highly conserved cyclins. Cyclins function as regulators of Cyclin Dependent Kinases (CDK). They exhibit a distinct expression and degradation pattern which aids coordination of each mitotic event. CCND1 regulates the activity of CDK4/CDK6 which are required for G1 to S transition[171]. *CCND1* has been shown to be deregulated by mutation, amplification and overexpression in many cancer types which alters cell cycle progression and contributes to tumorigenesis[172]. Exceptionally high *CCND1* levels have been detected in Mantle Cell lymphoma, where point mutations and genomic deletions created a more stable form of CCND1[173]. Deregulation of *CCND1* is observed in pancreatic and head and neck cancers. In these cancers, increased CCND1 expression is also associated with higher

tumour grade and poorer patient outcomes[174,175]. In the case of ccRCC, CCND1 is rarely mutated[170] (**Figure 6.3**).

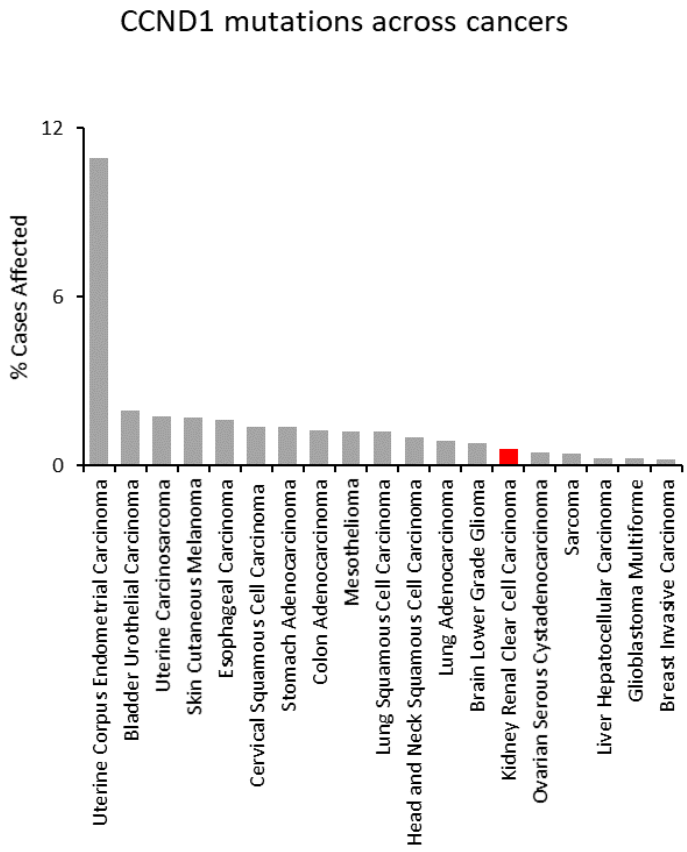

Figure 6.3 *CCND1* mutations across cancers. Source: TCGA

The regulation of *CCND1* gene has been previously associated with both *HIF2α* and *MYC*[176,177]. *CCND1* regulation by HIF2α in ccRCC has been suggested by observing that HIF2α overexpression, as observed in ccRCC, leads to enhanced expression of *CCND1*. HIF2α downregulation by siRNA downregulated *CCND1* mRNA[178]. The importance of *CCND1* in ccRCC has been demonstrated by Zhang and colleagues[179] by showing that suppression of *CCND1* by shRNA impaired tumour growth.

Our ChIP-seq data showed a prominent HIF2α peak upstream of *CCND1*, suggesting that there is an active enhancer of *CCND1.* In fact, Schodel *et al.*[135] revealed an RCC susceptibility locus

within this HIF2α bound *CCND1* enhancer. The RCC-protective SNP disrupts HIF2α binding, DNA accessibility and interaction with transcriptional apparatus. Interestingly, our ChIP-seq data also revealed an existence of an *in vivo* specific peak in the *CCND1* enhancer locus.

Role of TGFα in ccRCC

TGFα is a mitogenic polypeptide capable of binding and activating protein kinase receptors such as epidermal growth factor receptor (EGFR), leading to cell proliferation, differentiation and development[180]. TGFα is involved in transformation of normal cells into malignant cells and an increase in TGFα synthesis is commonly observed in many cancer types such as breast and lung cancers[181–183]. In ccRCC, mutations of *TGFα* are not very common (**Figure 6.4**)[170].

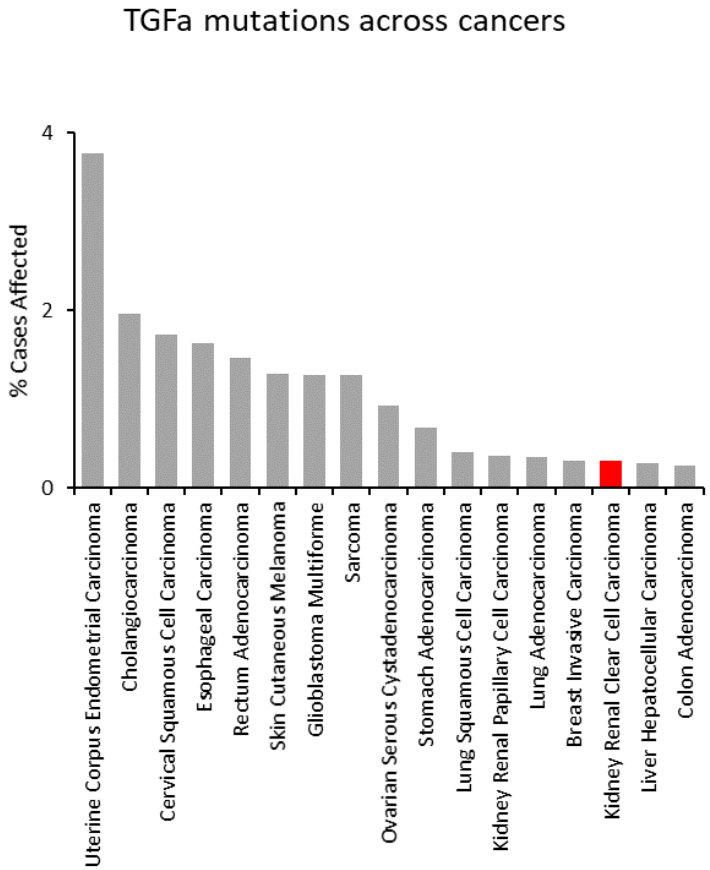

Figure 6.4 *TGFα* mutations across cancers. Source: TCGA

A study by Petrides and colleagues[184] demonstrated that TGFα is overexpressed in ccRCC patient tissue compared to normal tissue from the same subjects. They also found that increased TGFα expression levels correlated with a poorer patient prognosis[184,185]. Treatment with inhibitors of EGFR was effective in reducing tumour volume in RCC xenograft models and in tumours growing orthotopically in the renal subcapsule[186]. HIF2α has been shown to regulate the expression of TGFα in ccRCC by demonstrating that a dominant negative HIF2α and enzymatic inhibition of EGFR were equally effective in abolishing EGFR activation[187]. Furthermore, TGFα, unlike other HIF2α targets, can stimulate serum-independent growth of *VHL*$^{-/-}$ cells. In fact, ccRCC cells that expressed a mutant VHL which had the ability to degrade HIF2α failed to overproduce TGFα and proliferate in a serum-free medium[187].

Despite the fact that *MYC, CCND1* and *TGFα* are known to be highly deregulated in ccRCC, they are not mutated. An indirect link between these genes and HIF2α has been previously suggested, mostly based on *in vitro* studies. Here, I used a novel HIF2α-inducible genetic model to study the direct effects of HIF2α loss *in vivo*. Using this system, I showed that *MYC, CCND1* and *TGFα* and pathways associated with these genes are very significantly downregulated immediately after HIF2α is inactivated. Furthermore, the expression of these genes seems to be dependent on the activation of HIF2α bound distal enhancer elements present in the locus of each one of them.

6.5 Simultaneous inactivation of *MYC, CCND1* and *TGFα*

The data presented in this study suggests that HIF2α directly upregulates the expression of *MYC, CCND1* and *TGFα* by binding to their respective specific enhancer region. To test this hypothesis, CRISPRi was used to transcriptionally downregulate the activity of the *MYC, CCND1* and *TGFα* enhancers. Several sgRNAs targeting each one of the enhancers present in the locus of each of these genes were tested. *In vitro* characterisation of the generated cell lines was not optimal. Most of the sgMYC tested were not very efficient at downregulating *MYC* mRNA. This may be because cells *in vitro* do not depend on HIF2α and most likely acquired other mechanisms to upregulate *MYC*. Moderate downregulation of *CCND1* and *TGFα* was achieved by sgCCND1 and sgTGF*α,* respectively. These cells were injected subcutaneously into nude athymic mice. I suspect that the transcriptional repression of the *MYC, CCND1* and *TGFα* enhancers prevented HIF2α from binding to these elements and resulted in decreased tumour growth. Through this I demonstrated that HIF2α regulates tumour growth and progression by directly upregulating canonical oncogenic signalling such as upregulation of *MYC, CCND1* and *TGFα* via enhancer interaction.

Downregulation of *MYC, CCND1* and *TGFα* slowed down tumour growth, but it did not prevent tumour formation. HIF2α regulates many genes and it is possible that downregulation of these three genes alone was insufficient in preventing tumorigenesis. It is also possible that the tandem sgRNA approach did not downregulate the activation of the enhancers of these genes to a sufficient extent to prevent their expression and therefore completely abrogate tumour growth. Performing a ChIP-seq on these tumours could reveal whether CRISPRi targeting of these enhancer regions have worked.

6.6 Chromatin landscape and the role of enhancers in ccRCC

The importance of aberrations in cis-acting non-coding regulatory regions in ccRCC tumorigenesis has not been widely studied. However, recent studies suggest that VHL loss contributes considerably to enhancer remodelling in ccRCC cell lines and tumours[188]. A study by Yao *et al*. demonstrated that VHL, apart from its role in oxygen sensing, also safeguards the chromatin landscape[188]. They observed that VHL loss induced tumour-specific enhancer gains, whilst VHL restoration in ccRCC delayed tumour growth *in vivo* and caused more prominent changes to enhancers than to promoters. In fact, extensive enhancer malfunction has been associated with ccRCC, with binding of enhancer-centric HIF2α and recruitment of histone acetyltransferase p300 at pre-existing lineage-specific promoter–enhancer complexes[188]. A study by Smythies and colleagues[189] demonstrated that HIF2α binds to promoter-distal elements and HIF2α binding occurs predominantly in H3K27ac enriched regions, a marker of active enhancers. Their study showed that HIF2α interacted with tissue-specific transcription factors (such as *FOXA1* and *FOXA2*), suggesting that HIF2α may have a tissue specific role. Tissue specificity has been previously observed in case of HIF2α in ccRCC. SNPs located within the *MYC* and *CCND1* enhancers have been shown to be mediated by HIF2α only in renal cell lines[134,135].

HIF2α ChIP-seq analysis (performed in our lab) comparing HIF2α binding *in vivo* and *in vitro* demonstrated that there are specific *in vivo* HIF2α peaks suggesting the existence of *in vivo* exclusive interactions between HIF2α and other transcription factors (**Figure 6.5**). This data suggests possible interactions between HIF2α and PAX transcription factors. PAX2 and PAX8 are known to control the kidney development and are also expressed in RCC[190]. The

differences in the apparent role of HIF2α *in vivo* and *in vitro* may explain the HIF2α requirement for cell survival in each condition.

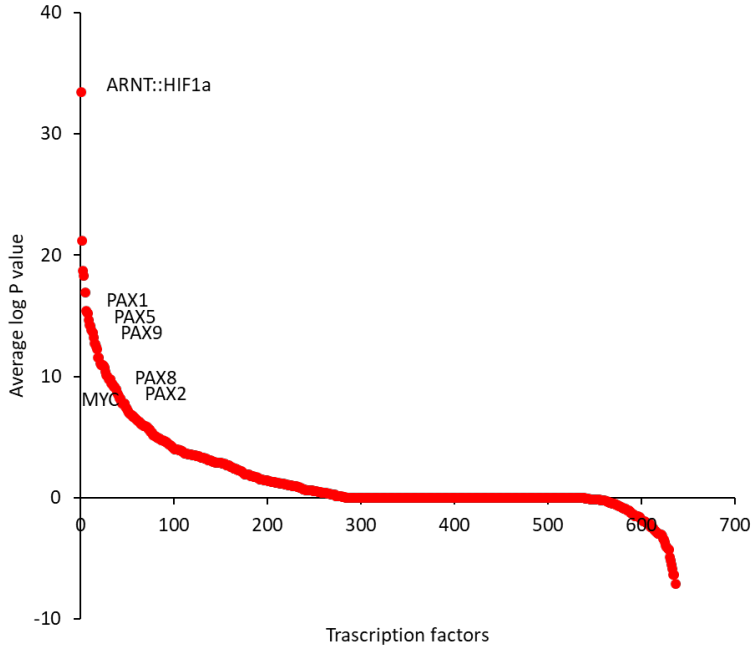

Figure 6.5 Transcription factor binding motif analysis in *in vivo* versus *in vitro* HIF2α ChIP-seq. All binding motifs present within 100bp around the HIF2α binding peaks are shown in red.

6.7 Implications for a novel ccRCC therapy

Improvements in understanding molecular mechanisms underlying ccRCC biology have led to the discovery of new targetable pathways. Several agents such as tyrosine kinase inhibitors, mTOR inhibitors and immune checkpoint inhibitors have been approved for treatment of advanced RCC. Combinations of these treatments showed promising clinical efficacy.

HIF2α inhibitors have only recently been developed and are currently undergoing early clinical trials. HIF2α inhibitors are well tolerated by patients, but the observed patient response was very variable. Only 2% of patients responded completely to the treatment, 12% responded partially and 52% of patients maintained stable disease[76].

The HIF2α controllable model I generated allows the study of molecular pathways underlying HIF2α inhibition and may be able to elucidate the reason behind the observed variations in patient response. Using this model, I observed complete tumour regression following HIF2α inhibition, reflecting the response of the small fraction (2%) of patients who responded completely to treatment. *MYC, CCND1* and *TGFα* and overall cell cycle progression signature appeared to be most significantly downregulated immediately following HIF2α inhibition. We suspect that the rest of the patients' tumours (those that responded partially or not at all) were able to maintain cell cycle progression independent of HIF2α.

Sustained proliferative ability is a hallmark of cancer. The regulation of cell cycle progression via CDKs and Cyclins is deregulated in many cancers[191]. A number of potent small molecule CDK inhibitors have been developed since early 1990s. Many of these inhibitors have lacked selectivity within the CDK family, leading to toxicity[192]. Development of novel, specific CDK inhibitors have emerged as a novel promising therapy for the treatment of advanced cancers. One of them, CDK4/6 inhibitor in particular, became recently approved as a single-agent treatment for breast cancer[193].

Data presented in this study, such as increased cell cycle progression in ccRCC and *CCND1* deregulation, suggests that ccRCC patients might benefit from combinatorial treatment such as HIF2α inhibitors in combination with CDK4/6 inhibitors. This is in agreement with a shRNA screen, where 88 kinases targeted in $VHL^{-/-}$ ccRCC cell lines showed sensitivity to loss of CDK6[194]. The study also found an increased sensitivity to CDK4/6 inhibitors in $VHL^{-/-}$ cells compared to VHL restored cells.

Summary and Model

ccRCC is characterised by inactivation of VHL, leading to stabilisation and accumulation of HIF2α. The role of HIF2α in ccRCC initiation has been previously demonstrated, but it remains unclear whether it is necessary for tumour maintenance. Therefore, the aim of this study was to investigate the role of HIF2α in ccRCC maintenance. To do that, I generated a novel HIF2α controllable system which was tested *in vitro* and *in vivo*. Our results confirmed that HIF2α is necessary for tumour formation and that HIF2α maintains tumour growth by upregulating oncogenes involved in cell cycle progression such as *MYC, CCND1* and *TGFα.* Studying the ccRCC chromatin landscape, we discovered that HIF2α binds to enhancers of *MYC, CCND1* and *TGFα.* Transcriptional inactivation of these regions confirmed that HIF2α interaction with these enhancer regions drives the expression of *MYC, CCND1* and *TGFα* in ccRCC. In conclusion, this study demonstrated that HIF2α drives the expression of *MYC, CCND1* and *TGFα* by directly interacting with their enhancers. This interaction is important for both tumour initiation and maintenance (**Figure 6.6**).

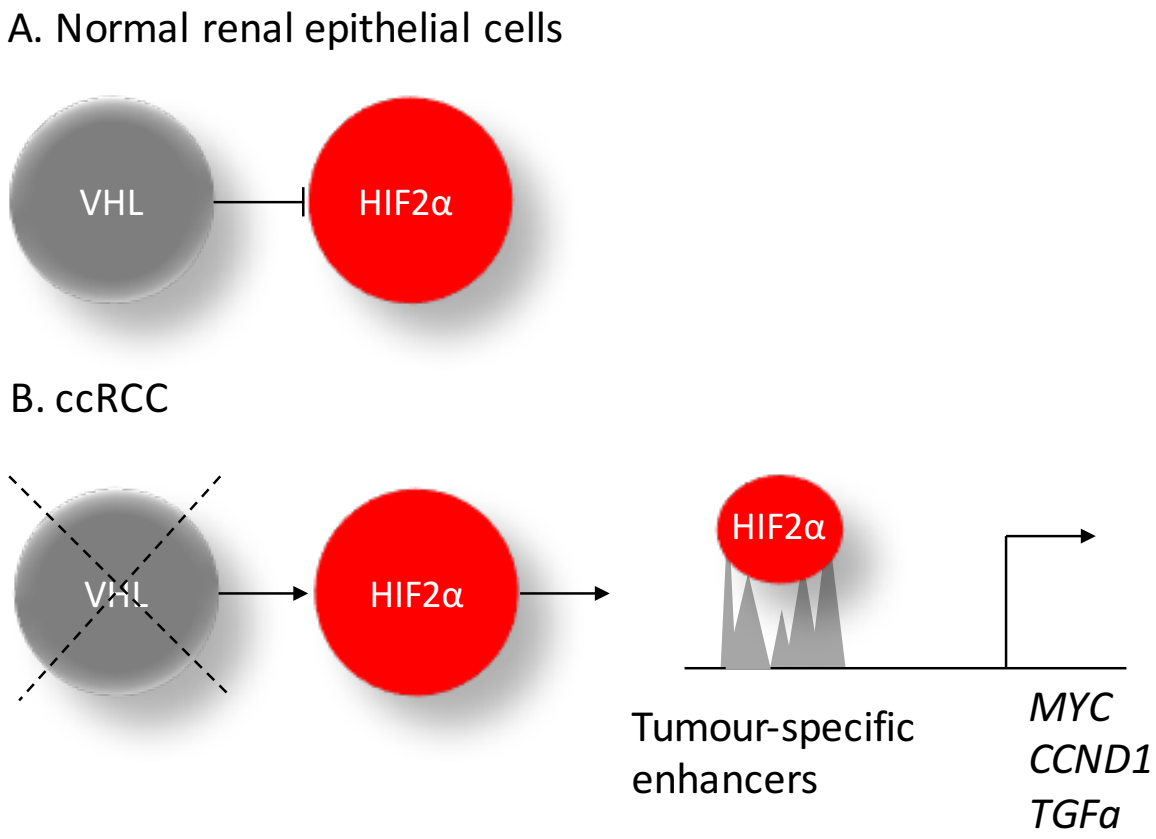

Figure 6.6 ccRCC model. (A) In normal epithelial cells, VHL targets HIF2α for degradation. (B) In ccRCC, VHL is inactivated, HIF2α is stabilized, it binds to enhancer regions of *MYC, CCND1* and *TGFα* and leads to their overexpression.

References

1. Molnar, C. & Gair, J. *Concepts of Biology—1st Canadian Edition*. (2013).

2. UK, K. R. The kidneys-a basic guide. Available at: https://www.kidneyresearchuk.org/health-information/resources/the-kidneys-a-basic-guide. (Accessed: 2nd January 2019)

3. Frew, I. J. & Moch, H. A Clearer View of the Molecular Complexity of Clear Cell Renal Cell Carcinoma. *Annu. Rev. Pathol.* **10,** 263–289 (2015).

4. Cancer Research UK. Available at: https://www.cancerresearchuk.org/healthprofessional/%250Acancer-statistics/statistics-by-cancer-type/kidneycancer/%250Aincidence. (Accessed: 4th January 2019)

5. Hunt, J. D., Van Der Hel, O. L., McMillan, G. P., Boffetta, P. & Brennan, P. Renal cell carcinoma in relation to cigarette smoking: Meta-analysis of 24 studies. *Int. J. Cancer* **114,** 101–108 (2005).

6. Renehan, A. G., Tyson, M., Egger, M., Heller, R. F. & Zwahlen, M. Body-mass index and incidence of cancer: a systematic review and meta-analysis of prospective observational studies. *Lancet* **371,** 569–78 (2008).

7. Chow, W.-H., Gridley, G., Fraumeni, J. F. & Järvholm, B. Obesity, Hypertension, and the Risk of Kidney Cancer in Men. *N. Engl. J. Med.* **343,** 1305–1311 (2000).

8. Shuch, B. *et al.* Understanding pathologic variants of renal cell carcinoma: Distilling therapeutic opportunities from biologic complexity. *Eur. Urol.* **67,** 85–97 (2015).

9. Henderson, A., Douglas, F., Perros, P., Morgan, C. & Maher, E. R. SDHB-associated renal oncocytoma suggests a broadening of the renal phenotype in hereditary paragangliomatosis. *Fam. Cancer* **8,** 257–260 (2009).

10. Verine, J. *et al.* Hereditary renal cancer syndromes: An update of a systematic review. *European Urology* **58,** 701–710 (2010).

11. Sato, Y. *et al.* Integrated molecular analysis of clear-cell renal cell carcinoma. *Nat. Genet.* **45,** 860–7 (2013).

12. Rini, B. I. & Atkins, M. B. Resistance to targeted therapy in renal-cell carcinoma. *Lancet Oncol.* **10,** 992–1000 (2009).

13. Gerlinger, M. *et al.* Intratumor Heterogeneity and Branched Evolution Revealed by Multiregion Sequencing. *N. Engl. J. Med.* **366,** 883–892 (2012).

14. Vanharanta, S., Shu, W., Brenet, F., Hakimi, A. A. & Heguy, A. Epigenetic expansion of VHL-HIF signal output drives multiorgan metastasis in renal cancer. *Nat Med* **19,** 50–56 (2013).

15. Creighton *et al.* Comprehensive molecular characterization of clear cell renal cell

carcinoma. *Nature* **499,** 43–49 (2013).

16. Wang, S.-S. *et al.* Bap1 is essential for kidney function and cooperates with Vhl in renal tumorigenesis. *Proc. Natl. Acad. Sci. U. S. A.* **111,** 16538–43 (2014).

17. Turajlic, S. *et al.* Deterministic Evolutionary Trajectories Influence Primary Tumor Growth: TRACERx Renal. *Cell* **173,** 595–610 (2018).

18. Turajlic, S. *et al.* Tracking Cancer Evolution Reveals Constrained Routes to Metastases: TRACERx Renal. *Cell* **173,** 581–594 (2018).

19. El-Mokadem, I. *et al.* Chromosome 9p deletion in clear cell renal cell carcinoma predicts recurrence and survival following surgery. *Br. J. Cancer* **111,** 1381–1390 (2014).

20. Monzon, F. A. *et al.* Chromosome 14q loss defines a molecular subtype of clear-cell renal cell carcinoma associated with poor prognosis. *Mod. Pathol.* **24,** 1470–1479 (2011).

21. Mitchell, T. J. *et al.* Timing the Landmark Events in the Evolution of Clear Cell Renal Cell Cancer: TRACERx Renal. *Cell* **173,** 611–623 (2018).

22. Ohh, M. *et al.* The von Hippel-Lindau Tumor Suppressor Protein Is Required for Proper Assembly of an Extracellular Fibronectin Matrix. *Mol. Cell* **1,** 959–968 (1998).

23. Grosfeld, A. *et al.* Interaction of hydroxylated collagen IV with the von Hippel-Lindau tumor suppressor. *J. Biol. Chem.* **282,** 13264–13269 (2007).

24. Schermer, B. *et al.* The von Hippel-Lindau tumor suppressor protein controls ciliogenesis by orienting microtubule growth. *J. Cell Biol.* **175,** 547–554 (2006).

25. Okuda, H. *et al.* Direct interaction of the beta-domain of VHL tumor suppressor protein with the regulatory domain of atypical PKC isotypes. *Biochem. Biophys. Res. Commun.* **263,** 491–7 (1999).

26. Kuznetsova, A. *et al.* von Hippel-Lindau protein binds hyperphosphorylated large subunit of RNA polymerase II through a proline hydroxylation motif and targets it for ubiquitination. *Proc. Natl. Acad. Sci. U. S. A.* **100,** 2706–2711 (2003).

27. Maxwell, P. H. *et al.* The tumour suppressor protein VHL targets hypoxia-inducible factors for oxygen-dependent proteolysis. *Nature* **399,** 271–275 (1999).

28. Ivan, M. *et al.* HIFalpha targeted for VHL-mediated destruction by proline hydroxylation: implications for O2 sensing. *Science* **292,** 464–468 (2001).

29. Lando, D. *et al.* FIH-1 is an asparaginyl hydroxylase enzyme that regulates the transcriptional activity of hypoxia-inducible factor. *Genes Dev.* **16,** 1466–1471 (2002).

30. Dayan, F., Roux, D., Brahimi-Horn, M. C., Pouyssegur, J. & Mazure, N. M. The oxygen sensor factor-inhibiting hypoxia-inducible factor-1 controls expression of distinct genes through the bifunctional transcriptional character of hypoxia-inducible factor-1α. *Cancer Res.* **66,** 3688–3698 (2006).

31. Liu, W., Shen, S. M., Zhao, X. Y. & Chen Dr., G. Q. Targeted genes and interacting proteins of hypoxia inducible factor-1. *Int. J. Biochem. Mol. Biol.* **3,** 165–178 (2012).

32. Harris, A. L. Hypoxia — a Key Regulatory Factor in Tumour Growth. *Nat. Rev. Cancer* **2,** 38–47 (2002).

33. Raval, R. R. *et al.* Contrasting Properties of HIF-2 in von Hippel-Lindau-Associated Renal Cell Carcinoma Contrasting Properties of Hypoxia-Inducible Factor 1 (HIF-1) and HIF-2 in von Hippel-Lindau-Associated Renal Cell Carcinoma. *Mol. Cell. Biol.* **25,** 5675–5686 (2005).

34. Li, L. *et al.* Hypoxia-inducible factor linked to differential kidney cancer risk seen with type 2A and type 2B VHL mutations. *Mol. Cell. Biol.* **27,** 5381–92 (2007).

35. Semenza, G. L. & Wang, G. L. A nuclear factor induced by hypoxia via de novo protein synthesis binds to the human erythropoietin gene enhancer at a site required for transcriptional activation. *Mol. Cell. Biol.* **12,** 5447–5454 (1992).

36. Ema, M. *et al.* A novel bHLH-PAS factor with close sequence similarity to hypoxia-inducible factor 1alpha regulates the VEGF expression and is potentially involved in lung and vascular development. *Proc. Natl. Acad. Sci. U. S. A.* **94,** 4273–8 (1997).

37. Tian, H., McKnight, S. L. & Russell, D. W. Endothelial PAS domain protein 1 (EPAS1), a transcription factor selectively expressed in endothelial cells. *Genes Dev.* **11,** 72–82 (1997).

38. Wood, S. M., Gleadle, J. M., Pugh, C. W., Hankinson, O. & Ratcliffe, P. J. The Role of the Aryl Hydrocarbon Receptor Nuclear Translocator (ARNT) in Hypoxic Induction of Gene Expression. *J. Biol. Chem.* **271,** 15117–15123 (1996).

39. Choi, S. M., Oh, H. & Park, H. Microarray analyses of hypoxia-regulated genes in an aryl hydrocarbon receptor nuclear translocator (Arnt)-dependent manner. *FEBS J.* **275,** 5618–5634 (2008).

40. Bracken, C. P. *et al.* Cell-specific regulation of hypoxia-inducible factor (HIF)-1a and HIF-2a stabilization and transactivation in a graded oxygen environment. *J. Biol. Chem.* **281,** 22575–22585 (2006).

41. Heikkila, M., Pasanen, A., Kivirikko, K. I. & Myllyharju, J. Roles of the human hypoxia-inducible factor (HIF)-3a variants in the hypoxia response. *Cell. Mol. Life Sci.* **68,** 3885–3901 (2011).

42. Koshiji, M. *et al.* HIF-1alpha induces cell cycle arrest by functionally counteracting Myc. *EMBO J.* **23,** 1949–56 (2004).

43. Gordan, J. D., Bertout, J. A., Hu, C. J., Diehl, J. A. & Simon, M. C. HIF-2a Promotes Hypoxic Cell Proliferation by Enhancing c-Myc Transcriptional Activity. *Cancer Cell* **11,** 335–347 (2007).

44. Chuan Shen, Rameen Beroukhim, Steven E. Schumacher, Jing Zhou, Michelle Chang, S. S. and W. G. K. J. Genetic and Functional Studies Implicate HIF1α as a 14q Kidney

Cancer Suppressor Gene. *Cancer Discov.* **1,** 222–235 (2011).

45. Maranchie, J. K. *et al.* The contribution of VHL subtrate binding and HIF-1a to the phenotype of vhl loss in renal cell carcinoma. *Cancer Cell* **1,** 247–253 (2002).

46. Kondo, K., Klco, J., Nakamura, E., Lechpammer, M. & Kaelin, W. G. Inhibition of HIF is necessary for tumor suppression by the von Hippel-Lindau protein. *Cancer Cell* **1,** 237–246 (2002).

47. Zimmer, M., Doucette, D., Siddiqui, N. & Iliopoulos, O. Inhibition of hypoxia-inducible factor is sufficient for growth suppression of VHL-/- tumors. *Mol. Cancer Res.* **2,** 89–95 (2004).

48. Kondo, K., Kim, W. Y., Lechpammer, M. & Kaelin, W. G. Inhibition of HIF2α is sufficient to suppress pVHL-defective tumor growth. *PLoS Biol.* **1,** 439–444 (2003).

49. Purdue, M. P. *et al.* Genome-wide association study of renal cell carcinoma identifies two susceptibility loci on 2p21 and 11q13.3. *Nat. Genet.* **43,** 60–65 (2010).

50. Schonenberger, D. *et al.* Formation of renal cysts and tumors in Vhl/Trp53-deficient mice requires HIF1α and HIF2α. *Cancer Res.* **76,** 2025–2036 (2016).

51. Chen, L., Endler, A. & Shibasaki, F. Hypoxia and angiogenesis: regulation of hypoxia-inducible factors via novel binding factors. *Exp. Mol. Med.* **41,** 849–857 (2009).

52. Hsieh, J. J., Mark P. Purdue , Sabina Signoretti, C. S., Laurence Albiges, M. S., , Daniel Y. Heng, J. L. & Ficarra, and V. Renal Cell Carcinoma. *Nat Rev Dis Prim* **3,** 1–19 (2013).

53. Curti, B. D. Renal cell carcinoma. *Curr.Opin.Oncol.* **15,** 213–216 (2004).

54. Goyal, R., Gersbach, E., Yang, X. J. & Rohan, S. M. Differential diagnosis of renal tumors with clear cytoplasm: Clinical relevance of renal tumor subclassification in the era of targeted therapies and personalized medicine. *Arch. Pathol. Lab. Med.* **137,** 467–480 (2013).

55. Law, T. M. *et al.* Phase iii randomized trial of interleukin-2 with or without lymphokine-activated killer cells in the treatment of patients with advanced renal cell carcinoma. *Cancer* **76,** 824–832 (1995).

56. Fyfe, G. *et al.* Results of treatment of 255 patients with metastatic renal cell carcinoma who received high-dose recombinant interleukin-2 therapy. *J. Clin. Oncol.* **13,** 688–96 (1995).

57. Escudier, B. *et al.* Sorafenib in Advanced Clear-Cell Renal-Cell Carcinoma. *N. Engl. J. Med.* **356,** 125–134 (2007).

58. Motzer, R. J. *et al.* Sunitinib versus Interferon Alfa in Metastatic Renal-Cell Carcinoma. *N. Engl. J. Med.* **356,** 115–124 (2007).

59. Rini, B. I. *et al.* Comparative effectiveness of axitinib versus sorafenib in advanced renal cell carcinoma (AXIS): A randomised phase 3 trial. *Lancet* **378,** 1931–1939 (2011).

60. Choueiri, T. & Motzer, R. J. Systemic Therapy for Metastatic Renal-Cell Carcinoma. *N. Engl. J. Med.* **376,** 354–366 (2017).

61. Sternberg, C. N. *et al.* Pazopanib in locally advanced or metastatic renal cell carcinoma: Results of a randomized phase III trial. *J. Clin. Oncol.* **28,** 1061–1068 (2010).

62. Escudier, B. *et al.* Phase III trial of bevacizumab plus interferon alfa-2a in patients with metastatic renal cell carcinoma (AVOREN): Final analysis of overall survival. *J. Clin. Oncol.* **28,** 2144–2150 (2010).

63. Motzer, R. J. *et al.* Efficacy of everolimus in advanced renal cell carcinoma: a double-blind, randomised, placebo-controlled phase III trial. *Lancet* **372,** 449–456 (2008).

64. Hudes, G. *et al.* Temsirolimus, interferon alfa, or both for advanced renal-cell carcinoma. *J. Urol.* **356,** 2271–81 (2008).

65. Négrier, S. *et al.* Temsirolimus and bevacizumab, or sunitinib, or interferon alfa and bevacizumab for patients with advanced renal cell carcinoma (TORAVA): A randomised phase 2 trial. *Lancet Oncol.* **12,** 673–680 (2011).

66. Brian I. Rini, Joaquim Bellmunt, Jill Clancy, Kongming Wang, Andreas G. Niethammer, Subramanian Hariharan, and B. E. Randomized Phase III Trial of Temsirolimus and Bevacizumab Versus Interferon Alfa and Bevacizumab in Metastatic Renal Cell Carcinoma: INTORACT Trial. *J. Clin. Oncol.* **32,** 752–759 (2013).

67. Motzer, R. J. *et al.* Lenvatinib, everolimus, and the combination in patients with metastatic renal cell carcinoma: A randomised, phase 2, open-label, multicentre trial. *Lancet Oncol.* **16,** 1473–1482 (2015).

68. Brahmer, J. R. *et al.* Safety and Activity of Anti–PD-L1 Antibody in Patients with Advanced Cancer. *N. Engl. J. Med.* **366,** 2455–2465 (2012).

69. Motzer, R. J. *et al.* Nivolumab for metastatic renal cell carcinoma: Results of a randomized phase II trial. *J. Clin. Oncol.* **33,** 1430–1437 (2015).

70. Atkins, M. B., Clark, J. I. & Quinn, D. I. Immune checkpoint inhibitors in advanced renal cell carcinoma: experience to date and future directions. *Ann. Oncol. Off. J. Eur. Soc. Med. Oncol.* **28,** 1484–1494 (2017).

71. Fontaine, F., Overman, J. & François, M. Pharmacological manipulation of transcription factor protein-protein interactions: opportunities and obstacles. *Cell Regen. (London, England)* **4,** 2 (2015).

72. Scheuermann, T. H. *et al.* Allosteric Inhibition of Hypoxia Inducible Factor-2 with Small Molecules. *Nat Chem Biol* **9,** 271–276 (2013).

73. Rogers, J. L. *et al.* Development of inhibitors of the PAS-B domain of the HIF-2a transcription factor. *J. Med. Chem.* **56,** 1739–1747 (2013).

74. Key, J., Scheuermann, T. H., Anderson, P. C., Daggett, V. & Gardner, K. H. Principles of ligand binding within a completely buried cavity in HIF2α PAS-B. *J. Am. Chem. Soc.*

131, 17647–17654 (2009).

75. Wallace, E. M. *et al.* A small-molecule antagonist of HIF2α is efficacious in preclinical models of renal cell carcinoma. *Cancer Res.* **76,** 5491–5500 (2016).

76. Courtney, K. D. *et al.* Phase I dose-escalation trial of PT2385, a first-in-class hypoxia-inducible factor-2a antagonist in patients with previously treated advanced clear cell renal cell carcinoma. *J. Clin. Oncol.* **36,** 867–874 (2018).

77. Chen, W. *et al.* Targeting renal cell carcinoma with a HIF-2 antagonist. *Nature* **539,** 112–117 (2016).

78. Cho, H. *et al.* On-Target Efficacy of a HIF2α Antagonist in Preclinical Kidney Cancer Models. *Nature* **539,** 107–111 (2016).

79. Papadopoulos, K. P., Janasch, E., Zojwalla, N. J., Wang, K. & Bauer, T. M. A first-in-human phase 1 dose-escalation trial of the oral HIF-2a inhibitor PT2977 in patients with advanced solid tumors. *J. Clin. Oncol.* **36,** 2508–2508 (2018).

80. Weinstein, I. B. & Joe, A. Oncogene addiction. *Cancer Res.* **68,** 3077–3080 (2008).

81. Arvanitis, C. & Felsher, D. W. Conditional transgenic models define how MYC initiates and maintains tumorigenesis. *Seminars in Cancer Biology* **16,** 313–317 (2006).

82. Felsher, D. W. & Bishop, J. M. Reversible tumorigenesis by MYC in hematopoietic lineages. *Mol. Cell* **4,** 199–207 (1999).

83. Pelengaris, S., Khan, M. & Evan, G. I. Suppression of Myc-induced apoptosis in β cells exposes multiple oncogenic properties of Myc and triggers carcinogenic progression. *Cell* **109,** 321–334 (2002).

84. Weinstein, I. B. & Joe, A. K. Mechanisms of disease: Oncogene addiction--a rationale for molecular targeting in cancer therapy. *Nat. Clin. Pract. Oncol.* **3,** 448–57 (2006).

85. Pagliarini, R., Shao, W. & Sellers, W. R. Oncogene addiction: pathways of therapeutic response, resistance, and road maps toward a cure. *EMBO Rep.* **16,** 280–96 (2015).

86. Gorre, M. E. *et al.* Clinical resistance to STI-571 cancer therapy caused by BCR-ABL gene mutation or amplification. *Science* **293,** 876–880 (2001).

87. Van Allen, E. M. *et al.* The genetic landscape of clinical resistance to RAF inhibition in metastatic melanoma. *Cancer Discov.* **4,** 94–109 (2014).

88. Solimini, N. L., Luo, J. & Elledge, S. J. Non-Oncogene Addiction and the Stress Phenotype of Cancer Cells. *Cell* **130,** 986–988 (2007).

89. Luo, J., Solimini, N. L. & Elledge, S. J. Principles of Cancer Therapy: Oncogene and Non-oncogene Addiction. *Cell* **136,** 823–837 (2009).

90. Chen, Z. *et al.* Selective Chk1 inhibitors differentially sensitize p53-deficient cancer cells to cancer therapeutics. *Int. J. Cancer* **119,** 2784–2794 (2006).

91. Bonnet, S. *et al.* A Mitochondria-K+ Channel Axis Is Suppressed in Cancer and Its

Normalization Promotes Apoptosis and Inhibits Cancer Growth. *Cancer Cell* **11,** 37–51 (2007).

92. Stolina, M. *et al.* Specific inhibition of cyclooxygenase 2 restores antitumor reactivity by altering the balance of IL-10 and IL-12 synthesis. *J Immunol* **164,** 361–370 (2000).

93. Loges, S., Schmidt, T. & Carmeliet, P. Mechanisms of resistance to anti-angiogenic therapy and development of third-generation anti-angiogenic drug candidates. *Genes Cancer* **1,** 12–25 (2010).

94. Mattarollo, S. R. *et al.* NKT cell adjuvant-based tumor vaccine for treatment of myc oncogene-driven mouse B-cell lymphoma. *Blood* **120,** 3019–3029 (2012).

95. Kawakami, Y. *et al.* Cancer-induced immunosuppressive cascades and their reversal by molecular-targeted therapy. *Ann. N. Y. Acad. Sci.* **1284,** 80–86 (2013).

96. Casey, S. C., Li, Y. & Felsher, D. W. An essential role for the immune system in the mechanism of tumor regression following targeted oncogene inactivation. *Immunol. Res.* **58,** 282–291 (2014).

97. Rakhra, K. *et al.* CD4+ T-cells Contribute to the Remodeling of the Microenvironment Required for Sustained Tumor Regression upon Oncogene Inactivation. *Cancer Cell* **18,** 485–498 (2010).

98. Acosta, J. C. *et al.* Chemokine Signaling via the CXCR2 Receptor Reinforces Senescence. *Cell* **133,** 1006–1018 (2008).

99. Beatty, G. L. & Paterson, Y. IFN-γ-Dependent Inhibition of Tumor Angiogenesis by Tumor-Infiltrating CD4 + T Cells Requires Tumor Responsiveness to IFN-γ. *J. Immunol.* **166,** 2276–82 (2001).

100. Kuilman, T. *et al.* Oncogene-Induced Senescence Relayed by an Interleukin-Dependent Inflammatory Network. *Cell* **133,** 1019–1031 (2008).

101. Kortlever, R. M. *et al.* Myc Cooperates with Ras by Programming Inflammation and Immune Suppression. *Cell* **171,** 1301–1315 (2017).

102. Soucek, L. *et al.* Mast cells are required for angiogenesis and macroscopic expansion of Myc-induced pancreatic islet tumors. *Nat. Med.* **13,** 1211–1218 (2007).

103. Reimann, M. *et al.* Tumor Stroma-Derived TGF-β Limits Myc-Driven Lymphomagenesis via Suv39h1-Dependent Senescence. *Cancer Cell* **17,** 262–272 (2010).

104. Kersten, K., de Visser, K. E., van Miltenburg, M. H. & Jonkers, J. Genetically engineered mouse models in oncology research and cancer medicine. *EMBO Mol. Med.* **9,** 137–153 (2017).

105. Adams, J. M. *et al.* The c-myc oncogene driven by immunoglobulin enhancers induces lymphoid malignancy in transgenic mice. *Nature* **318,** 533–538 (1985).

106. Hanahan, D. Heritable formation of pancreatic β-cell tumours in transgenic mice

expressing recombinant insulin/simian virus 40 oncogenes. *Nature* **315,** 115–122 (1985).

107. Lacey, M., Alpert, S. & Hanahan, D. Bovine papillomavirus genome elicits skin tumours in transgenic mice. *Nature* **322,** 609–612 (1986).

108. Shibata, H. *et al.* Rapid colorectal adenoma formation initiated by conditional targeting of the APC gene. *Science (80-.).* **278,** 120–123 (1997).

109. Vooijs, M., Jonkers, J. & Berns, A. A highly efficient ligand-regulated Cre recombinase mouse line shows that LoxP recombination is position dependent. *EMBO Rep.* **2,** 292–297 (2001).

110. Gossen, M. & Bujard, H. Tight control of gene expression in mammalian cells by tetracycline-responsive promoters. *Proc. Natl. Acad. Sci.* **89,** 5547–5551 (1992).

111. Baron, U. & Bujard, H. Tet repressor-based system for regulated gene expression in eukaryotic cells: Principles and advances. *Methods Enzymol.* **327,** 401–421 (2000).

112. Gossen, M. *et al.* Transcriptional activation by tetracyclines in mammalian cells. *Science (80-.).* **268,** 1766–1769 (1995).

113. Lewandoski, M. Conditional control of gene expression in the mouse. *Nat. Rev. Genet.* **2,** 743–755 (2001).

114. Dow, L. E. *et al.* Apc Restoration Promotes Cellular Differentiation and Reestablishes Crypt Homeostasis in Colorectal Cancer. *Cell* **161,** 1539–1552 (2015).

115. Dow, L. E. *et al.* Inducible in vivo genome editing with CRISPR-Cas9. *Nat. Biotechnol.* **33,** 390–394 (2015).

116. Fellmann, C. *et al.* An optimized microRNA backbone for effective single-copy RNAi. *Cell Rep.* **5,** 1704–1713 (2013).

117. Schmittgen, T. D. & Livak, K. J. Analyzing real-time PCR data by the comparative CTmethod. *Nat. Protoc.* **3,** 1101–1108 (2008).

118. Rodrigues, P. *et al.* NF-κB–dependent lymphoid enhancer co-option promotes renal carcinoma metastasis. *Cancer Discov.* **8,** 850–865 (2018).

119. Langmead, B. & Salzberg, S. L. Fast gapped-read alignment with Bowtie 2. *Nat. Methods* **9,** 357–359 (2012).

120. Li, H. *et al.* The Sequence Alignment/Map format and SAMtools. *Bioinformatics* **25,** 2078–2079 (2009).

121. Zhang, Y. *et al.* Model-based analysis of ChIP-Seq (MACS). *Genome Biol.* **9,** R137 (2008).

122. Horvath, P. & Barrangou, R. CRISPR/Cas, the immune system of bacteria and archaea. *Science* **327,** 167–170 (2010).

123. Müller, a *et al.* Involvement of chemokine receptors in breast cancer metastasis.

Nature **410,** 50–56 (2001).

124. Clontech. Tet-Off and Tet-On Gene Expression Systems User Manual. *Manual* **1,** (2005).

125. Kim, J. H. *et al.* High cleavage efficiency of a 2A peptide derived from porcine teschovirus-1 in human cell lines, zebrafish and mice. *PLoS One* **6,** (2011).

126. Scholzen, T. & Gerdes, J. The Ki-67 protein: From the known and the unknown. *J. Cell. Physiol.* **182,** 311–322 (2000).

127. BD Biosciences. Caspase-3 Activation: An Indicator of Apoptosis in Image-Based Assays. 1–4 (2012). Available at: https://www.bdbiosciences.com/documents/Bioimaging_AppNote_Apoptosis.pdf. (Accessed: 16th January 2019)

128. Boxer, R. B., Jang, J. W., Sintasath, L. & Chodosh, L. A. Lack of sustained regression of c-MYC-induced mammary adenocarcinomas following brief or prolonged MYC inactivation. *Cancer Cell* **6,** 577–586 (2004).

129. Shachaf, C. M. *et al.* MYC inactivation uncovers pluripotent differentiation and tumour dormancy in hepatocellular cancer. *Nature* **431,** 1112–1117 (2004).

130. River, C. Oncology Animal Models. (2011). Available at: https://www.criver.com/sites/default/files/resources/rm_rm_d_immunodeficient_models.pdf. (Accessed: 27th February 2019)

131. The Jackson Laboratory. NSG MOUSE STRAIN DATASHEET. (2019). Available at: https://www.jax.org/strain/005557. (Accessed: 17th January 2019)

132. QIAGEN. Ingenuity Pathway Analysis (IPA). (2014). Available at: http://pages.ingenuity.com/rs/ingenuity/images/IPA_data_sheet.pdf. (Accessed: 17th January 2019)

133. Broad Institute. GSEA User Guide. Available at: https://software.broadinstitute.org/gsea/doc/GSEAUserGuideFrame.html. (Accessed: 17th January 2019)

134. Grampp, S. *et al.* Genetic variation at the 8q24.21 renal cancer susceptibility locus affects HIF binding to a MYC enhancer. *Nat. Commun.* **7,** (2016).

135. Schödel, J. *et al.* Common genetic variants at the 11q13.3 renal cancer susceptibility locus influence binding of HIF to an enhancer of cyclin D1 expression. *Nat. Genet.* **44,** 420–425 (2012).

136. Tseng, Y. Y. *et al.* PVT1 dependence in cancer with MYC copy-number increase. *Nature* **512,** 82–86 (2014).

137. Janssen, J. W. G. *et al.* MYEOV, a gene at 11q13, is coamplified with CCND1, but epigenetically inactivated in a subset of esophageal squamous cell carcinomas. *J. Hum. Genet.* **47,** 460–464 (2002).

138. Janssen, J. W. G. *et al.* MYEOV: A candidate gene for DNA amplification events occurring centromeric to CCND1 in breast cancer. *Int. J. Cancer* **102,** 608–614 (2002).

139. Coccaro, N. *et al.* MYEOV gene overexpression in primary plasma cell leukemia with t(11;14)(q13;q32). *Oncol. Lett.* **12,** 1460–1464 (2016).

140. Joshi, R., Gilligan, D. M., Otto, E., McLaughlin, T. & Bennett, V. Primary structure and domain organization of human alpha and beta adducin. *J. Cell Biol.* **115,** 665–675 (1991).

141. Wenger, R. H., Stiehl, D. P. & Camenisch, G. Integration of Oxygen Signaling at the Consensus HRE. *Sci. Signal.* **2005,** re12 (2005).

142. Gilbert, L. A. *et al.* CRISPR-mediated modular RNA-guided regulation of transcription in eukaryotes. *Cell* **154,** 442–451 (2013).

143. Gilbert, L. A. *et al.* Genome-Scale CRISPR-Mediated Control of Gene Repression and Activation. *Cell* **159,** 647–661 (2014).

144. Ran, F. *et al.* Genome engineering using the CRISPR-Cas9 system. *Nat Protoc* **8,** 2281–2308 (2013).

145. Shen, C. *et al.* Genetic and Functional Studies Implicate HIF1 as a 14q Kidney Cancer Suppressor Gene. *Cancer Discov.* **1,** 222–235 (2011).

146. Ahler, E. *et al.* Doxycycline Alters Metabolism and Proliferation of Human Cell Lines. *PLoS One* **8,** (2013).

147. Bellovin, D., Das, B. & Felsher, D. Tumor Dormancy, Oncogene Addiction, Cellular Senescence and Self-Renewal Programs. *Adv Exp Med Biol* **734,** 91–107 (2013).

148. Cho, H. *et al.* On-Target Efficacy of a HIF2α Antagonist in Preclinical Kidney Cancer Models. *Nature* (2016). doi:10.1038/nature19795

149. Lin, W. *et al.* Dormant cancer cells contribute to residual disease in a model of reversible pancreatic cancer. *Cancer Res* **73,** 1821–1830 (2013).

150. Jain, M. *et al.* Sustained loss of a neoplastic phenotype by brief inactivation of MYC. *Science (80-.).* **297,** 102–104 (2002).

151. Flores, I., Murphy, D. J., Swigart, L. B., Knies, U. & Evan, G. I. Defining the temporal requirements for Myc in the progression and maintenance of skin neoplasia. *Oncogene* **23,** 5923–5930 (2004).

152. Balkwill, F. & Mantovani, A. Inflammation and cancer: Back to Virchow? *Lancet* **357,** 539–545 (2001).

153. Rakhra, K. *et al.* CD4+ T Cells contribute to the remodeling of the microenvironment required for sustained tumor regression upon oncogene inactivation. *Cancer Cell* **18,** 485–498 (2010).

154. Nishikawa, H. & Sakaguchi, S. Regulatory T cells in cancer immunotherapy. *Curr Opin*

Immunol **27,** 1–7 (2014).

155. De Palma, M. & Lewis, C. E. Macrophage regulation of tumor responses to anticancer therapies. *Cancer Cell* **23,** 277–286 (2013).

156. Pagès, F. *et al.* In situ cytotoxic and memory T cells predict outcome in patients with early-stage colorectal cancer. *J. Clin. Oncol.* **29,** 5944–5951 (2009).

157. Şenbabaoğlu, Y. *et al.* Tumor immune microenvironment characterization in clear cell renal cell carcinoma identifies prognostic and immunotherapeutically relevant messenger RNA signatures. *Genome Biol.* **17,** (2016).

158. Chevrier, S. *et al.* An Immune Atlas of Clear Cell Renal Cell Carcinoma. *Cell* **169,** 736–749 (2017).

159. Bertout, J. A. *et al.* HIF2 inhibition promotes p53 pathway activity, tumor cell death, and radiation responses. *Proc. Natl. Acad. Sci.* **106,** 14391–14396 (2009).

160. Dang, C. V. MYC on the path to cancer. *Cell* **149,** 22–35 (2012).

161. Meyer, N. & Penn, L. Z. Reflecting on 25 years with MYC. *Nat. Rev. Cancer* **8,** 976–990 (2008).

162. Coller, H. A. *et al.* Expression analysis with oligonucleotide microarrays reveals that MYC regulates genes involved in growth, cell cycle, signaling, and adhesion. *Proc. Natl. Acad. Sci.* **97,** 3260–3265 (2000).

163. Fernandez, P. C. *et al.* Genomic targets of the human c-Myc protein. *Genes Dev.* **17,** 1115–1129 (2003).

164. Beroukhim, R. *et al.* The landscape of somatic copy-number alteration across human cancers. *Nature* **463,** 899–905 (2010).

165. Collins, S. & Groudine, M. Amplification of endogenous myc-related DNA sequences in a human myeloid leukaemia cell line. *Nature* **298,** 679–681 (1982).

166. Schwab, M. *et al.* Amplified DNA with limited homology to myc cellular oncogene is shared by human neuroblastoma cell lines and a neuroblastoma tumour. *Nature* **305,** 245–248 (1983).

167. Nau, M. M. *et al.* L-myc, a new myc-related gene amplified and expressed in human small cell lung cancer. *Nature* **318,** 69–73 (1985).

168. Koboldt, D. C. *et al.* Comprehensive molecular portraits of human breast tumours. *Nature* **490,** 61–70 (2012).

169. Shou, Y., Martelli, M. L., Gabre, A., Qi, Y. & Brents, L. A. Diverse karyotypic abnormalities of the c-myc locus associated with c-myc dysregulation and tumor progression in multiple myeloma. *Proc. Natl. Acad. Sci.* **97,** 228–233 (2000).

170. National Cancer Institute. Available at: https://portal.gdc.cancer.gov/genes. (Accessed: 8th January 2019)

171. Schuuring, E. The involvement of the chromosome 11q13 region in human malignancies: Cyclin D1 and EMS1 are two new candidate oncogenes-a review. *Gene* **159,** 83–96 (1995).

172. Donnellan, R. & Chetty, R. Cyclin D1 and human neoplasia. *J. Clin. Pathol. - Mol. Pathol.* **51,** 1–7 (1998).

173. Wiestner, A. *et al.* Point mutations and genomic deletions in CCND1 create stable truncated cyclin D1 mRNAs that are associated with increased proliferation rate and shorter survival. *Blood* **109,** 5499–5606 (2007).

174. Bachmann, K. *et al.* Cyclin D1 is a strong prognostic factor for survival in pancreatic cancer: Analysis of CD G870A polymorphism, FISH and immunohistochemistry. *J. Surg. Oncol.* **111,** 316–323 (2015).

175. Dhingra, V., Verma, J., Misra, V., Srivastav, S. & Hasan, F. Evaluation of cyclin D1 expression in head and neck squamous cell carcinoma. *J. Clin. Diagnostic Res.* **11,** 1–4 (2017).

176. Bretones, G., Delgado, M. D. & León, J. Myc and cell cycle control. *Biochim. Biophys. Acta - Gene Regul. Mech.* **1849,** 506–516 (2015).

177. Baba, M. *et al.* Loss of von Hippel-Lindau protein causes cell density dependent deregulation of CyclinD1 expression through Hypoxia-inducible factor. *Oncogene* **22,** 2728–2738 (2003).

178. Raval, R. R. *et al.* Contrasting Properties of Hypoxia-Inducible Factor 1 (HIF-1) and HIF-2 in von Hippel-Lindau-Associated Renal Cell Carcinoma. *Mol. Cell. Biol.* **25,** 5675–5686 (2005).

179. Zhang, T., Niu, X., Liao, L., Cho, E. A. & Yang, H. The contributions of HIF-target genes to tumor growth in RCC. *PLoS One* **8,** (2013).

180. Prigent, S. A. & Lemoine, N. R. The type 1 (EGFR-related) family of growth factor receptors and their ligands. *Prog. Growth Factor Res.* **4,** 1–24 (1992).

181. Salomon, D. S., Brandt, R., Ciardiello, F. & Normanno, N. Epidermal growth factor-related peptides and their receptors in human malignancies. *Crit. Rev. Oncol. Hematol.* **19,** 183–232 (1995).

182. Ciardiello, F. *et al.* Expression of transforming growth factor alpha (TGF alpha) in breast cancer. *Ann. Oncol.* **2,** 169–182 (1991).

183. Hsieh, E., Shepherd, F. & Tsao, M. Co-expression of epidermal growth factor receptor and transforming growth factor-α is independent of ras mutations in lung adenocarcinoma. *Lung Cancer* **29,** 151–157 (2000).

184. Petrides, P., Bock, S., Bovens, J., Hofmann, R. & Jakse, G. Modulation of Pro-Epidermal Growth Factor, Pro-Transforming Growth Factor α and Epidermal Growth Factor Receptor Gene Expression in Human Renal Carcinomas. *Cancer Res.* **50,** (1990).

185. Lager, D., Slagel, D. & Palechek, P. The expression of epidermal growth factor

receptor and transforming growth factor alpha in renal cell carcinoma. *Mod Pathol* **7,** 544–548 (1994).

186. Prewett, M. *et al.* Mouse-human chimeric anti-epidermal growth factor receptor antibody C225 inhibits the growth of human renal cell carcinoma xenografts in nude mice. *Clin. Cancer Res.* **4,** 2957–2966 (1998).

187. Gunaratnam, L. *et al.* Hypoxia inducible factor activates the transforming growth factor-alpha/epidermal growth factor receptor growth stimulatory pathway in VHL(-/-) renal cell carcinoma cells. *J Biol Chem* **278,** 44966–74 (2003).

188. Yao, X. *et al.* VHL deficiency drives enhancer activation of oncogenes in clear cell renal cell carcinoma. *Cancer Discov.* **7,** 1284–1305 (2017).

189. Smythies, J. A. *et al.* Inherent DNA-binding specificities of the HIF-1α and HIF-2α transcription factors in chromatin. *EMBO Rep.* **20,** 1–17 (2018).

190. Ozcan, A., De La Roza, G., Ro, J. Y., Shen, S. S. & Truong, L. D. PAX2 and PAX8 expression in primary and metastatic renal tumors, A comprehensive comparison. *Arch. Pathol. Lab. Med.* **136,** 1541–1551 (2012).

191. Lim, S. & Kaldis, P. Cdks, cyclins and CKIs: roles beyond cell cycle regulation. *Development* **140,** 3079–3093 (2013).

192. Chohan, T. A., Qayyum, A., Rehman, K., Tariq, M. & Akash, M. S. H. An insight into the emerging role of cyclin-dependent kinase inhibitors as potential therapeutic agents for the treatment of advanced cancers. *Biomed. Pharmacother.* **107,** 1326–1341 (2018).

193. Abraham, J. Abemaciclib becomes first CDK inhibitor to clinch single-agent approval for breast cancer. *J. Community Support. Oncol.* **16,** (2018).

194. Bommi-Reddy, A. *et al.* Kinase requirements in human cells: III. Altered kinase requirements in VHL-/- cancer cells detected in a pilot synthetic lethal screen. *Proc. Natl. Acad. Sci.* **105,** 16484–16489 (2008).